Published in final edited form as:

J Med Chem. 2021 December 23; 64(24): 17656–17689. doi:10.1021/acs.jmedchem.1c01571.

The repertoire of small molecule PET probes for neuroinflammation imaging: challenges and opportunities beyond TSPO

Zhen Chen[1,†], **Ahmed Haider**[1,†], **Jiahui Chen**[1], **Zhiwei Xiao**[1], **Luca Gobbi**[2], **Michael Honer**[2], **Uwe Grether**[2], **Steven E. Arnold**[3], **Lee Josephson**[1], **Steven H. Liang**[1]

[1]Division of Nuclear Medicine and Molecular Imaging, Massachusetts General Hospital & Department of Radiology, Harvard Medical School, Boston, MA, 02114, United States

[2]Pharma Research and Early Development, F. Hoffmann-La Roche Ltd, CH-4070 Basel, Switzerland

[3]Department of Neurology and the Massachusetts Alzheimer's Disease Research Center, Massachusetts General Hospital, Harvard Medical School, 114 16th Street, Charlestown, Massachusetts 02129, USA

Abstract

Neuroinflammation is an adaptive response of the central nervous system to diverse potentially injurious stimuli, which is closely associated with neurodegeneration and typically characterized by activation of microglia and astrocytes. As a noninvasive and translational molecular imaging tool, positron emission tomography (PET) could provide a better understanding of neuroinflammation and its role in neurodegenerative diseases. Ligands to TSPO, a putative marker of neuroinflammation, have been the most commonly studied in this context, but suffer from serious limitations. Herein we present a repertoire of different structural chemotypes and novel PET ligand design for classical and emerging neuroinflammatory targets beyond TSPO. We believe that this review will support multidisciplinary collaborations in academic and industrial institutions working on neuroinflammation and facilitate the progress of neuroinflammation PET probe development for clinical use.

GRAPHICAL ABSTRACT

Corresponding Authors: Steven H. Liang – Division of Nuclear Medicine and Molecular Imaging, Massachusetts General Hospital, and Department of Radiology, Harvard Medical School, Boston, Massachusetts 02114, United States; Phone: +16177266107; liang.steven@mgh.harvard.edu; Fax: +1-617-726-6165.

[†]These authors contribute equally.

The authors declare no competing financial interest.

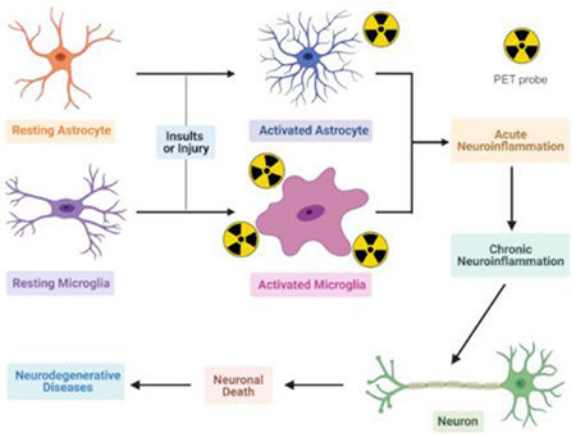

Keywords

Neuroinflammation; Neurodegenerative disease; Microglia; Astrocyte; positron emission tomography (PET)

1. Introduction

Neuroinflammation is an adaptive response of nervous tissue to a variety of stimuli or insults, including infection, toxins, misfolded proteins and autoantigens. It typically involves the activation of glia cells (i.e., microglia and astrocyte) in the central nervous system (CNS) through release of second lipid messenger and inflammatory mediators such as reactive oxygen/nitrogen species (ROS/RNS), chemokines and cytokines (Figure 1).[1] Inflammatory mediators govern the response to inflammatory stimuli and minimize the damage from the inflammatory insult.

Microglia are the principal immune cells in the CNS, constantly sensing the cellular environment and responding to maintain homeostasis. Of note, microglia have a very high sensitivity to stimuli and their activation is typically transient with a response time of 20-40 minutes.[2] Initially, a theory of the M0/M1/M2 continuum was proposed to describe microglial phenotypes. Within this theory, in response to a stimuli, such as lipopolysaccharide (LPS), the homeostatic M0 microglia can be activated into an amoeboid-like morphology, which can be polarized to two forms, namely M1 microglia and M2 microglia.[3–5] While M1 microglia are proinflammatory and primarily responsible for removing the stimuli or insult by release of various inflammatory factors such as reactive oxygen species (ROS), TNF-α and prostaglandins, the major role of M2 microglia is to mitigate the inflammatory response and protect the neurons by expressing growth factors and other neuroprotective factors.[6] However, this M0/M1/M2 conceptualization appears to be oversimplified, leading to conflicting interpretations of findings in some PET inflammatory imaging work.[7] More recent studies have identified at least eight microglial phenotypes, based on transcriptomic profiling of microglial in different disease and response modes. Some current phenotypes are named LPS-related transcriptomic signature microglia, microglia neurodegenerative

phenotype, disease-associated microglia, proliferation-related transcriptomic signature microglia, and interferon-related transcriptomic signature microglia.[7] As research continues to characterize more microglial phenotypes, an understanding of the microglial function in neuroinflammation and neurodegenerative diseases will grow.

Astrocytes are another type of CNS-resident glial cells, which have high expression in the white and gray matter and are best known for their role in the regulating brain energy metabolism, extracellular glutamate uptake, and maintenance of CNS homeostasis via several ion channels.[8–11] In response to CNS insults, such as brain injury or CNS diseases, astrocytes are activated to undergo astrogliosis and fibrosis, which exerts an important role in the recovery of injured tissue, blood-brain barrier (BBB) repair, restricting infection or inflammatory cell spread, and neuroprotection against CNS diseases.[12–15] Despite these benefits, dysfunction of reactive astrocyte may contribute to or exacerbate neuroinflammation or neurodegenerative disorders either by gain of detrimental functions or by loss of normal effects.[16] Previously, reactive astrocytes have been proposed to constitute two subtypes, namely A1 astrocyte and A2 astrocyte. A2 astrocytes are protective to synapses through upregulation of various neurotrophic factors, while A1 astrocytes, which are activated by M1 microglia, are toxic or destructive to synaptic integrity and neuronal survival.[17, 18] Particularly, high densities of A1 astrocytes are observed in various human neurodegenerative disorders including Alzheimer's disease (AD), Huntington's disease (HD), Parkinson's disease (PD), amyotrophic lateral sclerosis (ALS), and multiple sclerosis (MS), suggesting a central role of A1 astrocyte in the pathophysiology of neurodegeneration. Nevertheless, this classification of A1/A2 astrocytes is also likely too simplistic, and more recent studies have determined multifarious activation states of astrocytes, which are not only associated with the type of insult or disease state, but also with the cell type and CNS region.[19]

Neuroinflammation can exert both, neurotoxic and neuroprotective effects, dependent on different activation states of immune cells. Generally, neuroinflammatory responses could be beneficial to the CNS through activation of the innate immune system to minimize and repair the damage caused by insults.[20, 21] However, in chronic neuroinflammatory conditions such as neurodegenerative disorders, microglia and astrocytes are persistently activated with sustained generation of pro-inflammatory factors, resulting in vicious cycles of inflammation, cellular dysregulation, injury and degeneration.[22–25] As such, neuroinflammation has emerged as a common driver of multiple neurodegenerative diseases.[26] Neurodegenerative diseases are pathological defined by characteristic misfolded protein inclusions in neuronal cells, or in the case of Alzheimer's disease, extracellular aggregates as well. Such lesions include extracellular amyloid beta plaque (Aβ) and intracellular tau protein in AD, tau protein in some frontotemporal dementias (FTD), progressive supranuclear palsy and corticobasal degeneration, α-synuclein in PD and related Lewy body diseases and multiple system atrophy, TDP-43 in amyotrophic lateral sclerosis and some frontotemporal dementias, and huntingtin in HD. In general, these aggregated misfolded proteins are toxic to neuronal cells, disrupting intracellular trafficking and other functions. In a prion-like fashion, protein misfolding and intracellular aggregation in these neurodegenerative diseases propagate from neuron to neuron, spreading progressively through the brain. As they do, sickened and dying cells release distress signals, eliciting

neuroinflammation, which in turn, can accelerate death in vicious cycles, and this toxicity might spread to all brain regions to trigger neuroinflammation and neurodegeneration. For example, in AD, extracellular fibrillar and soluble oligomeric species of Aβ are recognized as exogenous stimuli, leading to uncontrolled neuroinflammation together with upregulated ROS levels and oxidative stress, and ultimately resulting in neuronal death, propagation of neuroinflammation, as well as exacerbation of tau and Aβ pathology.[27–30] In addition, mounting data indicated that neuroinflammation is also inextricably involved in pain,[31–33] cancers,[34, 35] and other neurodegenerative disorders including PD, epilepsy, and MS.[36–38]

Positron emission tomography (PET) has emerged as a noninvasive and translational imaging technique to visualize and quantify in vivo biochemical processes in real-time.[39–41] Compared with other imaging methods, such as fluorescence imaging, PET is characterized by greater tissue penetration, better quantification and facile animal-to-human translatability. At typical PET probe doses of less than 100 ug/person, biological responses to the probe are negligible, allowing PET to support and mitigate the risk for clinical translation of therapeutic drug candidates through an improved understanding of their pharmacokinetics, target engagement, and mode-of-action. PET has provided a better understanding of neuroinflammation, neurological disorders and neurodegenerative diseases.[42–51] Despite these benefits, developing novel suitable radioligands for PET imaging of neuroinflammation-related targets is still a demanding task, which must meet several selection criteria. The first step entails the identification and validation of a suitable protein target, which acts as a surrogate or proxy index for neuroinflammatory conditions. The target of interest should have adequate number of binding sites (B_{max}) and/or dynamic range to encompass levels across disease and physiological conditions. In other words, the B_{max} of this target must vary adequately to allow detectable pathological-to-normal signals using PET ligands. Secondly, radioligands must have excellent binding affinity (K_d) and selectivity to a specific target to enable an adequate signal to noise ratio against noise coming from off-target and non-specific binding. A B_{max}/K_d ratio of ≥10 has been proposed to be able to successfully detect a biological target with a PET tracer. Thirdly, radioligands must rapidly cross the BBB, which might be impeded by poor intrinsic permeability or/and intensive interaction with the efflux transporters in the BBB, such as P-glycoprotein (Pgp) and breast cancer resistance protein (Bcrp). Generally, a radioligand with low molecular weight (MW < 500 Da), moderate lipophilicity (log*D* = 1.5–3.0), low polar surface area (PSA ≤ 75 $Å^2$), and low hydrogen-bonding capability (≤ 1 hydrogen bond donor) exhibits good permeability across the BBB.[52–54] Finally, the short lived nuclides typically used for labelling of small molecules (^{11}C: $t_{1/2}$ = 20.4 min, ^{18}F: $t_{1/2}$ = 109.8 min) impose additional limits in tracer candidate selection with regard to fast and efficient radiochemistry methodology, despite significant improvements in the radiochemical synthesis methods in most recent times.[48, 55]

For a very long time, a central player in imaging neuroinflammation with PET has been the translocator protein (TSPO), which has been reviewed by our group and others.[42–47] While TSPO PET still constitutes the most widespread application in current clinical neuroinflammation imaging, its use and interpretation is largely limited by several quantification-related caveats, including polymorphism associated difference in binding affinity, incomplete cellular specificity for microglia and a microglial phenotype, as well

as its inability to distinguish between pro- and anti-inflammatory microglia. Furthermore, TSPO PET imaging represents only one of many aspects of neuroinflammatory responses that may differ across people and diseases. Beyond recent developments of next generation TSPO ligands, novel enzymes, receptors and intracellular signalling molecules are under development and investigation for PET imaging of neuroinflammation, especially in neurodegenerative disorders.[56–62] Compared with the existing review articles that primarily focus on PET imaging evaluation, we present herein a repertoire of novel PET ligands designed for classical and emerging biological targets (beyond TSPO) involved in the neuroinflammatory pathway as well as different structural chemotypes and radiolabeling strategies for these PET ligands. We have two explicit inclusion criteria for the topics in this work, including (1) PET ligands that have shown their potential in preclinical models and/or validated in higher species for future translation or extended study in disease population; and (2) emerging or not fully validated biological targets that could be the focus of next generation PET ligands towards imaging of neuroinflammation (Figure 1 and Table 1). We believe that this review will support multidisciplinary collaborations in academic and industrial institutions working on neuroinflammation and facilitate the progress of neuroinflammation PET probe development for clinical use.

1. PET probes for cyclooxygenase (COX)

Cyclooxygenase (COX), also termed prostaglandin H synthase, is the key enzyme regulating the transformation of arachidonic acid and plays an important role in activating the inflammatory pathway by the production of prostaglandins, cytokines, chemokines, and ROS.[117] In mammals, COX exists in two major subtypes, namely COX-1 and COX-2, which share 63% amino acid sequence identity and differ in distribution patterns, functions and regulatory mechanisms.[118, 119]

1.1 PET probes for cyclooxygenase 1 (COX-1)

COX-1 is widely distributed in most brain tissues with enrichment in medulla, midbrain, and pons, and mainly functions to control the transformation of arachidonic acid to prostaglandins. Of note, COX-1 participates in several processes related to cellular homeostasis and is thus deemed a “housekeeping” enzyme. As well, recent studies have demonstrated that changes in COX-1 expression and/or activity are closely involved in neuroinflammation. For example, in a chronic neuroinflammation mouse model induced by interleukin-1β overexpression, the expression of COX-1 was elevated and this variation could be fully abolished by pharmacological blockade or genetic deletion of COX-1.[120] Consistent with this report, LPS or $A\beta_{1–42}$ induced inflammatory response and neuronal damage could also be attenuated by pharmacological blockade or genetic deletion of COX-1.[63, 121] In addition, COX-1 inhibition has been shown to attenuate tau phosphorylation and Aβ deposition as well as to prompt improvement of learning and memory in AD mice.[122]

The evident role of COX-1 in neuroinflammation has stimulated the research on the development of potent and selective COX-1 PET probes. [^{11}C]**1** ([^{11}C]ibuprofen) and ketoprofen methyl ester [^{11}C]**2** ([^{11}C]KTP-Me) were initially reported as potential COX-1

PET ligands (Figure 2).[123] However, [^{11}C]ibuprofen exhibited relatively low binding affinity (IC_{50} COX-1 = 7.6 μM), no selectivity between COX-1 and COX-2 (IC_{50} COX-2 = 7.2 μM with human whole blood assay), as well as high plasma binding, thus impeding its further evaluation.[124] In contrast, [^{11}C]KTP-Me has emerged as the first promising COX-1 PET probe with reasonable in vitro binding affinity and selectivity (COX-1: IC_{50} = 0.047 μM, COX-2: IC_{50} = 2.9 μM).[64] The selective binding of [^{11}C]KTP-Me to COX-1 was also confirmed by ex vivo autoradiography, wherein a remarkably decreased uptake of [^{11}C]KTP-Me in the brain was observed in COX-1 deficient mice, but not in COX-2-deficient mice, when compared with the wild-type controls. PET imaging studies of [^{11}C]KTP-Me indicated significantly elevated radioactivity accumulation in the LPS-injected striatum (standard uptake value, SUV = 0.97) compared with the contralateral control (SUV = 0.26), which was consistent with the increased COX-1 expression. Further translation into human use revealed favorable brain uptake, reaching a plateau of 1.5 SUV in the cortex at 2 min p.i., followed by a gradual elimination with 40% of peak radioactivity remaining at 60 min p.i.[125] Metabolic analysis revealed that the parent [^{11}C]KTP-Me disappeared from plasma within the initial 2–3 min, forming a hydrophilic metabolite [^{11}C]KTP, which may hamper the interpretation and quantification of the PET signal in the brain. Other recent studies rendered the discovery of three 1,2,4-triazole-based COX-1 PET ligands with high binding affinities and selectivity over COX-2 (>200 fold), namely [^{11}C]**3** ([^{11}C]PS1) (human COX-1: IC_{50} = 5.0 nM, human COX-2: IC_{50} > 1 μM), [^{11}C]**4** ([^{18}F]PS2) (human COX-1: IC_{50} = 4.0 nM, human COX-2: IC_{50} = 0.84 μM), and [^{11}C]**5** ([^{11}C]PS13) (human COX-1: IC_{50} = 1.0 nM, human COX-2: IC_{50} > 1 μM).[65, 126] PET imaging studies of [^{18}F]PS2 in rhesus monkeys indicated high initial brain uptake with a peak SUV of 4.11 at 7 min p.i., followed by a rapid washout (SUV = 1.05 at 85 min). However, its further development was likely discouraged by skull uptake due to radiodefluorination in vivo. [^{11}C]PS1 and [^{11}C]PS13 also revealed high radioactivity accumulations in non-human primate (NHP) brains with 4.26 and 4.29 peak SUV, respectively. Compared with [^{11}C]PS1 (SUV = 0.62 at 85 min p.i.) and [^{18}F]PS2, [^{11}C]PS13 exhibited a much slower elimination rate from the brain, declining by 54% to 1.99 SUV at 85 min p.i., which likely suggested the highest specific binding in the brain for [^{11}C]PS13. Compartmental modeling revealed that the total volume of distribution (V_T) of [^{11}C]PS13 could be reduced by 87% and 72% by unlabeled PS13 and KTP-Me, respectively, without any influence by the COX-2 inhibitor MC1, confirming its high specific signal for COX-1. More importantly, in a neuroinflammatory monkey model with [^{11}C]PS13, the LPS- or ibotenic acid-injected ipsilateral basal ganglia exhibited higher radioactivity accumulation compared with the untreated contralateral control.[127] Moving forward into COX-1 imaging in healthy human, [^{11}C]PS13 revealed excellent test-retest variability and good time-stability, together with high uptake in the hippocampus (SUV_{max} = ca. 2.5), occipital cortex (SUV_{max} = ca. 2.7), thalamus, and brainstem.[128] It was also demonstrated that V_T of [^{11}C]PS13 correlated well with COX-1 transcript and expression levels in healthy individuals. Altogether COX-1 represents a promising target for neuroinflammation imaging and [^{11}C]PS13 merits further investigation in preclinical models of neuroinflammation and clinical research study.

1.2 PET probes for cyclooxygenase 2 (COX-2)

By contrast to the wide distribution of COX-1 in most brain tissues, COX-2 is typically expressed at a low level in normal brain tissues, but its expression can be dramatically changed by challenge with inflammatory stimuli. [57, 119] In contrast to the established role of COX-1, the role of COX-2 in neuroinflammation is controversial.[129] In one study, higher levels of COX-2 were observed in several inflammatory animal models, and inhibition of COX-2 revealed some anti-inflammatory effects.[66] In other studies, by contrast, COX-2 was demonstrated to play a prominent role in neuroprotection, and detrimental effects were induced by pharmacological blockade or genetic deletion of COX-2. For example, COX-2 deficient mice exhibited exacerbated LPS-induced neuroinflammatory response compared with wild-type mice.[130] Nonetheless, there is a consensus that COX-2 is closely implicated in neuroinflammatory processes.

So far, a number of COX-2 inhibitors have been labeled with carbon-11 or fluorine-18 and evaluated for in vivo COX-2 imaging. [^{18}F]**6** ([^{18}F]desbromo-DuP-697) was initially disclosed as COX-2 ligand with moderate binding affinity (K_i = 250 nM) (Figure 3).[131] As demonstrated by ex vivo biodistribution and autoradiography studies in rats, [^{18}F]desbromo-DuP-697 revealed heterogeneous distribution with high radioactivity levels in most cortical regions, and good binding specificity with 40% displaceable binding by the COX-2 inhibitor NS-398. Unfortunately, it failed to demonstrate any specificity in inflamed paw, as similar radioactivity levels were accumulated in the inflamed paw (SUV = 0.17 at 2 h p.i.) and the healthy control paw (SUV = 0.20 at 2 h p.i.). Further, the radioactivity in the inflamed paw was not displaced by NS-398, which was possibly attributed to the low expression levels of COX-2 in paws. Subsequently, a potent and selective COX-2 inhibitor, Celecoxib (IC_{50} COX-2 = 40 nM; IC_{50} COX-1 = 8 μM), containing a diarylpyrazole core, was labeled with carbon-11 or fluorine-18. Although [^{11}C]**7** ([^{11}C]Celecoxib)[132–134] and [^{18}F]**8** ([^{18}F]Celecoxib)[135] revealed reasonable brain uptake in both rodents (3 %ID/mL at 10-15 min p.i.) and NHPs (SUV_{max} = 1.2-2.0 in various brain regions at 3-10 min p.i.), these two tracers failed to demonstrate specific binding in the brain. In addition, a rapid metabolic rate was observed for [^{11}C]Celecoxib in baboons with < 25% parent fraction at 10 min p.i. One ^{11}C-labeled and two ^{18}F-labeled Celecoxib derivatives ([^{11}C]**9** (IC_{50} COX-2 = 8 nM; IC_{50} COX-1 = 2.6 μM),[136] [^{18}F]**10** (IC_{50} COX-2 = 0.36 μM; IC_{50} COX-2 > 100 μM)[137] and [^{18}F]**11** (IC_{50} COX-2 = 1.7 nM; IC_{50} COX-2 = 0.38 μM)[138] were also disclosed and all of them exhibited good metabolic stability in rodents. While [^{11}C]**9** failed to cross the BBB in rats (0.20 %ID/g at 15 min p.i.), [^{18}F]**10** exhibited low uptake and retention in COX-2 expressing HCA-7 (human colorectal cancer cell line) tumors in mice. Considering the reasonable brain uptake of [^{18}F]**11** in mice, a more efficient method for its radiolabeling other than electrochemical radiofluorination needs to be established to address the issues in regard to the poor radiochemical yield (2% RCY) and low molar activity (~0.11 GBq/μmol). In addition to the diarylpyrazole core in Celecoxib and its derivatives, several COX-2 inhibitors containing a diaryl pentacyclic core were also radiolabeled with carbon-11 or fluorine-18, such as diarylfuranone [^{11}C]**12** ([^{11}C]Rofecoxib, IC_{50} COX-2 = 18 nM; IC_{50} COX-2 > 50 μM),[133, 139, 140] diarylimidazole [^{11}C]**13** (IC_{50} COX-2 = 4 nM; IC_{50} COX-2 > 10 μM) and [^{11}C]**14** (IC_{50} COX-2 = 5 nM; IC_{50} COX-1 = 3.3 μM),[141] diarylindole [^{11}C]**15** (IC_{50} COX-2 = 0.006 nM; IC_{50} COX-1 > 10 μM),[141] diaylcyclopentene [^{11}C]**16**

(IC_{50} COX-2 = 5 nM; IC_{50} COX-1 = 9.9 μM),[142] diarylindazole [^{18}F]**17** (IC_{50} COX-2 = 0.4 μM; IC_{50} COX-1 > 30 μM),[143] as well as diarylisoxazole [^{18}F]**18** (IC_{50} COX-2 = 2 nM; IC_{50} COX-1 > 100 μM),[144] [^{11}C]**19** ([^{11}C]TMI, IC_{50} COX-2 < 1 nM; IC_{50} COX-1 ≥ 500 μM),[145] and [^{11}C]**20** ([^{11}C]MOV, IC_{50} value not available).[146] However, almost all these ligands failed in preclinical studies due to limited brain uptake and/or lack of specific signal. Remarkably, [^{11}C]TMI exhibited favourable brain uptake, heterogeneous distribution (SUV_{max} = 2-5 in various brain regions), 20–30% displaceable binding by the COX-2 inhibitor meloxicam and excellent metabolic stability in baboons. Strenuous efforts have rendered the discovery of two promising COX-2 ligands: [^{18}F]**21** ([^{18}F]Pyricoxib, IC_{50} COX-2 = 40 nM; IC_{50} COX-1 = 8 μM)[147] with a diaryl heterohexacyclic core and its analogue, [^{11}C]**22** ([^{11}C]MC1, IC_{50} COX-2 = 1 nM; IC_{50} COX-1 > 1 μM).[148–152] More recently, two ^{18}F-labeled analogues of MC1 were also reported ([^{18}F]**23** and [^{18}F]**24**), albeit without in vivo evaluation.[150] Although [^{18}F]Pyricoxib entered mouse brains (1.74 %ID/g at 60 min p.i.), no specific signal was demonstrated under healthy conditions as suggested by an even higher radioactivity accumulation in the brain (3.79 % ID/g at 60 min p.i.) under Celecoxib-pretreatment conditions. However, in COX-2 expressing HCA-7 mouse xenografts, specific binding was confirmed. Similar to [^{18}F]Pyricoxib, [^{11}C]MC1 did not reveal any binding specificity in most organs of NHPs including the brain under normal conditions, despite high brain uptake (SUV_{max} = 2.9 at 2 min p.i.). In contrast, in the LPS-treated putamen of monkeys, [^{11}C]MC1 exhibited a significantly increased radioactivity accumulation (41%) compared to the healthy control.[67] These results suggested that the lack of specific binding in the brain for almost all COX-2 PET probes might be attributed to the low expression levels of COX-2. More importantly, [^{11}C]MC1 could also enable the diagnosis of patients with rheumatoid arthritis, a kind of peripheral inflammatory disorder, which exhibited increased COX-2 binding in inflamed joints of patients compared with that of healthy control. The binding specificity of [^{11}C]MC1 towards COX-2 was further validated by the blocking effect in a pretreatment experiment with a COX-2 inhibitor celecoxib. Considering the fact that COX-2 expression can be induced by neuroinflammation, COX-2 may be of more interest for neuroinflammation imaging compared with COX-1 and more efforts need to be devoted to improve binding specificity of COX-2 PET probes.

2. PET probes for reactive oxygen species (ROS)

ROS is a class of highly reactive molecules, which is generated through electron introduction to oxygen in a diversity of enzymatic processes and chemical reactions and includes superoxide anion ($O_2^{\bullet -}$), hydroxyl radical ($^{\bullet}OH$) and other radicals.[153] ROS is responsible for oxidative stress and expression of some ROS is vital for various physiological processes, including cell survival, proliferation, differentiation, and apoptosis.[154] Generally, the ROS level is low due to instant anti-oxidant regulation.[68] Following an inflammatory insult, microglial cells are activated into the proinflammatory M1 isoform to evoke a fast elevation of the ROS level, which would further upregulate the activated M1 phenotype. In some cases, this is a beneficial acute cellular response to eliminate the inflammatory insult, however, sustained microglial activation and persistent ROS generation might contribute to tissue injury in chronic neuroinflammation and

neurodegenerative disorders. It has been demonstrated that the cerebral ROS level is prone to increase with age, which possibly coincides with the elevated MAO-B activity.[155] In addition, overexpression of ROS was observed in diverse AD cellular and animal models as well as AD patients.[156] In PD, increased ROS levels are also deemed as a contributor to the degeneration of dopaminergic neurons.[157] Therefore, PET imaging of ROS may serve as a promising strategy for in vivo mapping of neuroinflammation in neurodegenerative diseases.

To this end, [^{11}C]**25** ([^{11}C]ascorbic acid, also known as [^{11}C]vitamin C) was developed as a ROS PET probe, which can be readily oxidized by ROS to form [^{11}C]dehydroascorbic acid (DHA) and has demonstrated an increased radioactivity uptake in several cellular models with either exogenous or endogenous ROS generation, such as U87 glioma cells, human HL60 promeylocyctic leukemia cells and neutrophils (Figure 4A).[158] However, since [^{11}C]ascorbic acid is not capable of penetrating the BBB, no further evaluation was pursued. Recently, [^{11}C]**26** ([^{11}C]HM) and its deuterated isotopolog [^{11}C]**27** ([^{11}C]HM-D) were reported as promising ROS PET probes.[69] Herein [^{11}C]HM was selectively oxidized by superoxide anion to generate a charged species [^{11}C]**32** ([^{11}C]ox-HM), which was then trapped in tissues as an imaging agent (Figure 4B). Preliminary evaluation of [^{11}C]HM and [^{11}C]HM-D in rat brains revealed fast radioactivity uptake and SUV plateaus of 1.8 and 1.65 at 2 min p.i., respectively. After initial high uptake, a rapid clearance was observed for both probes with the SUV declining to 0.22 and 0.13 at 40 min p.i., respectively. The latter provided a low background for accurate detection of increased ROS levels under diseased conditions. Moreover, ex vivo autoradiography and in vivo PET imaging both indicated a significantly increased [^{11}C]HM uptake in the cerebral hemisphere that was treated with sodium nitroprusside (SNP), a reagent that prompted ROS production by blocking the oxidative phosphorylation. Three ^{18}F-labeled analogs of [^{11}C]HM were also reported, namely [^{18}F]**28** ([^{18}F]FDMT),[159] [^{18}F]**29** ([^{18}F]ROStrace),[70] and [^{18}F]**30** ([^{18}F]FDHM).[71] While [^{18}F]FDMT failed to penetrate the BBB of mice, rendering it impossible to map the increased ROS levels in neuroinflammation, both [^{18}F]ROStrace and [^{18}F]FDHM exhibited high initial uptake in mouse brains with the uptake up to ca. 10 %ID/cm^{-3} and ca. 2.3 SUV, respectively. Furthermore, in LPS-treated mice exhibiting neuroinflammation, [^{18}F]ROStrace revealed an approximately 150% increased brain uptake compared to the control group. Similar to [^{11}C]HM, [^{18}F]FDHM also exhibited higher uptake in the SNP-treated cerebral hemisphere compared with the contralateral side. [^{11}C]**31** ([^{11}C]DHQ1) is another promising PET probe for in vivo imaging of ROS, which readily entered the mouse brains (ca. 3.5 SUV at 3 min p.i.) with its oxidative product generated from the reaction with ROS trapped in the brain.[72] Pretreatment with apocyanin, a NOX2 inhibitor capable of regulating the brain redox status, led to a faster elimination of radioactivity from the brain, which indicated that the oxidation of [^{11}C]DHQ1 to *N*-methylquninolinium species, a kind of trapping mechanism, was inhibited. Despite favorable in vivo characteristics, further studies need to be performed to validate and quantify the oxidized forms of these probes as well as the changes of ROS levels in neuroinflammation.

3. PET probes for cannabinoid type 2 receptor (CB2R)

Notwithstanding the relatively low physiological levels of cannabinoid type 2 receptor (CB2R) in the CNS, studies have shown that neuroinflammation is accompanied by CB2R

upregulation on activated microglia that infiltrate the brain and spinal cord.[73, 160, 161] Notably, CB2R activation was linked to protective anti-inflammatory effects, thus channeling the development of various CB2 agonists for CNS-related and peripheral pathologies.[162] Indeed, the CB2R is considered a promising target for the management of neuroinflammatory disorders such as AD,[163] MS, PD and ALS.[164] Along this line, CB2R agonists were found to reduce pro-inflammatory cytokine release and the migration of immune cells.[165, 166] In contrast to cannabinoid type 1 receptor (CB1R)-targeted pharmacotherapy, however, CB2R agonists lack psychoactive side effects due to the relatively low abundancy of CB2R in the healthy CNS.[167, 168] In addition to the various drug development programs, CB2R has been suggested as a biomarker for neuroinflammation. As such, the development of CB2R-targeted PET probes for *in vivo* receptor quantification is currently ongoing. Nonetheless, despite considerable efforts, CB2R-targeted PET radioligand development has only yielded marginal progress in the past several years. In particular, previously reported radioligands were plagued by high nonspecific binding, limited brain uptake, rapid extensive metabolism and poor selectivity over CB1R. Although the vast majority of probes did not meet their expectations during in vivo studies, some of the examples presented below harbor potential for successful clinical translation. A summary of selected CB2R PET radioligands is provided in Figure 5.

Thiazole derivatives **33** (A-836339) and **34** have been initially discovered as highly potent and selective CB2R agonists. Indeed, A-836339 exhibited a subnanomolar binding affinity for CB2R (K_i = 0.7 nM) and high selectivity over CB1R (K_i = 270 nM).[74] The carbon-11 labeled version, [^{11}C]**33** ([^{11}C]A-836339), was obtained from the respective desmethyl precursor. PET imaging experiments revealed a significantly increased brain uptake in LPS-treated CD1 mice (SUV_{max} = 2.3), as compared to control animals (SUV_{max} = 0.5).[74] Similarly, in the APP/PS1 mouse model of Alzheimer's disease, an enhanced brain uptake was observed in the AD group, as compared to wild-type animals.[74] Encouraged by these findings, Moldovan et al. developed a radiofluorinated analog, [^{18}F]**34**, with improved potency (*K*i CB2R = 0.4 nM) and selectivity (*K*i CB1R = 380 nM).[169] However, [^{18}F]**34** was plagued by metabolic instability, as well as the presence of radiometabolites in the brain.[169] While further reports on a suitable radiofluorinated analog of [^{11}C]A-836339 are pending, Savonenko et al. investigated the utility of [^{11}C]A-836339 as a PET biomarker for neuroinflammation in a mouse model of Aβ amyloidosis.[170] Similar to the observations in APP/PS1 animals, the authors found an increased tracer uptake in Aβ amyloidosis mice, which was significantly reduced by co-administration of non-radioactive CB2R ligand AM630. Conversely, in two distinct rodent models of cerebral ischemia (involving LPS or AMPA treatment), [^{11}C]A-836339 failed to monitor the changes of CB2R expression by PET imaging.[171]

Oxoquinolines have served as a structural basis for the development of a series of CB2R PET radioligands. Indeed, the most extensively studied oxoquinoline-based probe, [^{11}C]**35** ([^{11}C]NE40), has been translated into the clinic.[172] The synthesis of [^{11}C]NE40 was accomplished by ^{11}C-methylation of the respective phenolic precursor with either [^{11}C]CH_3I or [^{11}C]methyl triflate.[173, 174] NE40 exhibited a binding affinity of 9.6 nM (K_i CB2R) and a selectivity factor (preference for CB2R over CB1R) of ~ 100. Furthermore, [^{11}C]NE40

proved to be CB2R specific in the rodent spleen, an organ that inherently contains high number of CB2R expressing immune cells, while showing a fast washout from the CB2R-deficient healthy rodent brain.[174] In contrast, CB2R specific binding of [^{11}C]NE40 was observed in the brain of rats that underwent stereotactic injection of an adeno-associated viral vector (AAV2/7) encoding for hCB2R in the right striatum, and therefore displayed local hCB$_2$R overexpression.[75] Evens et al. further reported a moderate initial tracer uptake in the rhesus monkey brain (SUV_{max} = 1.5), thus indicating that [^{11}C]NE40 is able to penetrate the BBB. Nonetheless, when translated into the clinic, [^{11}C]NE40 PET did not show the anticipated CB2R upregulation in the brains of AD patients. Similarly, there was no relationship between [^{11}C]NE40 brain uptake on PET and regional or global amyloid load.[175] While the authors stated that the attenuated uptake in AD patients may have been attributed to neuronal degeneration, concerns have also been raised about the suitability of this probe for CB2R-targeted PET imaging in AD.[175] Indeed, considering the high baseline expression of CB1R in the CNS, a high selectivity factor is required to prevent off-target binding to the CB1R.

Slavik et al. synthesized a series of novel 4-oxoquinoline derivatives based on the structure of KD2, a CB2 ligand that exhibited a K_i of 1.7 nM for CB2R.[176, 177] Upon structure-activity relationship (SAR) studies, compound **36** (RS-016) exhibited the most favorable in vitro performance characteristics, thereby showing an improved affinity (K_i = 0.7 nM) and lipophilicity (Log$D_{7.4}$ = 2.8), as compared to KD2.[178] Moreover, in a mouse model of LPS-induced neuroinflammation, PET scans with [^{11}C]**36** ([^{11}C]RS-016) revealed higher CB2R expression levels in different brain regions of LPS-treated animals including the hippocampus, cortex and cerebellum. [^{11}C]RS-016 was further employed for the detection of atherosclerosis, whereby the probe was successfully employed to visualize the CB2R in vivo in rodent and in vitro in human atherosclerotic lesions.[178] Subsequently, a radiofluorinated analog of [^{11}C]RS-016 was developed, namely, [^{18}F]**37** ([^{18}F]RS-126).[179] Despite the encouraging *in vitro* results obtained with [^{18}F]RS-126, including high CB2R specificity on autoradiograms of the rodent spleen, no specific binding was detected in the brain of LPS-treated mice with [^{18}F]RS-126. Similarly, [^{18}F]RS-126 did not detect CB2R overexpression in transgenic R6/2 HD mice, despite evident CB2R mRNA upregulation.[180] In addition, given the relatively high nonspecific binding, [^{18}F]RS-126 did not exhibit any CB2 specificity by autoradiography using human post-mortem ALS spinal cord tissue. Conversely, a close derivative of [^{11}C]RS-016 bearing an additional hydroxyl group, [^{11}C]**38** ([^{11}C]RS-028) exhibited less nonspecific binding and allowed the visualization of CB2R upregulation in autoradiograms of post-mortem human ALS spinal cord sections. Unfortunately, the application of [^{11}C]RS-028 was limited by a rapid washout from CB2-rich organs such as the spleen, thus resulting in poor in vivo specificity. The authors suggested that [^{11}C]RS-028 may suffer from rapid enzymatic degradation. As such, to assess the influence of the O-alkyl chain length and oxygen position on metabolic fate, [^{18}F]**39** ([^{18}F]AH-040) and [^{18}F]**40** ([^{18}F]AH-043) were designed and synthesized. Despite their improved metabolic stability, the selectivity of [^{18}F]AH-040 and [^{18}F]AH-043 towards CB2R over the CB1R was significantly reduced. Given that a high selectivity over CB1R is crucial for successful CNS-targeted visualization of CB2R, the reduced selectivity hampered the further evaluation of [^{18}F]AH-040 and [^{18}F]AH-043.[180]

Although some thiophene-based derivatives, such as **41** (AAT-015, Ki CB2R = 3.3 ± 0.5 nM, Ki CB1R = 1.0 ± 0.2 μM) and AAT-778 (Ki CB2R = 4.3 ± 0.7 nM, Ki CB1R = 1.1 ± 0.1 μM), showed promising pharmacology data, the corresponding radiolabeled analogues did not achieve any specific binding – neither by *in vitro* autoradiography nor by PET imaging.[179] Accordingly, this class of compounds was deemed unsuitable for CB2R-targeted PET imaging. Another class of reported CB2R ligands constitutes the potent *N*-arylamide oxadiazole derivatives, **42** (MA2) and **43** (MA3).[181] The radioligands, [^{11}C]**42** ([^{11}C]MA2) and [^{18}F]**43** ([^{18}F]MA3) revealed high brain uptake in PET experiments. While specific accumulation of [^{18}F]MA3 was observed in brain regions overexpressing human CB2R in rodents, no CB2R specificity was evident in PET experiments with [^{18}F]MA3 in nonhuman primates.[182] Another structural scaffold, that is based on a triazine core, has been exploited for the purpose of CB2R PET radioligand development.[183] As such, a deuterated high-affinity CB2R ligand, [^{18}F]**44**, was found to readily cross the BBB in baboons and rhesus macaques. In another study, [^{18}F]**45** was selected as the compound with the most ideal in vitro performance characteristics, however, [^{18}F]**45**-based PET imaging was plagued by rapid metabolism and elimination, prompting the termination of its further development as a CB2R PET radioligand.[184]

To date, 2,5,6-trisubstituted pyridines constitute the most promising class of CB2R PET radioligands for clinical translation. While initial PET experiments with [^{11}C]**46** ([^{11}C]RSR-056) revealed a substantial increase in brain uptake following LPS-induced treatment in rodents, it is worthwhile mentioning that the increased [^{11}C]RSR-056 accumulation in the brain was only in part attributed to CB2R binding. The latter was evident from the relatively weak signal reduction under blockade conditions, which did not reduce the signal to baseline levels observed in control animals.[185] It has been suggested that neuroinflammation may have resulted in partial damage of the BBB, leading to an enhanced CNS penetration of the tracer in LPS treated animals.[186] In a subsequent study, the same authors designed a series of fluorinated derivatives by introducing structural diversity at positions 2 and 5 of the pyridine ring. Indeed, these efforts resulted in the discovery of the radiofluorinated analog, [^{18}F]**47**, with a binding affinity of 6 nM, a prolonged physical half-life of 109.8 min as well as a selectivity index of ~ 600 over CB1R.[187] By in vitro autoradiography studies on rodent spleen sections, [^{18}F]**47** proved to be CB2R-specific. Further, [^{18}F]**47** was sensitive to the CB2R receptor upregulation in ALS postmortem spinal cord tissues. Despite these encouraging *in vitro* findings, [^{18}F]**47** showed only limited *in vivo* specificity for the CB2R-rich rodent spleen. To address this issue, the influence of structural modifications at position 6 of the pyridine ring was assessed, ultimately prompting the discovery of [^{18}F]**48** ([^{18}F]RoSMA-18), a pyridine derivative with outstanding target affinity (Ki hCB2R = 0.7 nM) and selectivity (>12,000) over CB1R across different species.[76] Indeed, [^{18}F]RoSMA-18 showed excellent specificities for the CB2R-positive spleen tissue by *in vitro* autoradiography as well as by PET imaging and *ex vivo* biodistribution in rodents. Further, [^{18}F]RoSMA-18 was successfully employed to detect CB2R upregulation in human ALS spinal cord tissue. While the high selectivity and specificity of [^{18}F]RoSMA-18 was confirmed in CB2R knockout mice, PET experiments in Wistar rats corroborated the specific and reversible CB2R binding in the CB2-positive spleen. Although only intact tracer was detected in the

rat brain upon intravenous injection of [^{18}F]RoSMA-18, *in vivo* defluorination was evident by the considerable amount of skull and spinal radioactivity uptake, which was not reduced under blockade conditions. Notably, substitution of the hydrogen atoms in the fluoropropyl side chain with deuterium atoms afforded [^{18}F]**49** ([^{18}F]RoSMA-18-d$_6$**)**, in which case no defluorination and radioactivity accumulation in the skull was observed.[76] Given the outstanding performance characteristics, [^{18}F]RoSMA-18-d$_6$ is currently considered a promising candidate for clinical translation.

4. PET probes for monoamine oxidase B (MAO-B)

Monoamine oxidase (MAO) is a flavoenzyme mainly residing in the outer mitochondrial membrane.[188–191] MAO is predominantly responsible for the oxidative deamination of a number of monoamine neurotransmitters with concomitant release of ROS, which may contribute to the generation of oxidative stress and neuroinflammation.[192] MAO can be divided into two isoforms, namely MAO-A and MAO-B. Despite a certain degree (ca. 70%) of amino acid sequence identity, MAO-A and MAO-B exhibit different distributions, substrates and clinical implications. While MAO-A is primarily located in catecholaminergic neurons and preferentially degrades 5-hydroxytryptamine (5-HT) in human brain, MAO-B, as the major enzyme responsible for dopamine metabolism in human CNS, has higher expression in glial cells as well as histaminergic and serotonergic neurons.[77] For clinical applications, MAO-A deficiency is involved in aggression and its inhibitors could serve to treat mood and depression disorders,[193–197] whereas MAO-B inhibitors, such as rasagiline and selegiline (deprenyl), are generally used as neuroprotective drugs for PD, a dopamine-deficiency disease,[198–203] as well as AD.[204, 205] In this review, we particularly focus on the recent development of MAO-B targeted PET ligands attributed to the involvement of MAO-B in astroglial cells in the neuroinflammation and neurodegenerative diseases. It has been demonstrated that high levels of MAO-B, but not MAO-A, are expressed in astrocytes, and particularly in reactive astrocytes, suggesting the potential usefulness of MAO-B PET probes for in vivo astrogliosis imaging.[206] Moreover, increased MAO-B expression in astrocytes might contribute to the parkinsonian pathologies and exacerbate the degenerative process, implicating that inhibition of MAO-B function likely provides protection from harmful activation of astrocytes as well as neuroinflammation and neurodegenerative diseases.

In the development of MAO-B-specific PET ligands, a promising irreversible radioligand [^{11}C]**50** ([^{11}C]*L*-deprenyl, K_i = 0.97 μM)[207] was developed for human studies, which demonstrated high brain uptake and binding specificity in both mice[208] and humans (Figure 6).[78] By in vitro autoradiography studies, a remarkably increased binding of [^{11}C]*L*-deprenyl was observed in the temporal lobe and white matter of AD patient tissues, as compared with healthy controls.[209] The accumulated radioactivity could be efficiently blocked by the MAO-B inhibitor rasagiline, but not by the MAO-A inhibitor, pirlindole. A ^{18}F-labeled analog of *L*-deprenyl ([^{18}F]**52** ([^{18}F]fluorodeprenyl)) was also developed, and demonstrated high brain uptake (ca. 6.0 SUV), heterogeneous distribution pattern and specific binding in cynomolgus monkeys.[210] In addition, the limitation regarding the quantification of MAO-B activity with irreversible PET probes could be partially addressed by use of α-deuterium substituted radioligands, leading to the development of

[^{11}C]**51** ([^{11}C]*L*-deprenyl-D_2) and [^{18}F]**53** ([^{18}F]fluorodeprenyl-D_2), which attenuated the reaction rate between the radioligand and MAO-B, thus enabling the calculation of net blood-brain washout for *L*-deprenyl.[211, 212] So far, [^{11}C]*L*-deprenyl-D_2 has demonstrated its usefulness in assessing the MAO-B occupancy for a specific drug in human brains[213] and indicated a decrease of MAO-B density in brains of tobacco smokers.[214, 215] Moreover, several applications of [^{11}C]*L*-deprenyl-D_2 have also been validated in patients. While in patients with temporal lobe epilepsy, [^{11}C]*L*-deprenyl-D_2 exhibited significantly higher binding within the epileptogenic lobe, compared with the contralateral loci,[216–218] in patients with AD or mild cognitive impairment, [^{11}C]*L*-deprenyl-D_2 enabled the assessment of astrocytosis levels, which is positively correlated with Aβ deposition and negatively correlated with decreased gray matter density.[219, 220] Another irreversible MAO-B PET probe, [^{18}F]**54** ([^{18}F]fluororasagiline)[221], and its isotopologue, [^{18}F]**55** ([^{18}F]fluororasagiline-D_2)[222], were also shown to provide good uptake in NHP brains (ca. 2.5 SUV). However, the BBB penetration of radiometabolites of these irreversible MAO-B PET probes rendered in vivo quantification challenging.[223]

Compared with irreversible PET probes, reversible variants might provide advantages with regard to in vivo quantification. In this scenario, the potent reversible MAO-B inhibitor Ro-19-6327 (IC_{50} = 20 nM) was radiolabeled for studies in humans, leading to the formation of [^{123}I]**56** ([^{123}I]Ro-43-0463) and [^{18}F]**57** ([^{18}F]Ro-43-0463).[224, 225] While [^{123}I]Ro-43-0463 demonstrated good in vivo characteristics for SPECT imaging, only limited brain radioactivity accumulation was observed for [^{18}F]Ro-43-0463, which is possibly attributed to its lower lipophilicity. A more promising reversible MAO-B PET probe, [^{11}C]**58** ([^{11}C]MD230254), was synthesized with [^{11}C]phosgene, which revealed high binding affinity (IC_{50} = 4 nM) and ca. 70% specific binding in NHP brains.[79] The ^{18}F-labeled analogue of MD230254 was also reported ([^{18}F]**59** ([^{18}F]FBPO)), but was hampered for further application by in vivo defluorination.[226] Another reversible radioligand, [^{11}C]**60** ([^{11}C]SL25.1188), with high binding affinity (K_i = 2.9 nM for human MAO-B) was afforded by use of a novel [^{11}C]CO_2 fixation strategy, which could partially overcome the production site restriction with [^{11}C]phosgene.[227] Preclinical evaluation of [^{11}C]SL25.1188 in NHP indicated good BBB penetration with the highest radioactivity accumulated in striatum (V_T = 10.3) and thalamus (V_T = 10.9).[228] Moreover, high in vivo metabolic stability and good specific binding (55-70% of total radioactivity) were corroborated in NHP brains. More importantly, [^{11}C]SL25.1188 is the first reversible MAO-B PET probe validated for human use.[80] Ongoing exploration has led to the development of ^{18}F-labeled analogue [^{18}F]**61**.[229] However, reduced binding affinity and selectivity, fast kinetics, and in vivo defluorination impeded its further application. Most recently, a promising ^{18}F-labeled reversible MAO-B PET probe [^{18}F]**62** ([^{18}F]SMBT-1) was developed with high in vitro binding affinity (K_d = 3.7 nM) and selectivity.[230] Notably, [^{18}F]SMBT-1 is a repurposing of the first generation tau ligand scaffold based on [^{18}F]THK-5351, which was found to be non-selective against MAO-B.[231] Autoradiography studies of [^{18}F]SMBT-1 demonstrated higher radioactivity levels in AD brain sections compared with that in the normal control, and the radioactivity could be completely displaced by the MAO-B inhibitor lazabemide, indicating higher specific binding of [^{18}F]SMBT-1 to MAO-B in AD brains. Further biodistribution studies revealed a high initial uptake (7.85 %ID/g at 2 min p.i.), rapid washout (0.20 %ID/g at

60 min p.i.), and no radiometabolites in normal mouse brains. These promising results provoked the translation of [^{18}F]SMBT-1 into first-in-human studies, wherein [^{18}F]SMBT-1 demonstrated robust and reversible binding to MAO-B.[81] Pretreatment with the selective MAO-B inhibitor *L*-deprenyl resulted in 85% diminished radioactivity, indicating high selectivity of [^{18}F]SMBT-1 to MAO-B. All these results suggest that [^{18}F]SMBT-1 warrants more evaluations under normal and disease conditions in preclinical and clinical trials.

4.2 Alternative approach for the mapping of MAO activity

The utilization of metabolic trapping is an alternative approach for the in vivo mapping of MAO activity. In this scenario, the radiotracer is selectively oxidized or deaminated by brain MAO to generate a more polar and/or charged radiometabolite, which could not pass the biological membranes, including the BBB, and is thus trapped in the brain as an imaging agent. On the other hand, the unmetabolized radiotracer will be rapidly eliminated from the brain. To this end, [^{11}C]**50** ([^{11}C]MPTP) was first synthesized and evaluated in baboons as a metabolic trapping agent for MAO-B (Figure 7).[232] The radioactivity accumulated in baboon striatum and substantia nigra was attributed to trapping of in situ generated pyridinium radiometabolite [^{11}C]MPP^{+}, which could be decreased by the MAO-B inhibitor tranylcypromine. Then [^{11}C]**64** ([^{11}C]DMPEA) was developed for MAO-B PET imaging with [^{11}C]dimethylammonium as the trapped radiometabolite.[233] In mice, [^{11}C]DMPEA readily penetrated the BBB, reached a plateau of 7.9 %ID/g in the brain at 1 min p.i., and decreased to 2.8 %ID/g at 60 min. Of note, the radioactivity in mouse brains was significantly reduced by pretreatment with the MAO-B inhibitor *L*-deprenyl, whereas no obvious influence was detected with the MAO-A inhibitor clorgyline, indicating specificity and selectivity of [^{11}C]DMPEA towards MAO-B. When translated to human use, [^{11}C]DMPEA also demonstrated good BBB penetrating ability with gradually increased radioactivity accumulation in the brain. The different elimination pattern of [^{11}C]DMPEA in mice and humans were attributed to a much slower elimination rate of unmetabolized [^{11}C]DMPEA in human brain. Recently, [^{11}C]**65** ([^{11}C]PHXY) and [^{11}C]**66** ([^{11}C]COU) were also disclosed as promising metabolic trapping agents for MAO.[234] Although in rat brain, both probes failed to demonstrate any selectivity between MAO-A and MAO-B, in NHP brains, [^{11}C]PHXY exhibited good specificity to MAO-A, whereas [^{11}C]COU exhibited more sensitivity to MAO-B inhibition.

5. PET probes for sphingosine-1-phosphate receptor (S1PR)

Sphingosine 1-phosphate receptor (S1PR) is a family of G-protein-coupled receptors with five subtypes (S1PR1-5).[235–238] The S1PR employs several mechanisms by directly interacting with its substrates and modulates extracellular signaling pathways and functions involved with cyclic adenosine monophosphate, protein kinase B, mitogen-activated protein kinase, protein kinase C, and phospholipase D.[239, 240] Regulation of S1PR is essential in both physiological and pathological states, particularly in immune systems, cardiovascular and CNS.

5.1 PET probes for sphingosine-1-phosphate receptor subtype 1 (S1PR1)

S1PR1, the primary receptor, is widely expressed in neurons and glia in the CNS[241] and plays an important role in anti-inflammatory processes and neuroprotection.[82, 242, 243] The expression and activity of S1PR1 is maintained in a balance between the synthesis by sphingosine kinase-1 (SphK1) and degradation by sphingosine 1-phosphate lyase (SPL). Delisle[244] demonstrated that the activity of SphK1 could be reduced, whereas the expression of SPL was increased by Aβ peptides, which finally led to a significant decrease of S1PR1 in AD patients' frontal cortex as well as the hippocampus. Besides the loss of the neuroprotective function in AD pathogenesis, S1PR1 over-activity was also reported to be involved in PD. The evidence showed that α-Synuclein, associated with PD progression, caused the expulsion of S1PR1 from neurons and led to impaired inhibitory G-protein signaling.[245] Additionally, the mRNA level of S1PR1 was also observed as decreased in the brain of experimental PD and AD models[246]. Studies in mice models also revealed the participation of S1PR1 in the progress of multiple sclerosis (MS) and EAE.[247, 248] More importantly, the neuroinflammation could be attenuated by S1PR1 deletion or activity inhibition in mice.[249] All these evidence suggested S1PR1 within the CNS as target for neuroinflammation and neurodegenerative diseases.

As a potential therapeutic target for the treatment of neuroinflammation and neurodegenerative diseases, S1PR1-specific imaging would help understanding the pathophysiology of S1PR1 in the CNS[250–252]. However, the development of S1PR1 imaging agents suitable for clinical studies is still a challenge. The primary effort to develop S1PR1 PET tracers was focused on radiolabeling of the derivative of fingolimod (FTY720, IC_{50} = 603.75 nM), which is an oral immunomodulatory drug approved by the US Food and Drug Administration (FDA) in 2010 for treating the relapsing form of multiple sclerosis (Gilenya®) and chronic inflammatory demyelinating polyneuropathy.[253, 254] The iodinated analogue of FTY720, **67** (BZM055), showed similar pharmacokinetic properties and was first labeled with iodine-123 for SPECT imaging ([^{123}I]**67** (Figure 8).[255] However, the low phosphorylation rate (9%) by SphK2, limited brain penetrating capability, and a fast clearance rate prevented its translation into clinical investigations. Further radiolabeling of FTY720 derivatives rendered two S1PR1 radioligands [^{18}F]**68** and [^{18}F]**69**.[256] In the spleen typically containing S1PR1 positive immune cells, both [^{18}F]**69** and [^{18}F]**69** demonstrated high radioactivity levels, which amounted to 7% ID/mL at 10 min p.i. and 7.8% ID/mL at 30 min p.i., respectively. Unfortunately, the biodistribution studies of [^{18}F]**69** and [^{18}F]**69** revealed fast kinetics in mice and it is also unclear how rapidly and efficiently these two FTY720 derived radioligands undergo phosphorylation. All these factors mentioned above rendered them less suitable tracers for in vivo imaging studies.

Considering the required phosphorylation step for FTY720 derivatives, a novel S1PR1 PET probe [^{18}F]**70** was developed and tested in vivo, which is an analogue of the S1PR1 ligand W146 (Ki = 4.1 nM) and does not require the phosphorylation step for binding.[257] Although [^{18}F]**70** revealed favorable mouse brain uptake (8 %ID/cm^3 p.i. at 2 min) and good in vitro stability in mouse serum, the fast in vivo metabolic rate and defluorination impeded its application as a suitable PET imaging ligand.

The next generation of S1PR1 therapeutics and PET ligands mainly focused on compound **71** (TZ3321) with excellent binding potency (IC_{50} = 2.13 nM) and selectivity (> 450 fold) over S1PR2 and S1PR3. Preliminary biodistribution studies of radioligand [^{11}C]**71** ([^{11}C]TZ3321, also known as [^{11}C]CS1P1) in mice revealed favorable brain uptake (7 %ID/g at 60 min).[83, 258] As demonstrated by PET imaging and autoradiography studies, [^{11}C]TZ3321 revealed significantly higher uptake in EAE mouse models compared with the vehicle, which is consistent with higher S1PR1 expression levels in EAE. Subsequently, two S1PR1 PET ligands [^{18}F]**72** (IC_{50} = 2.63 nM) and [^{18}F]**73** (IC_{50} = 9.65 nM) based on an oxadiazole scaffold were explored.[259, 260] Evaluation of [^{18}F]**72** in the LPS-induced acute liver injury mouse models suggested that the high uptake of [^{18}F]**72** in the liver (SUV = 7 at 10 min p.i.) was associated with the S1PR1 expression. However, both [^{18}F]**72** and [^{18}F]**73** failed to penetrate the rat BBB with limited brain uptake of 0.027 and 0.46 %ID/g at 5 min p.i., respectively. More recently, four novel oxadiazole-derived radioligands with different hydroxyl alkyl tails were developed ([^{18}F]**74**-[^{18}F]**77**).[84] PET imaging studies in NHPs indicated high brain uptakes for radioligands [^{18}F]**74** (IC_{50} = 6.7 nM, SUV ≈ 3.8 at 4 min p.i.), [^{18}F]**75**(IC_{50} = 14 nM, SUV ≈ 3.2 at 5 min p.i) and [^{18}F]**77** (IC_{50} = 15.4 nM, SUV ≈ 2.5 at 4 min p.i.), whereas [^{18}F]**76** only revealed a minimum brain uptake of ~0.7 SUV. Motivated by these promising preclinical results and the fact that one S1PR1 PET probe [^{11}C]CS1P1 ([^{11}C]TZ3321) has been advanced into clinical trials,[261] more efforts are warranted to validate these ligands in preclinical disease models and clinical translation.

5.2 PET probes for sphingosine-1-phosphate receptor subtype 2 (S1PR2)

Among the five subtype receptors, S1PR2 plays a pivotal role in regulating blood brain barrier (BBB) functions in the CNS. S1PR2 is widely expressed in neuronal and vascular cells, and is essential for the growth of injured neurons and vascular systems. It was demonstrated that genetic deletion of S1PR2 promoted vascular repair and reduced neurological deficits in stroke mouse models.[262] Moreover, the increased expression of S1PR2 was observed in EAE mice and MS patients, and genetic deletion or pharmacological blockade of S1PR2 could reduce the severity of neuroinflammation.[263] Consequently, S1PR2 may serve as a promising imaging target for assessing the progress of neuroinflammation and related disorders. JTE-013 (IC_{50} = 68.5 nM) is a well-known S1PR2 selective antagonist,[264] and radiolabeling of its derivative led to the discovery of radioligand [^{11}C]**78** ([^{11}C]TZ34125), which revealed favorable binding affinity (IC_{50} = 9.52 ± 0.70 nM) and good selectivity over S1PR1 and S1PR3 (>100 fold) (Figure 8).[265] Despite limited brain uptake in mice due to interaction with P-gp, [^{11}C]TZ34125 was sensitive to sexual dimorphism of S1PR2 expression in SJL mice (SUV = 0.58 and 0.48, respectively in female and male mouse cerebellum at 30 min p.i.). Most recently, a ^{125}I-labeled ligand [^{123}I]**79** ([^{123}I]TZ6544) was disclosed with excellent binding affinity (K_d = 4.31 nM), high selectivity (>300 fold over S1PR1, S1PR3, S1PR4, and S1PR5), and binding specificity towards S1PR2.[266]

6. PET probes for purinergic receptors

Purinergic receptors constitute key elements of the CNS by mediating cellular neuroinflammatory responses and regulating functions of microglia, astrocytes and

neurons.[267] As such, purinergic receptors are broadly implicated in CNS disorders such as AD, ALS, PD, MS, HD, traumatic brain injury (TBI), cerebral ischemia, epilepsy, neuropathic pain and psychiatric disorders.[268–272] Depending on their endogenous ligands, purinergic receptors can be classified into either P1 (activated by adenosine) and P2 receptors (activated by extracellular nucleotides). P2 receptors are typically subdivided into P2X that are ATP-gated ion channels and P2Y metabotropic receptors that constitute G-protein–coupled receptors.[273] Following an insult of the brain, a rapid release of adenosine triphosphate (ATP) or uridine triphosphate (UTP) has been observed in damaged brain regions, ultimately triggering microglial activation.[272, 274–276] Given their implications in contemporary neuroinflammation imaging, this chapter focuses on recent advances in the development of probes for imaging P2X ligand-gated ion channel type 7 receptor (P2X7R) and purinergic metabotropic 12 receptor (P2Y12R).

P2X7R is involved in microglial activation, proliferation and apoptosis.[85] Of note, P2X7R encompasses one extracellular loop, bearing the ATP-binding site, two transmembrane domains as well as intracellular N- and C-terminal domains.[277] Under normal physiological conditions, P2X7R expression in the CNS is rather limited.[85, 278] However, following brain injury, the expression of P2X7R increases substantially, thereby promoting inflammasome formation as well as the release of proinflammatory cytokines/chemokines.[85, 273] Notably, long-lasting high extracellular ATP levels and excessive release of proinflammatory cytokines have been linked to neuroinflammation. Further, P2X7R overexpression was shown to promote microglial activation and proliferation in primary hippocampal cultures of rat brains.[279] Along this line of reasoning, P2X7R expression was significantly enhanced in various preclinical neuroinflammation models as well as in postmortem brain samples of AD patients.[280] Therefore, imaging P2X7R may offer a promising diagnostic and prognostic approach for neurodegenerative diseases.

A series of P2X7R ligands have been radiolabeled with either carbon-11 or fluorine-18 (Figure 9). [^{11}C]**80** ([^{11}C]JNJ-54173717, IC_{50} hP2X7R = 4.2 nM) is one of the first brain penetrant ^{11}C-labeled radioligands for P2X7R-targeted imaging.[281] Indeed, biodistribution experiments in rats unveiled that [^{11}C]JNJ-54173717 readily crossed the BBB. In the striatum of a rat model of hP2X7R overexpression, high tracer uptake was detected, whereby striatal tracer uptake was substantially reduced by pretreatment with a non-radioactive antagonist, JNJ-42253432, indicating hP2X7R-specific binding of [^{11}C]JNJ-54173717 in vivo. Further, [^{11}C]JNJ-54173717 exhibited considerable brain uptake in rhesus monkeys (SUV_{max} = ca. 3.2), suggesting that the probe is brain penetrant in NHPs and warrants clinical translation.[281] As such, the first-in-man study of [^{11}C]JNJ-54173717 has recently been reported, and demonstrated its utility in quantifying P2X7R expression in the CNS.[86] Given the encouraging results obtained with [^{11}C]JNJ-54173717, a radiofluorinated analog, [^{18}F]**81** ([^{18}F]JNJ-64413739, IC_{50} hP2X7R = 1.0 nM) was developed.[87] Indeed, PET imaging with [^{18}F]JNJ-64413739 in NHPs revealed high specificity for P2X7R. The latter was further corroborated by blocking experiments of [^{18}F]JNJ-64413739 in rodents, thus highlighting the utility of this probe to visualize P2X7R. Indeed, a dose-dependent inhibition of tracer binding with P2X7R antagonists was observed on rodent brain tissue as well as the human brain.[87, 282, 283] Although the overall promising characteristics

strongly support the further use of [^{18}F]JNJ-64413739 for imaging P2X7R in clinical neuroinflammation, the lack of a suitable brain reference region not expressing the target, which would allow the non-invasive assessment of P2X7 abundancy in different brain regions as well as the binding potential, precluded the exploitation of the full potential for kinetic modeling with this probe.[87] In contrast to [^{18}F]JNJ-64413739, attempts to develop a P2X7R-targeted PET radioligand based on the structure of A-740003 (IC_{50} hP2X7R = 40 nM) were unsuccessful.[284] In particular, biodistribution studies in healthy rats showed only traces of [^{11}C]**82** ([^{11}C]A-740003) in the brain, possibly owing to low BBB permeability. Similarly, a radiofluorinated derivative of A-804598 with reduced bulkiness, [^{18}F]**83** ([^{18}F]EFB, Ki hP2X7R = 2.9 nM), suffered from low brain uptake in vivo – despite exhibiting high in vitro affinities for human and rat P2X7R.[285] Given the implication of P2X7R in neuroinflammation, continuous research efforts prompted the development of another class of successful PET radioligands that were based on a benzamide core structure. The most extensively investigated candidate of this class was [^{11}C]**84** ([^{11}C]GSK1482160, IC_{50} hP2X7R = 3 nM).[88, 286, 287] Of note, biodistribution studies with [^{11}C]GSK1482160 showed enhanced radiotracer uptake in the brain of LPS-treated mice, as compared to control animals.[88] Pretreatment with non-radioactive GSK1482160 resulted in a significant reduction of brain uptake in LPS-treated mice. In a rodent EAE model, [^{11}C]GSK1482160 uptake in the CNS correlated with P2X7R-positive cell counts, number of activated microglia and overall disease severity.[287] Further, PET studies with [^{11}C]GSK1482160 showed homogeneous distribution in healthy NHP brains (SUV_{max} in NHP ca. 2.5).[287] Overall, these studies indicate that [^{11}C]GSK1482160 is a suitable PET radioligand to visualize P2X7R expression on activated microglia. A radiofluorinated analog of [^{11}C]GSK1482160, [^{18}F]**85** ([^{18}F]IUR-1601, IC_{50} P2X7R = 7.9 nM), was recently developed by Gao et al.[288] Although [^{18}F]IUR-1601 has been successfully evaluated in vitro, no in vivo data has been reported to date. PET studies with [^{11}C]**86** ([^{11}C]SMW139, IC_{50} hP2X7R = 24.5 nM), another ^{11}C-labeled P2X7R-targeted PET radioligand, were conducted in rats, with the peak SUV value of ca. 3.5. Of note, a 1.5-fold higher radioactivity uptake was observed in the right striatum of rats locally overexpressing hP2X7R (induced by striatal injection of adeno-associated viral (AAV) vector), as compared to the contralateral striatum, and this effect was successfully reversed by pretreatment of the animals with JNJ-4796556.[89, 289, 290] Although [^{11}C]SMW139 was not sensitive to P2X7R overexpression on postmortem brain tissues of AD patients,[289, 290] first-in-man studies as well as studies in MS patients have been recently reported, with promising initial findings that warrant further clinical evaluation of this novel probe.[89, 289, 290]

In contrast to P2X7R, P2Y12R is a metabotropic chemoreceptor that is primarily expressed in platelets within the circulatory system. In the CNS, P2Y12R is primarily localized on microglial cells.[291, 292] P2Y12R activation is triggered by adenosine diphosphate (ADP), with an EC_{50} of 60 nM.[293] Due to the key function of P2Y12R in promoting platelet aggregation, a number of P2Y12R antagonists are currently used to prevent thromboembolic events in clinical practice.[294] Further, given the established role in microglial chemotaxis and cytokine signaling, P2Y12R is an attractive diagnostic target, particularly, when exploited for non-invasive imaging modalities with high sensitivity such as PET.[278] In the healthy brain, P2Y12R expression is relatively high on M2-type microglia,[90] however,

P2Y12R expression was downregulated under neuroinflammatory conditions following LPS treatment.[90, 295] Similarly, P2Y12R expression was reduced in human postmortem AD brain tissues.[90] Although P2Y12R-targeted imaging is considered a promising approach to further elucidate the differential role of microglial subtypes, there is only one reported P2Y12R PET radioligand, [^{11}C]**87** (IC_{50} P2Y12 = 6 nM) to date (Figure 9).[296, 297] By in vitro autoradiography, [^{11}C]**87** was found to specifically bind to mouse brain tissue sections, as evidenced by blocking studies with ticagrelor, a P2Y12R antagonist.[91] Nonetheless, subsequent in vivo imaging experiments in rats indicated low metabolic stability of [^{11}C]**87** as well as limited brain uptake, potentially owing to Pgp efflux.[278] Despite the abovementioned challenges in P2Y12R-targeted PET tracer development, P2Y12R is one of few targets that seems to be selectively expressed on M2 microglia. Accordingly, there is a consensus that a suitable P2Y12R PET radioligand would substantially facilitate the classification of microglial cells, thereby potentially enabling non-invasive staging of neuroinflammatory conditions.

7. PET probes for colony stimulating factor 1 receptor (CSF1R)

Colony stimulating factor 1 receptor (CSF1R) is a cell-surface tyrosine kinase expressed in microglia and microphages.[298] CSF1R is a receptor for the cytokine CSF1 (colony stimulating factor 1) and is directly responsible for the survival, differentiation, and function of microglia and microphages. Emerging evidence has indicated a close association of CSF1R with neuroinflammation. For example, in brains with severe neuroinflammation such as AD, MS, hypoxic-ischemic encephalopathy (HIE) and glioblastomas, CSF1R levels were substantially upregulated, as evidenced by either animal models or post-mortem analysis of patient samples.[92, 299–306] Moreover, inhibition of CSF1R offered an attenuation of neuroinflammation and prevented the progression of these diseases. Therefore, CSF1R has emerged as an interesting PET imaging target for neuroinflammation.

Thus far, only a few PET probes have been disclosed for CSF1R. [^{18}F]**88** (IC_{50} = 169 nM) is the first reported CSF1R PET ligand,[307] derived from the orally bioactive CSF1R inhibitor GW2580 (IC_{50} = 0.47 μM with freshly isolated human monocytes) (Figure 10).[308] However, neither in vitro nor in vivo evaluation was provided. Subsequently, another CSF1R PET ligand, [^{11}C]**89** ([^{11}C]AZ683), was reported.[93] [^{11}C]AZ683 exhibited a high binding affinity (K_i = 8 nM, IC_{50} = 6 nM) and good selectivity for CSF1R (>250 fold over 95 other kinases). Preclinical evaluation of [^{11}C]AZ683 demonstrated some brain influx and retention in both rats (SUV_{max} = 0.5) and rhesus macaques (SUV_{max} = 1.1). Although the initial brain uptake of [^{11}C]AZ683 in NHPs was slightly higher than that in rats, it remains to be validated whether the uptake is suitable for distinguishing the PET signal differences between neuroinflammatory models and healthy controls. More recent work led to the development of [^{11}C]**90** ([^{11}C]CPPC) with higher binding affinity (IC_{50} = 0.8 nM).[94] Although [^{11}C]CPPC did not exhibit very high brain influx in healthy mice (ca. 0.6 SUV), the PET signal was significantly increased in LPS-treated AD (59% increased signal vs. control group), transgenic AD (31% increase vs. control group) and EAE (100% increase vs. control group) mouse models. These observations were consistent with the elevated expression levels of CSF1R in the neuroinflammatory mouse brains.[92, 299–306] In LPS-treated baboons, [^{11}C]CPPC revealed an even bigger increase in the brain uptake (120%

compared with controls). Postmortem autoradiography with [^{11}C]CPPC demonstrated a remarkable increase of tracer binding (75-99%) in brain sections of AD patients. Notably, the tracer binding could be partially blocked by several CSF1R inhibitors. Recently, [^{11}C]CPPC was further translated into imaging studies in rhesus monkeys with the peak SUV up to 2.4-4.6 in various brain regions.[309] Although these preliminary results are promising, a major issue with [^{11}C]CPPC is the low specific binding towards CSF1R. For example, in a microglia-depleted mouse model, only 14% reduction of the radioactivity was observed in the brain, while CSF1R-knockout mice indicated comparable brain uptake compared with healthy control animals. Soon after, considerable nonspecific binding of CPPC was further demonstrated with [^{3}H]**91** ([^{3}H]CPPC) in the CNS, as evidenced by low displacement of the radioactivity by CSF1R inhibitors PLX3397, PLX5622, and BLZ945 (15%, 16%, and 25%, respectively).[310] Most recently, a novel CSF1R PET probe [^{11}C]**92** ([^{11}C]GW2580) was disclosed, which exhibited improved sensitivity to capture inflammatory microgliosis compared with [^{11}C]CPPC.[309] Despite only with moderate binding affinity (IC_{50} = 470 nM), [^{11}C]GW2580 rapidly penetrated the BBB of mice and rhesus monkeys with the brain SUV up to 1.2 and 3.1, respectively. More importantly, remarkably increased radioactivity uptake was found in the lesioned striatum of LPS-treated mice and in the forebrains of $App^{NL\text{-}G\text{-}F/NL\text{-}G\text{-}F}$-knock-in mice, which was in agreement with the elevated CSF1R expression levels. Pretreatment with unlabeled GW2580 resulted in significantly reduced uptake in the whole brain and complete abolishment of the difference between LPS-treated striatum and non-treated counterpart. Accordingly, [^{11}C]GW2580 may represent a promising chemical phenotype for CSF1R, which may require more efforts in medicinal chemistry development to improve binding affinity and validation in the preclinical models.

8. Emerging biological targets in neuroinflammatory processes for PET ligand development

8.1 The receptor for advanced glycation end products (RAGE)

The receptor for advanced glycation end products (RAGE), which was named after its initially identified ligands, AGEs (advanced glycation end products), belongs to the immunoglobulin receptor superfamily.[95] Recent studies have demonstrated that RAGE plays an important role in various neurodegenerative diseases, including AD, MS, stroke, and ALS.[311] Under healthy conditions, the expression levels of RAGE are low in almost all organs except the liver. However, in acute and chronic inflammatory disorders, RAGE expression levels are significantly upregulated.[95] In humans, RAGE exists in two isoforms, namely membrane-bound full length RAGE (flRAGE) and soluble RAGE (sRAGE).[311] In particular, sRAGE keeps the extracellular ligand-binding region, which can capture endogenous RAGE ligands and offer a remarkable blockade of their binding to flRAGE, thus relieving cellular inflammation and stress mediated by uncontrolled RAGE activity. Therefore, sRAGE may serve as a potential therapeutic and predictive imaging target for disease protection. [^{18}F]**93** ([^{18}F]RAGER), which is based on the RAGE inhibitor FPS-ZM1, is the first RAGE PET ligand with good in vitro binding affinity (K_d = 15 nM) and sufficient binding potential (B_{max}/K_d = 2) (Figure 11).[96, 312] Although [^{18}F]RAGER exhibited an in vitro off-target binding to the human melatonin MT1 receptor (K_i = 90

nM),[313] in vivo PET imaging studies demonstrated specific binding of [^{18}F]RAGER to RAGE in both rats and NHPs, which warrants further evaluations to probe the selectivity of [^{18}F]RAGER between flRAGE and sRAGE isomers. Subsequently, [^{11}C]FPS-ZM1 was successfully synthesized by palladium-catalyzed carbonylation with [^{11}C]CO.[314, 315] However, high nonspecific binding was observed for [^{11}C]**94** ([^{11}C]FPS-ZM1) in both wild-type and AD mice by in vitro autoradiography experiments, which was possibly attributed to its high lipophilicity (cLogP = 5.25). Most recently, [^{18}F]**95** ([^{18}F]InRAGER) was reported as a selective PET ligand for flRAGE (K_d = 1 nM), which was achieved via isotopic exchange with [^{18}F]KF.[97] Although high initial brain uptake (SUV_{max} = ca. 2.0) was observed in rats, the development of new radiosynthetic methods is necessary to address poor radiochemical yield and low molar activity.

8.2 MER tyrosine kinase (MERTK)

MER tyrosine kinase (MERTK) is a macrophage cell-surface protein in the TAM (namely TYRO3, AXL, MER) tyrosine kinase family.[316] In the brain, MERTK shows high expression in the microglia and astrocytes and emerging data have indicated the implication of MERTK in neuroinflammation.[98] In addition, a close association between polymorphism of the MERTK gene and MS susceptibility was reported.[317] Despite extremely low or even undetectable levels in the healthy brain, the expression of MERTK is significantly elevated in a variety of neuroinflammatory diseases. For instance, by postmortem analysis, soluble MERTK was upregulated in the brain of MS patients.[318] Although the precise role that MERTK exerts in neuroinflammation remains elusive, a suitable MERTK PET probe would provide a valuable tool to better understand the underlying mechanisms. To date, only one MERTK PET probe has been reported, namely [^{18}F]**96** ([^{18}F]JHU16907) (Figure 11).[99] [^{18}F]JHU16907 revealed good binding affinity (IC_{50} = 2.5 nM) and high initial brain uptake in mice. Preliminary evaluation of [^{18}F]JHU16907 in LPS-treated mice demonstrated a remarkably increased radioactivity accumulation (35%) in the brain. Moreover, the radioactivity in LPS-treated mouse brains could be significantly blocked (62%) by unlabeled JHU16907, suggesting a good specific binding of [^{18}F]JHU16907. Despite these promising preliminary results, evaluation of [^{18}F]JHU16907 in higher species is yet to be reported.

8.3. Soluble epoxide hydrolase (sEH)

Epoxide hydrolases, which include soluble epoxide hydrolase (sEH) and microsomal epoxide hydrolase (mEH), are key enzymes responsible for the degradation of epoxyeicosatrienoic acids (EETs).[100] EETs, which are generally produced from arachidonic acid by a cytochrome P450-catalyzed epoxidation reaction, represent an important class of signalling lipids with anti-inflammatory and anti-apoptotic effects as well as a function to regulate cerebral blood flow. The pharmacological blockade or genetic deletion of sEH represents a predominant approach for elevating the levels of EETs in vivo, which have demonstrated to provide protection against neuroinflammation in several disorders, such as AD, PD, vascular cognitive impairment, ischemia, seizure, and depression.[100] As such, sEH has emerged as a potential PET imaging target in these diseases. To date, [^{18}F]**97** ([^{18}F]FNDP) is the only one available sEH PET probe, which exhibited good potency (IC_{50} = 8.7 nM) (Figure 11).[319] In CD-1 mice, [^{18}F]FNDP demonstrated good BBB permeability (5.24 %ID/g at 5 min in striatum) and regional brain uptake. In sEH knock-out mice, a

remarkable decrease of [^{18}F]FNDP uptake (~90%) was also demonstrated. These results indicated excellent specific binding of [^{18}F]FNDP to sEH. Further evaluation of [^{18}F]FNDP in baboons suggested rapid and heterogeneous brain uptakes with higher radioactivity levels in putamen, insula, frontal cortex and amygdala, and lower levels in white matter and cerebellum.[319, 320] Blocking experiments demonstrated excellent specific binding of [^{18}F]FNDP to sEH in NHPs (~90%). Clinically, validation of [^{18}F]FNDP in heathy adults indicated excellent BBB permeability with high uptake in all brain regions ranging from ~2.4-3.4 SUV except corpus callosum (SUV_{max} = 1.5).[101] The heterogeneous distribution of [^{18}F]FNDP is aligned with the expression patterns of sEH in human brains. Accordingly, [^{18}F]FNDP may represent a promising radioligand for human sEH imaging in normal and disease conditions, and more efforts for validation of [^{18}F]FNDP in the preclinical neuroinflammatory models and clinical translation are warranted.

8.4. Phosphodiesterase subtypes (PDE4B, PDE4D and PDE7)

As a subtype of the cyclic nucleotide phosphodiesterases (PDEs), phosphodiesterase-4 (PDE4) is specifically responsible for the hydrolysis of the second messenger cyclic adenosine monophosphate (cAMP), a critical regulator for microglia homeostasis. PDE4 can be further divided into four subtypes, namely PDE4A, PDE4B, PDE4C, and PDE4D.[51, 102] In particular, PDE4B is widely expressed in most immune and inflammatory cells, such as T cells, B cells, microglia, monocytes and macrophages. It has been demonstrated that PDE4B exerts a critical role in neuroinflammation in a range of injury and neurological disorders, and PDE4B inhibition could provide improved efficacy in treating patients with neuroinflammation. Although selective PDE4B inhibitors remain in preclinical evaluation and initial forays seem promising, two PDE4 pan-inhibitors, apremilast and roflumilast, have been approved for the treatment of peripheral inflammation related conditions. To date, [^{18}F]**98** ([^{18}F]PF-06445974) is the only available PDE4B-preferring PET probe with excellent in vitro binding affinity (IC_{50} <1 nM) and good selectivity among PDE4A (> 4 fold), PDE4C (> 17) and PDE4D (> 36) (Figure 12).[103] PET imaging studies of [^{18}F]PF-06445974 in NHPs demonstrated excellent BBB permeability with a peak SUV of ~3. A heterogeneous radioactivity distribution pattern was observed with the highest level in the thalamus, followed by putamen, caudate, cortex, cerebellum, and hippocampus in a decreasing order. Pre-treatment with a Pfizer-proprietary PDE4B inhibitor led to marked reduction of the radioactivity levels of [^{18}F]PF-06445974 in various brain regions. In all, [^{18}F]PF-06445974 represents an excellent starting point to develop PDE4B-selective PET probe warranting further development in preclinical disease models as well as clinical trials.

PDE4D has been demonstrated to be involved in neuroinflammation and inhibition of PDE4D could attenuate neuroinflammation and provide neuroprotection in AD.[104] Recently, four lead PDE4D inhibitors were labeled with carbon-11 and evaluated in mice and monkeys with PET ([^{11}C]**99** ([^{11}C]T1953), [^{11}C]**100** ([^{11}C]T2525), [^{11}C]**101** ([^{11}C]T1650), and [^{11}C]**102** ([^{11}C]T1660)), which exhibited excellent binding affinity (IC_{50} = 5.12, 0.5, 3.9, and 2.8 nM, respectively), high selectivity (> 100 fold over PDE4B), and moderate brain uptake in mouse and, in particular in monkey brains (mice: SUV_{max} = 0.94, 1.44, 1.76, and 1.76, respectively, monkeys: SUV_{max} = 4.32, 5.09, 3.28, and 3.52, respectively) (Figure 12).[105] While radioligands [^{11}C]T1953 and [^{11}C]T2525 failed to deliver any specific PET

binding in monkey brains, both [^{11}C]T1650 and [^{11}C]T1660 exhibited considerable PDE4D-specific binding (37-48% decreased V_T values), as demonstrated by pharmacological block experiments with a PDE4 inhibitor rolipram or a selective PDE4D inhibitor BPN14770. [^{11}C]T1650 was further progressed into a first-in-human study with favorable brain uptake (SUV_{max} = 4.39) and specific binding (30% decreased $SUV_{60\text{-}120\ min}$ by pretreatment with PDE4D-selective inhibitor BPN14770). However, the V_T value increased steadily over scan duration, indicating the accumulation of radiometabolites in the brain. Overall, these results indicate the feasibility of PDE4D PET imaging in NHPs, but further radioligand optimization remains necessary to avoid problematic brain penetrant radiometabolites.

PDE7 is another subtype of PDEs, which is involved in pro-inflammatory processes. It has been indicated that inhibition of PDE7 function may be beneficial for the treatment of neuroinflammation and confer neuroprotection.[106] In contrast to diverse therapeutics agents, the development of PDE7-selective PET probes has lagged far behind. In 2015, two radioligands [^{18}F]**103** ([^{18}F]MICA-003, IC_{50} = 17.0 nM) and [^{11}C]**104** ([^{11}C]MICA-005, IC_{50} = 1.7 nM) were disclosed as potential PDE7 PET probes (Figure 12).[321, 322] Evaluation in mice indicated that both radioligands rapidly penetrated the BBB with a peak uptake of 5% ID/g and 1.74 SUV, respectively. Nonetheless, the homogenous distribution for both radioligands and the brain penetrating radiometabolite for [^{18}F]MICA-003 rendered them unfavorable for in vivo quantification of PDE7. Most recently, a promising PDE7 radioligand [^{11}C]**105** ([^{11}C]MTP38, IC_{50} < 10 nM)[323] was prepared via ^{11}C-cyanation of an appropriate bromo precursor with [^{11}C]HCN.[107] In vivo evaluation of [^{11}C]MTP38 demonstrated favorable BBB penetration and highest uptake was observed in the striatum with a peak SUV of approximating 4.5 in rats and 5 in monkeys. Pretreatment with unlabeled MTP38 or a selective PDE7 inhibitor MTP-X led to remarkably reduced radioactivity retention, indicating moderate binding specificity of [^{11}C]MTP38 to PDE7.[324] However, it is worth mentioning that the lead MTP38 shows equal potency towards PDE7 subtypes, namely PDE7A and PDE7B. First-in human PET studies of [^{11}C]MTP38 were subsequently conducted, which exhibited good BBB penetration, reversible binding, and heterogeneous distribution with SUV of 4-8 in various brain regions. As proof of concept, [^{11}C]MTP38 demonstrated high feasibility of imaging PDE7 in human and served as a novel chemical scaffold for further modification to improve specific binding and subtype selectivity.

8.5. CX3C chemokine receptor 1(CX3CR1)

The CX3C chemokine receptor 1 (CX3CR1) is also known as fractalkine (CX3CL1) receptor or G-protein coupled receptor 13 (GPR13). In the brain, CX3CR1 plays an important role in neuroinflammation of sustaining the microglial hemostasis in the brain and is used as immune histological marker for microglia.[108, 325] It has been demonstrated that CX3CR1 deficiency led to the dysregulation of microglial responses and microglial neurotoxicity, which further contributed to the generation of ischemic damage.[108] In 2015, [^{18}F]**106** ([^{18}F]FBTTP, K_i = 23 nM) was reported as a potential CX3CR1 PET probe.[326] Initial PET imaging studies in mice demonstrated the ability to cross the BBB, but further information about in vitro and in vivo validation remains to be reported (Figure 13).[109, 327] In addition, a ^{64}Cu-labeled macromolecule ([^{64}Cu]vMIP-II-comb) was synthesized by

conjugating the viral macrophage inflammatory protein-II (vMIP-II) with a ^{64}Cu-linked nanoparticle.[328] [^{64}Cu]vMIP-II-comb was specific for chemokine receptors, and proved to be useful for in vivo macrophage mapping in mouse models of peripheral diseases, such as vascular injury and inflammatory atherosclerosis. Overall, CX3CR1 is a promising imaging target for neuroinflammation, and further studies are warranted to develop a suitable brain-penetrant small-molecule PET ligand.

8.6. Nucleotide oligomerization domain (NOD)- like receptor protein 3 (NLRP3)

Nucleotide oligomerization domain (NOD)-like receptor protein 3 (NLRP3) represents one subtype of the NOD-like receptor (NLR) family, which is widely expressed in microglia and macrophages, and functions as an intracellular sensor for the detection of various insult or stimuli, such as pathogen and endogenous danger signals.[110] Upon activation, NLRP3 is transformed into inflammasome, which is a cytosolic multiprotein oligomer, serving to mediate the proinflammatory cytokine release. Overall, NLPR3 is closely associated with neuroinflammation and multiple neurodegenerative diseases, such as PD and AD, and inhibition of NLPR3 represents an emerging and promising strategy for treatment of these disorders.[110]

To date the development of NLPR3 PET probes remains in its infancy. In 2020, [^{11}C]**107** ([^{11}C]MCC950) was disclosed as the first potential NLRP3 PET radioligand, with favorable binding affinity (IC_{50} = 8 nM) (Figure 13).[111] However, PET imaging studies indicated no brain uptake and rapid washout in several species, such as mice (SUV_{max} = 0.06), rats (SUV_{max} = 0.06), and rhesus monkeys (SUV_{max} = 0.48), impeding its further investigation. Soon after, another radioligand [^{11}C]**108** was prepared and evaluated in mice.[329] Despite some specific binding (26%) towards NLRP3 in thyroid gland, the in vivo application of [^{11}C]**108** for neuroinflammation was hampered by unfavorable binding affinity (IC_{50} = 900 nM) and limited brain uptake in mice (1.7 %ID/g). Further optimization on improved binding affinity and increased brain uptake will be necessary to identify lead PET ligands for NLPR3.

8.7. Myeloperoxidase (MPO)

Myeloperoxidase (MPO) is a heme-containing peroxidase catalyzing the generation of ROS and other reactive oxidants, which displays high expression in several proinflammatory innate immune cells, such as microglia, monocytes, neutrophils, and macrophages.[112] Emerging evidence indicates that excessive MPO activity is closely associated with tissue damage in diverse diseases, especially those characterized by inflammation. As such, inhibition of harmful MPO activity represents an emerging and promising therapeutic strategy for inflammation-related diseases. AZD3241 is a recently reported MPO inhibitor with moderate in vitro binding affinity (IC_{50} = 1.2 μM) and its radiolabeling with carbon-11 led to the development of radioligand [^{11}C]**109** ([^{11}C]AZD3241; Figure 13).[113] PET imaging studies of [^{11}C]AZD3241 in monkeys revealed a good brain uptake with maximum SUV of 3.0. The homogeneously distributed radioactivity and rapid washout in monkey brains was proposed to be attributed to low MPO expression levels in healthy monkey brains. More recently, [^{18}F]**110** ([^{18}F]MAPP) was prepared and evaluated in mice, which exhibited favorable BBB penetration.[114] Notably, in a complete Freund's adjuvant (CFA)

paw inflammation model, [^{18}F]MAPP exhibited 4 times higher radioactivity accumulation on the CFA-treated side than that on the PBS-treated side. Moreover, the radioactivity on the CFA-treated side could be markedly blocked (57%) by pretreatment with the MPO-specific inhibitor PF-1355, indicating some binding specificity of [^{18}F]MAPP towards MPO. Overall, [^{18}F]MAPP is a promising MPO-specific PET probe warranting further development and validation in preclinical disease models as well as potential clinical trials.

8.8. Glycogen synthase kinase 3 (GSK-3)

Glycogen synthase kinase 3 (GSK-3) is a serine/threonine kinase mediating the phosphorylation at the serine or threonine residues of a specific substrate.[330–332] In mammals, GSK-3 is present in two highly related isoforms GSK-3α and GSK-3β, sharing 85% overall amino acid identity and 97% identity in the ATP binding pocket. It has been demonstrated that GSK-3 possesses diverse substrates including the AD-related tau protein. Further, dysfunction of GSK-3 is implicated in multiple neurological disorders, such as neuroinflammation and AD.[333–335] Of note, GSK-3β exhibits extremely high levels in neural tissues, where it contributes to the development of the adult mammalian brain.[115] Accordingly, it is not surprising that GSK-3β has emerged as a key component of neuroinflammation. For example, following LPS administration, upregulated GSK-3β activity was observed in rats.[336] Postmortem immunoblotting studies of brain samples from AD patients also revealed elevated GSK-3β levels, as consistent with most cellular and transgenic rodent experiments, and the increased GSK-3β levels were mainly co-localized with neurofibrillary tangles (NFTs) that are composed of hyperphosphorylated tau protein.[337–339] Therefore, GSK-3 inhibition might provide a rational approach for the treatment of neurological disorders, and GSK-3 PET imaging may present a useful tool to validate GSK-3 drug candidates and to monitor the progress of AD or non-AD tauopathies.

Despite the great potential of GSK-3, so far, no GSK-3 PET probe has been advanced to clinical trials. The major obstacle possibly arises from the lack of highly potent and selective GSK-3 radioligands with sufficient BBB penetration. To date, only a handful of GSK-3 PET probes have been disclosed for in vivo evaluation (Figure 14). Among them, [^{11}C]**111** ([^{11}C]AR-A014418, K_i = 170 nM),[340, 341] [^{11}C]**112** ([^{11}C]PyrATP-1, K_i = 4.9 nM),[342] oxadiazole-based radioligands [^{11}C]**113-115** (IC_{50} = 35-66 nM)[343] and [^{11}C]**116** ([^{11}C]A1070722, K_i = 0.6 nM) failed to substantiate appropriate brain uptake in rodents and NHPs. Although [^{11}C]**117** ([^{11}C]SB-216763, K_i = 9 nM, IC_{50} = 34 nM) exhibited favorable BBB penetration with a peak SUV of 2.5 at 3 min p.i. in mice and 1.9 at 5 min p.i. in baboons, respectively, homogeneous distribution and the lack of selectivity over structurally similar kinases impeded its further application.[189, 344] A ^{18}F-labeled derivative of SB-216763 ([^{18}F]**118**, IC_{50} = 1.7 nM) was also synthesized and evaluated in Sprague−Dawley rats, but exhibited inadequate brain uptake (ca. 0.45 %ID/cc) and high non-displaceable binding.[345] The failure of these radioligands for in vivo GSK-3 imaging may be attributed to their low binding affinity to GSK-3, insufficient lipophilicity and interactions with efflux proteins (Pgp and BCRP) at the BBB. We have recently developed a highly potent and selective GSK inhibitor, **119** (PF-367, GSK-3β IC_{50} = 2.1 nM determined by a recombinant human enzyme assay), which demonstrated good efficacy in the regulation of tau phosphorylation both in vitro and in vivo, as well as exquisite selectivity towards

GSK-3 over a panel of kinases.[346] The radiolabeling of PF-367 with carbon-11 gave rise to a promising GSK-3 PET probe, [^{11}C]**119** ([^{11}C]PF-367), which readily penetrated the BBB of NHPs with a peak SUV of 1.0 at 5 min p.i. Pharmacological blocking with unlabeled PF-367 resulted in a faster washout of [^{11}C]PF-367 and decreased brain radioactivity levels were thus observed at late time points with approximately 30% of displaceable binding. Nonetheless, one concern about [^{11}C]PF-367 arose from its virtually homogeneous distribution pattern and considerable skull uptake. Ongoing efforts rendered the discovery of several ^{11}C-labeled analogues of PF-367 with comparable or better binding affinity, selectivity and in vivo brain exposure (SUV_{max} = 0.84-3.08 in rodents), such as [^{11}C]**120** ([^{11}C]PF-618, GSK-3β IC_{50} = 2.5 nM), [^{11}C]**121** ([^{11}C]PF-627, GSK-3β IC_{50} = 3.6 nM), [^{11}C]**122** ([^{11}C]OCM-37, GSK-3β IC_{50} = 1.5 nM), [^{11}C]**123** ([^{11}C]OCM-44, GSK-3β IC_{50} = 2.0 nM), and [^{11}C]**124** ([^{11}C]OCM-51, GSK-3β IC_{50} = 0.031 nM).[116] Despite exhibiting the highest binding affinity, [^{11}C]OCM-51 showed the lowest BBB penetration (SUV_{max} = 0.84) in rat brains, which is possibly due to substantial peripheral binding to GSK-3 before entering the brain and a more rapid elimination from the circulation. In contrast, [^{11}C]PF-618 and [^{11}C]OCM-44 exhibited the highest radioactivity accumulation in rat brains with a peak SUV of up to 3.08. Further, evaluation of [^{11}C]PF-618, [^{11}C]OCM-37 and [^{11}C]OCM-44 in rhesus monkeys revealed high brain radioactivity levels (SUV_{max} = 3.0-4.0) and favourable binding kinetics. Moreover, the gray matter exhibited higher uptake than the white matter, which coincided with the brain distribution of GSK-3 and contrasted with the in vivo profile of [^{11}C]PF-367. Overall, these findings suggest that [^{11}C]PF-618, [^{11}C]OCM-37 and [^{11}C]OCM-44 represent lead GSK-3 PET probes and warrants detailed kinetic profiling in higher species.

Outlook and Conclusion

The development of PET probes that selectively bind to different neuroinflammation-related targets is an exciting research area that has received much attention from academia and industry. It is envisioned that these efforts will substantially contribute to a better understanding of neuroinflammation and neurodegenerative diseases, as well as ultimately their clinical diagnosis and management. One major challenge in PET imaging of neuroinflammation lies in the identification of suitable targets, which must satisfy the following criteria: (1) The target must have adequate expression (high B_{max}) and high binding affinity (K_i/K_d) of the corresponding ligand for successful PET visualization ($B_{max}/K_d \geq 10$); (2) The target must serve as a proxy for one aspect in the neuroinflammatory process and a substantial change of target expression/density must result from such processes in order to distinguish pathological states from a healthy situation; and (3) The target must be druggable or traceable, which means that the target should contain some pharmacophores or pockets for the binding of a small molecule ligand. Additionally, it's also critical to continuously develop suitable PET molecules for the existing and validated biological targets that concurrently lack excellent binding affinity, high selectivity, high BBB penetration, suitable brain kinetics and reasonable metabolic profile.

To date, several promising targets have been elucidated for neuroinflammation imaging, whereas a number of PET probes were translated to humans. These probes are targeted towards TSPO, COX-1, CB2R, MAO-B, S1PR1, P2X7R, sEH, PDE4D and PDE7. Given

that neuroinflammation is a key hallmark of neurodegeneration, it is not surprising that strenuous efforts have been made to overcome the limitations of TSPO imaging, which undoubtedly remains the current reference standard in the clinic. Nonetheless, the diverse landscape of critical biological targets in neuroinflammation underscores the complexity of inflammatory processes in the central nervous system. The availability of suitable probes for these targets not only harbours potential to provide a superior diagnostic readout but will also contribute to an improved understanding in the field. In recent years, a rapidly growing number of novel targets, including enzymes, intracellular signalling molecules, G-protein coupled receptors, ion channels and members of the immunoglobulin receptor superfamily, have been exploited for neuroinflammation imaging. In addition, attributed to the length and focus of this review, we exclude many exciting druggable targets in neuroinflammatory pathway due to the lack of companion PET ligands. These targets, to name a few, prostaglandin EP2 receptor,[347] p38 mitogen-activated protein kinases,[348] tumor necrosis factor[349] and autotaxin,[350] represent new research directions and unmet clinical need for PET ligand development for neuroinflammation. Furthermore, recent development of PET neuroligands for the endocannabinoid pathway,[50] metabotropic/ionotropic glutamate signalling receptors[49] and phosphodiesterases,[51] for example, $mGluR_2$, TARP g8, NMDAR (GluN2B), AMPAR[351–354] offers a great opportunity to study crosstalk and signalling interaction under neuroinflammatory conditions and physiopathology of neurodegenerative diseases. In all, it is of paramount significance to take advantage of modern drug discovery efforts and establishment of translational preclinical disease models to drive future development of innovative PET probes. We hope that this review will draw attention from academia and industry, thereby nourishing future projects that focus on the diagnosis and management of neuroinflammation and neurodegenerative disorders..

ACKNOWLEDGMENTS

We thank the Division of Nuclear Medicine and Molecular Imaging, Radiology, MGH and Harvard Medical School, USA for general support. We also gratefully acknowledge the financial support from the NIH grants (DA038000, DA043507, MH117125, MH120197, AG063290, AG070060, AG073428 & AG074218 to S.H.L.) and the Swiss National Science Foundation for postdoctoral fellowship to Dr. Ahmed Haider.

Biographies

Zhen Chen received his BS degree in Applied Chemistry in 2013 from Tianjin University (China). He completed his PhD in 2019 under the supervision of Prof. Jun-An Ma in Tianjin University (China). From 2017 to 2020, he studied radiochemistry as an exchange PhD student and postdoctoral fellow with Prof. Steven H. Liang at Harvard Medical School / Massachusetts General Hospital (HMS/MGH). From 2020 to 2021, he worked as a postdoctoral research fellow in the group of Prof. Nicolai Cramer at EPFL. Currently, he is a full professor at Nanjing Forestry University. His research interests focus on novel transformations of diazo compounds, development of novel imaging biomarkers, and total synthesis of peptidic natural products.

Ahmed Haider obtained his M.S. in Pharmaceutical Sciences at ETH Zurich, Switzerland, where he subsequently earned his Ph.D. in Radiochemistry and Molecular Imaging with Professor Simon M. Ametamey in 2018. In the same year, he moved to the Department of

Nuclear Medicine at the University Hospital Zurich, working with Prof. Catherine Gebhard to advance cardiovascular gender medicine with particular focus on preclinical and clinical cardiovascular PET imaging. Recently, Dr. Haider joined Professor Steven H. Liang's research group at the Division of Nuclear Medicine and Molecular Imaging at Harvard Medical School and Massachusetts General Hospital in Boston, United States.

Jiahui Chen obtained his BS degree in Pharmacy in 2012 from Guangzhou University of Chinese medicine (China). He earned his Ph.D. in Chemical Biology from Peking University with Professor Zhengying Pan in 2018. In the same year, he started as a postdoctoral fellow with Prof. Steven H. Liang at the Division of Nuclear Medicine and Molecular Imaging at Harvard Medical School / Massachusetts General Hospital (HMS/MGH). His research interests include constructing and evaluating of neuroinflammatory and degenerative disease models, development and clinical translation of new PET tracers for the central nervous system.

Zhiwei Xiao obtained his B.Sc. degrees in Applied Chemistry in East China Normal University (ECNU) in 2013, followed by his Ph.D. in Organic Chemistry with Professor Qing-yun Chen in Shanghai Institute of Organic Chemistry (SIOC), Chinese Academy of Sciences (CAS) in 2019. After that, he joined Professor Hao Xu's group at the First Affiliated Hospital of Jinan University and then Professor Steven H. Liang's group at Division of Nuclear Medicine and Molecular Imaging, Department of Radiology, Massachusetts General Hospital (MGH) and Harvard Medical School (HMS) for his postdoctoral. His research interests include novel methodology development of ^{11}C-/^{18}F-labeling and development of PET tracers for neurodegenerative diseases.

Uwe Grether received his Diploma degree in Chemistry at the University of Karlsruhe, Germany, where he subsequently earned his Ph.D. in Organic Chemistry with Professor Herbert Waldmann in 2000. After that, he joined Professor James D. White's group at Orgeon State University for his postdoctoral research. In 2001, Dr. Grether started at the Pharma Research and Early Development unit of F. Hoffmann-La Roche Ltd. in Basel, Switzerland. His research interests include medicinal chemistry and chemical probes focussing on holistic approaches toward a clinical end-goal.

Michael Honer obtained his Diploma Degree in Biochemistry and Pharmacology at ETH Zurich, where he subsequently also earned his PhD in Neuropharmacology and Radiopharmacology. He then moved as a Research Scientist to the Center for Radiopharmaceutical Science at Paul Scherrer Institute & University Hospital Zurich, working on in vitro and in vivo characterization of novel PET tracers and preclinical & clinical PET imaging. In 2005, he was appointed as Team Leader of the PET Pharmacology Lab at the newly established Animal Imaging Center at ETH Zurich. In 2010, he joined Roche as group leader of the Translational PET Lab. Within the Neuroscience Disease and Therapeutic Area, he is responsible for PET tracer discovery and development and oversees all preclinical and many clinical PET activities.

Luca Gobbi obtained his Diploma Degree in Chemistry from the Federal Institute of Technology (ETH) in Zürich, Switzerland, where he subsequently earned his Ph.D. in

Organic Chemistry with Professor François Diederich in 2000. After postdoctoral studies with Professor Steven V. Ley in the Department of Chemistry at the University of Cambridge, UK, in 2001 he joined F. Hoffmann-La Roche Ltd. in the Pharma Research and Early Development unit in Basel, Switzerland. His research interests span from medicinal chemistry to PET tracer discovery, with a focus on the central nervous system.

Steven E. Arnold is Professor of Neurology at Harvard Medical School and Translational Neurology Head and Managing Director of the Interdisciplinary Brain Center at Massachusetts General Hospital. After receiving his M.D. from Boston University, Dr. Arnold trained and is dual board-certified in Neurology and Psychiatry. Dr. Arnold has conducted longstanding research on neurodegenerative disease pathology, molecular biomarkers and therapeutics for cognitive decline and neuropsychiatric syndromes in late life and has led broad clinical and translational research programs to accelerate therapeutics discovery and development.

Lee Josephson obtained his B.S. in Chemistry from the University of Wisconsin and his Ph.D. in Chemical Biology at Stony Brook University (1975). He did a postdoctoral fellowship in the Department of Molecular and Cellular Biology at Harvard University. He was a cofounder of AMAG Pharmaceuticals (AMAG, AMEX Exchange) where he served as Chief Scientific Officer. He then joined the Department of Radiology at MGH, where he pioneered the use of magnetic nanoparticles and was a cofounder of T2 Biosystems (TTOO, NASDQ). His research interests include magnetic nanoparticles, imaging biomarkers for cell death and cell health, and peptide PEGylation. He is currently Associate Professor at HMS and a partner in MedChem Imaging LLC which supplies radiotracers to the pharmaceutical industry.

Steven H. Liang obtained his B.S. at Tianjin University in 2003, followed by his Ph.D. in Chemistry with Professor Marco Ciufolini at the University of British Columbia in 2010. Then he started as a NSERC Fellow with Professor E. J. Corey at Harvard University. In 2012, Dr. Liang accepted a junior faculty position at HMS and MGH. Dr. Liang is currently the Director of Radiochemistry and Biomarker Development, Nuclear Medicine and Molecular Imaging at MGH, and Associate Professor of Radiology at HMS. Dr. Liang's research interests include novel radiochemistry, imaging biomarker and radiotherapy development, and clinical translation.

ABBREVIATION

Aβ	amyloid beta plaque
AD	Alzheimer's disease
ALS	amyotrophic lateral sclerosis
ATP	adenosine triphosphate
BBB	blood-brain barrier
Bcrp	breast cancer resistance protein

CB1R	cannabinoid type 1 receptor
CB2R	cannabinoid type 2 receptor
CNS	central nervous system
COX	cyclooxygenase
CSF1	colony stimulating factor 1
CSF1R	colony stimulating factor 1 receptor
CX3CR1	CX3C chemokine receptor 1
EET	epoxyeicosatrienoic acids
flRAGE	membrane-bound full length RAGE
GPR13	G-protein coupled receptor 13
GSK-3	glycogen synthase kinase 3
HD	Huntington’s disease
HIE	hypoxic-ischemic encephalopathy
%ID/g	% percentage injected dose per gram of tissue
LPS	lipopolysaccharide
MAO	monoamine oxidase
mEH	microsomal epoxide hydrolase
MerTK	Mer tyrosine kinase
MPO	myeloperoxidase
MS	multiple sclerosis
NHP	non-human primate
NLRP3	NOD-like receptor protein 3
P2X7R	P2X ligand-gated ion channel type 7 receptor
P2Y12R	purinergic metabotropic 12 receptor
PD	Parkinson’s disease
PDE	phosphodiesterase
PET	positron emission tomography
Pgp	P-glycoprotein
RAGE	receptor for advanced glycation end products

RNS	reactive nitrogen species
ROS	reactive oxygen species
S1PR	sphingosine-1-phosphate receptor
sEH	soluble epoxide hydrolase
SphK1	sphingosine kinase-1
sRAGE	soluble RAGE
SUV	standard uptake value
TBI	traumatic brain injury
TSPO	translocator protein
UTP	uridine triphosphate
NOD	nucleotide oligomerization domain

REFERENCES

1. Disabato DJ; Quan N; Godbout JP Neuroinflammation: the devil is in the details. J. Neurochem 2016, 139, 136–153. [PubMed: 26990767]
2. Davalos D; Grutzendler J; Yang G; Kim JV; Zuo Y; Jung S; Littman DR; Dustin ML; Gan W-B ATP mediates rapid microglial response to local brain injury in vivo. Nat. Neurosci 2005, 8, 752–758. [PubMed: 15895084]
3. Mantovani Alberto; Sica Antonio; Locati M Macrophage polarization comes of age. Immunity 2005, 23, 344–346. [PubMed: 16226499]
4. Glass CK; Saijo K; Winner B; Marchetto MC; Gage FH Mechanisms underlying inflammation in neurodegeneration. Cell 2010, 140, 918–934. [PubMed: 20303880]
5. Graeber MB Changing face of microglia. Science 2010, 330, 783–788. [PubMed: 21051630]
6. Réus GZ; Fries GR; Stertz L; Badawy M; Passos IC; Barichello T; Kapczinski F; Quevedo J The role of inflammation and microglial activation in the pathophysiology of psychiatric disorders. Neuroscience 2015, 300, 141–154. [PubMed: 25981208]
7. Werry EL; Bright FM; Piguet O; Ittner LM; Halliday GM; Hodges JR; Kiernan MC; Loy CT; Kril JJ; Kassiou M Recent developments in TSPO PET imaging as a biomarker of neuroinflammation in neurodegenerative disorders. Int. J. Mol. Sci. 2019, 20, 3161.
8. Bélanger M; Allaman I; Magistretti Pierre J. Brain energy metabolism: Focus on astrocyte-neuron metabolic cooperation. Cell Metab. 2011, 14, 724–738. [PubMed: 22152301]
9. Deitmer JW; Theparambil SM; Ruminot I; Noor SI; Becker HM Energy dynamics in the brain: Contributions of astrocytes to metabolism and pH homeostasis. Front. Neurosci 2019, 13, 1301. [PubMed: 31866811]
10. Halassa MM; Haydon PG Integrated brain circuits: Astrocytic networks modulate neuronal activity and behavior. Annu. Rev. Physiol 2010, 72, 335–355. [PubMed: 20148679]
11. Clarke LE; Barres BA Emerging roles of astrocytes in neural circuit development. Nat. Rev. Neurosci 2013, 14, 311–321. [PubMed: 23595014]
12. Okada S; Nakamura M; Katoh H; Miyao T; Shimazaki T; Ishii K; Yamane J; Yoshimura A; Iwamoto Y; Toyama Y; Okano H Conditional ablation of Stat3 or Socs3 discloses a dual role for reactive astrocytes after spinal cord injury. Nat. Med 2006, 12, 829–834. [PubMed: 16783372]
13. Herrmann JE; Imura T; Song B; Qi J; Ao Y; Nguyen TK; Korsak RA; Takeda K; Akira S; Sofroniew MV STAT3 is a critical regulator of astrogliosis and scar formation after spinal cord injury. J. Neurosci 2008, 28, 7231–7243. [PubMed: 18614693]

14. Wanner IB; Anderson MA; Song B; Levine J; Fernandez A; Gray-Thompson Z; Ao Y; Sofroniew MV Glial scar borders are formed by newly proliferated, elongated astrocytes that interact to corral inflammatory and fibrotic cells via STAT3-dependent mechanisms after spinal cord injury. J. Neurosci 2013, 33, 12870–12886. [PubMed: 23904622]
15. Anderson MA; Burda JE; Ren Y; Ao Y; O'Shea TM; Kawaguchi R; Coppola G; Khakh BS; Deming TJ; Sofroniew MV Astrocyte scar formation aids central nervous system axon regeneration. Nature 2016, 532, 195–200. [PubMed: 27027288]
16. Sofroniew MV Molecular dissection of reactive astrogliosis and glial scar formation. Trends Neurosci. 2009, 32, 638–647. [PubMed: 19782411]
17. Zamanian JL; Xu L; Foo LC; Nouri N; Zhou L; Giffard RG; Barres BA Genomic analysis of reactive astrogliosis. J. Neurosci 2012, 32, 6391–6410. [PubMed: 22553043]
18. Liddelow SA; Guttenplan KA; Clarke LE; Bennett FC; Bohlen CJ; Schirmer L; Bennett ML; Münch AE; Chung W-S; Peterson TC; Wilton DK; Frouin A; Napier BA; Panicker N; Kumar M; Buckwalter MS; Rowitch DH; Dawson VL; Dawson TM; Stevens B; Barres BA Neurotoxic reactive astrocytes are induced by activated microglia. Nature 2017, 541, 481–487. [PubMed: 28099414]
19. Lana D; Ugolini F; Nosi D; Wenk GL; Giovannini MG The emerging role of the interplay among astrocytes, microglia, and neurons in the hippocampus in health and disease. Front. Aging Neurosci 2021, 13, 651973. [PubMed: 33889084]
20. Crutcher KA; Gendelman HE; Kipnis J; Perez-Polo JR; Perry VH; Popovich PG; Weaver LC Debate: "Is increasing neuroinflammation beneficial for neural repair?". J. Neuroimmune Pharmacol 2006, 1, 195–211. [PubMed: 18040798]
21. Popovich PG; Longbrake EE Can the immune system be harnessed to repair the CNS? Nat. Rev. Neurosci 2008, 9, 481–493. [PubMed: 18490917]
22. Yang W-X; Terasaki T; Shiroki K; Ohka S; Aoki J; Tanabe S; Nomura T; Terada E; Sugiyama Y; Nomoto A Efficient delivery of circulating poliovirus to the central nervous system independently of poliovirus receptor. Virology 1997, 229, 421–428. [PubMed: 9126254]
23. Block ML; Hong J-S Microglia and inflammation-mediated neurodegeneration: Multiple triggers with a common mechanism. Prog. Neurobiol 2005, 76, 77–98. [PubMed: 16081203]
24. Tansey MG; McCoy MK; Frank-Cannon TC Neuroinflammatory mechanisms in Parkinson's disease: Potential environmental triggers, pathways, and targets for early therapeutic intervention. Exp. Neurol 2007, 208, 1–25. [PubMed: 17720159]
25. Schmid CD; Melchior B; Masek K; Puntambekar SS; Danielson PE; Lo DD; Gregor Sutcliffe J; Carson MJ Differential gene expression in LPS/IFNγ activated microglia and macrophages: in vitro versus in vivo. J. Neurochem 2009, 109, 117–125. [PubMed: 19393017]
26. Guzman-Martinez L; Maccioni RB; Andrade V; Navarrete LP; Pastor MG; Ramos-Escobar N Neuroinflammation as a common feature of neurodegenerative disorders. Front. Pharmacol 2019, 10, 1008. [PubMed: 31572186]
27. Sheng JG; Bora SH; Xu G; Borchelt DR; Price DL; Koliatsos VE Lipopolysaccharide-induced-neuroinflammation increases intracellular accumulation of amyloid precursor protein and amyloid β peptide in APPswe transgenic mice. Neurobiol. Dis 2003, 14, 133–145. [PubMed: 13678674]
28. Lee J; Goericke F; King WP Temperature-dependent thermomechanical noise spectra of doped silicon microcantilevers. Sens. Actuator A Phys 2008, 145-146, 37–43.
29. Sy M; Kitazawa M; Medeiros R; Whitman L; Cheng D; Lane TE; LaFerla FM Inflammation induced by infection potentiates tau pathological features in transgenic mice. Am. J. Pathol 2011, 178, 2811–2822. [PubMed: 21531375]
30. Jack CR; Knopman DS; Jagust WJ; Petersen RC; Weiner MW; Aisen PS; Shaw LM; Vemuri P; Wiste HJ; Weigand SD; Lesnick TG; Pankratz VS; Donohue MC; Trojanowski JQ Tracking pathophysiological processes in Alzheimer's disease: an updated hypothetical model of dynamic biomarkers. Lancet Neurol. 2013, 12, 207–216. [PubMed: 23332364]
31. DeLeo JA; Yezierski RP The role of neuroinflammation and neuroimmune activation in persistent pain. Pain 2001, 90, 1–6. [PubMed: 11166964]
32. Ellis A; Bennett DLH Neuroinflammation and the generation of neuropathic pain. Br. J. Anaesth 2013, 111, 26–37. [PubMed: 23794642]

33. Ji R-R; Xu Z-Z; Gao Y-J Emerging targets in neuroinflammation-driven chronic pain. Nat. Rev. Drug Discov 2014, 13, 533–548. [PubMed: 24948120]
34. Mao-Ying Q-L; Wang X-W; Yang C-J; Li X; Mi W-L; Wu G-C; Wang Y-Q Robust spinal neuroinflammation mediates mechanical allodynia in Walker 256 induced bone cancer rats. Mol. Brain 2012, 5, 16. [PubMed: 22607655]
35. Molfino A; Gioia G; Fanelli FR; Laviano A Contribution of neuroinflammation to the pathogenesis of cancer cachexia. Mediators Inflamm. 2015, 2015, 801685. [PubMed: 26504362]
36. Chen WW; Zhang X; Huang WJ Role of neuroinflammation in neurodegenerative diseases. Mol. Med. Rep 2016, 13, 3391–3396. [PubMed: 26935478]
37. Ransohoff RM How neuroinflammation contributes to neurodegeneration. Science 2016, 353, 777–783. [PubMed: 27540165]
38. Gordon R; Woodruff TM Chapter 3 - Neuroinflammation as a therapeutic target in neurodegenerative diseases. In Disease-Modifying Targets in Neurodegenerative Disorders, Baekelandt V; Lobbestael E, Eds. Academic Press: 2017; pp 49–80.
39. Ametamey SM; Honer M; Schubiger PA Molecular imaging with PET. Chem. Rev 2008, 108, 1501–1516. [PubMed: 18426240]
40. Willmann JK; van Bruggen N; Dinkelborg LM; Gambhir SS Molecular imaging in drug development. Nat. Rev. Drug Discov 2008, 7, 591–607. [PubMed: 18591980]
41. Miller PW; Long NJ; Vilar R; Gee AD Synthesis of 11C, 18F, 15O, and 13N radiolabels for positron emission tomography. Angew. Chem. Int. Ed 2008, 47, 8998–9033.
42. Airas L; Rissanen E; Rinne JO Imaging neuroinflammation in multiple sclerosis using TSPO-PET. Clin. Transl. Imaging 2015, 3, 461–473. [PubMed: 27331049]
43. Alam MM; Lee J; Lee S-Y Recent progress in the development of TSPO PET ligands for neuroinflammation imaging in neurological diseases. Nucl. Med. Mol. Imaging 2017, 51, 283–296. [PubMed: 29242722]
44. Largeau B; Dupont A-C; Guilloteau D; Santiago-Ribeiro M-J; Arlicot N TSPO PET imaging: From microglial activation to peripheral sterile inflammatory diseases? Contrast Media Mol. Imaging 2017, 2017, 6592139. [PubMed: 29114179]
45. Best L; Ghadery C; Pavese N; Tai YF; Strafella AP New and old TSPO PET radioligands for imaging brain microglial activation in neurodegenerative disease. Curr. Neurol. Neurosci. Rep 2019, 19, 24. [PubMed: 30941587]
46. Werry EL; Bright FM; Piguet O; Ittner LM; Halliday GM; Hodges JR; Kiernan MC; Loy CT; Kril JJ; Kassiou M Recent developments in TSPO PET imaging as a biomarker of neuroinflammation in neurodegenerative disorders. Int. J. Mol. Sci 2019, 20.
47. Zhang L; Hu K; Shao T; Hou L; Zhang S; Ye W; Josephson L; Meyer JH; Zhang M-R; Vasdev N; Wang J; Xu H; Wang L; Liang SH Recent developments on PET radiotracers for TSPO and their applications in neuroimaging. Acta Pharmaceutica Sinica B 2021, 11, 373–393. [PubMed: 33643818]
48. Deng X; Rong J; Wang L; Vasdev N; Zhang L; Josephson L; Liang SH Chemistry for positron emission tomography: Recent advances in 11C-, 18F-, 13N-, and 15O-labeling reactions. Angew. Chem. Int. Ed 2019, 58, 2580–2605.
49. Fu H; Chen Z; Josephson L; Li Z; Liang SH Positron emission tomography (PET) ligand development for ionotropic glutamate receptors: Challenges and opportunities for radiotracer targeting N-methyl-d-aspartate (NMDA), α-amino-3-hydroxy-5-methyl-4-isoxazolepropionic acid (AMPA), and kainate receptors. J. Med. Chem 2019, 62, 403–419. [PubMed: 30110164]
50. Hou L; Rong J; Haider A; Ogasawara D; Varlow C; Schafroth MA; Mu L; Gan J; Xu H; Fowler CJ; Zhang M-R; Vasdev N; Ametamey S; Cravatt BF; Wang L; Liang SH Positron emission tomography imaging of the endocannabinoid system: Opportunities and challenges in radiotracer development. J. Med. Chem 2021, 64, 123–149. [PubMed: 33379862]
51. Sun J; Xiao Z; Haider A; Gebhard C; Xu H; Luo H-B; Zhang H-T; Josephson L; Wang L; Liang SH Advances in cyclic nucleotide phosphodiesterase-targeted PET imaging and drug discovery. J. Med. Chem 2021, 64, 7083–7109. [PubMed: 34042442]

52. Ghose AK; Herbertz T; Hudkins RL; Dorsey BD; Mallamo JP Knowledge-based, central nervous system (CNS) lead selection and lead optimization for CNS drug discovery. ACS Chem. Neurosci 2012, 3, 50–68. [PubMed: 22267984]

53. Piel M; Vernaleken I; Rösch F Positron emission tomography in CNS drug discovery and drug monitoring. J. Med. Chem 2014, 57, 9232–9258. [PubMed: 25144329]

54. Honer M; Gobbi L; Martarello L; Comley RA Radioligand development for molecular imaging of the central nervous system with positron emission tomography. Drug Discov. Today 2014, 19, 1936–1944. [PubMed: 25173703]

55. Pipal RW; Stout KT; Musacchio PZ; Ren S; Graham TJA; Verhoog S; Gantert L; Lohith TG; Schmitz A; Lee HS; Hesk D; Hostetler ED; Davies IW; MacMillan DWC Metallaphotoredox aryl and alkyl radiomethylation for PET ligand discovery. Nature 2021, 589, 542–547. [PubMed: 33238289]

56. Narayanaswami V; Dahl K; Bernard-Gauthier V; Josephson L; Cumming P; Vasdev N Emerging PET radiotracers and targets for imaging of neuroinflammation in neurodegenerative diseases: Outlook beyond TSPO. Mol. Imaging 2018, 17, 1536012118792317. [PubMed: 30203712]

57. Janssen B; Mach RH Chapter 7 - Development of brain PET imaging agents: Strategies for imaging neuroinflammation in Alzheimer's disease. In Progress in Molecular Biology and Translational Science, Becker JT; Cohen AD, Eds. Academic Press: 2019; Vol. 165, pp 371–399. [PubMed: 31481170]

58. Jain P; Chaney A; Carlson ML; Jackson IM; Rao A; James ML Neuroinflammation PET imaging: Current opinion and future directions. J. Nucl. Med 2020, 61, 1107–1112. [PubMed: 32620705]

59. Meyer JH; Cervenka S; Kim M-J; Kreisl WC; Henter ID; Innis RB Neuroinflammation in psychiatric disorders: PET imaging and promising new targets. Lancet Psychiatry 2020, 7, 1064–1074. [PubMed: 33098761]

60. Lagarde J; Sarazin M; Bottlaender M In vivo PET imaging of neuroinflammation in Alzheimer's disease. J.Neural Transm 2018, 125, 847–867. [PubMed: 28516240]

61. Carter SF; Herholz K; Rosa-Neto P; Pellerin L; Nordberg A; Zimmer ER Astrocyte biomarkers in Alzheimer's disease. Trends Mol. Med 2019, 25, 77–95. [PubMed: 30611668]

62. Kreisl WC; Kim M-J; Coughlin JM; Henter ID; Owen DR; Innis RB PET imaging of neuroinflammation in neurological disorders. Lancet Neurol. 2020, 19, 940–950. [PubMed: 33098803]

63. Choi S-H; Langenbach R; Bosetti F Genetic deletion or pharmacological inhibition of cyclooxygenase-1 attenuate lipopolysaccharide- induced inflammatory response and brain injury. FASEB J. 2008, 22, 1491–1501. [PubMed: 18162486]

64. Shukuri M; Takashima-Hirano M; Tokuda K; Takashima T; Matsumura K; Inoue O; Doi H; Suzuki M; Watanabe Y; Onoe H In vivo expression of cyclooxygenase-1 in activated microglia and macrophages during neuroinflammation visualized by PET with 11C-ketoprofen methyl ester. J. Nucl. Med. 2011, 52, 1094–1101. [PubMed: 21680698]

65. Shrestha S; Singh P; Cortes-Salva MY; Jenko KJ; Ikawa M; Kim M-J; Kobayashi M; Morse CL; Gladding RL; Liow J-S; Zoghbi SS; Fujita M; Innis RB; Pike VW 3-Substituted 1,5-diaryl-1H-1,2,4-triazoles as prospective PET radioligands for imaging brain COX-1 in monkey. Part 2: selection and evaluation of [11C]PS13 for quantitative imaging. ACS Chem. Neurosci 2018, 9, 2620–2627. [PubMed: 29792035]

66. Anderson GD; Hauser SD; McGarity KL; Bremer ME; Isakson PC; Gregory SA Selective inhibition of cyclooxygenase (COX)-2 reverses inflammation and expression of COX-2 and interleukin 6 in rat adjuvant arthritis. J. Clin. Invest 1996, 97, 2672–2679. [PubMed: 8647962]

67. Shrestha S; Kim M-J; Eldridge M; Lehmann ML; Frankland M; Liow J-S; Yu Z-X; Cortes-Salva M; Telu S; Henter ID; Gallagher E; Lee J-H; Fredericks JM; Poffenberger C; Tye G; Ruiz-Perdomo Y; Anaya FJ; Montero Santamaria JA; Gladding RL; Zoghbi SS; Fujita M; Katz JD; Pike VW; Innis RB PET measurement of cyclooxygenase-2 using a novel radioligand: upregulation in primate neuroinflammation and first-in-human study. J. Neuroinflammation 2020, 17, 140. [PubMed: 32359360]

68. Rojo AI; McBean G; Cindric M; Egea J; López MG; Rada P; Zarkovic N; Cuadrado A Redox control of microglial function: Molecular mechanisms and functional significance. Antioxid. Redox Signal. 2014, 21, 1766–1801. [PubMed: 24597893]
69. Wilson AA; Sadovski O; Nobrega JN; Raymond RJ; Bambico FR; Nashed MG; Garcia A; Bloomfield PM; Houle S; Mizrahi R; Tong J Evaluation of a novel radiotracer for positron emission tomography imaging of reactive oxygen species in the central nervous system. Nucl. Med. Biol 2017, 53, 14–20. [PubMed: 28719807]
70. Hou C; Hsieh C-J; Li S; Lee H; Graham TJ; Xu K; Weng C-C; Doot RK; Chu W; Chakraborty SK; Dugan LL; Mintun MA; Mach RH Development of a positron emission tomography radiotracer for imaging elevated levels of superoxide in neuroinflammation. ACS Chem. Neurosci 2018, 9, 578–586. [PubMed: 29099578]
71. Egami H; Nakagawa S; Katsura Y; Kanazawa M; Nishiyama S; Sakai T; Arano Y; Tsukada H; Inoue O; Todoroki K; Hamashima Y 18F-Labeled dihydromethidine: positron emission tomography radiotracer for imaging of reactive oxygen species in intact brain. Org. Biomol. Chem 2020, 18, 2387–2391. [PubMed: 32073113]
72. Okamura T; Okada M; Kikuchi T; Wakizaka H; Zhang M-RA 11C-labeled 1,4-dihydroquinoline derivative as a potential PET tracer for imaging of redox status in mouse brain. J. Cereb. Blood Flow Metab 2015, 35, 1930–1936. [PubMed: 26082015]
73. Maresz K; Carrier EJ; Ponomarev ED; Hillard CJ; Dittel BN Modulation of the cannabinoid CB2 receptor in microglial cells in response to inflammatory stimuli. J. neurochem 2005, 95, 437–445. [PubMed: 16086683]
74. Horti AG; Gao Y; Ravert HT; Finley P; Valentine H; Wong DF; Endres CJ; Savonenko AV; Dannals RF Synthesis and biodistribution of [11C]A-836339, a new potential radioligand for PET imaging of cannabinoid type 2 receptors (CB2). Bioorg. Med. Chem 2010, 18, 5202–5207. [PubMed: 20554448]
75. Evens N; Vandeputte C; Coolen C; Janssen P; Sciot R; Baekelandt V; Verbruggen AM; Debyser Z; Van Laere K; Bormans GM Preclinical evaluation of [11C]NE40, a type 2 cannabinoid receptor PET tracer. Nucl. Med. Biol 2012, 39, 389–399. [PubMed: 22154685]
76. Haider A; Gobbi L; Kretz J; Ullmer C; Brink A; Honer M; Woltering TJ; Muri D; Iding H; Bürkler M; Binder M; Bartelmus C; Knuesel I; Pacher P; Herde AM; Spinelli F; Ahmed H; Atz K; Keller C; Weber M; Schibli R; Mu L; Grether U; Ametamey SM Identification and preclinical development of a 2,5,6-trisubstituted fluorinated pyridine derivative as a radioligand for the positron emission tomography imaging of cannabinoid type 2 receptors. J. Med. Chem 2020, 63, 10287–10306. [PubMed: 32787079]
77. Shih JC; Chen K; Ridd MJ Monoamine oxidase: From genes to behavior. Annu. Rev. Neurosci 1999, 22, 197–217. [PubMed: 10202537]
78. Fowler J; MacGregor R; Wolf A; Arnett C; Dewey S; Schlyer D; Christman D; Logan J; Smith M; Sachs H; al., e. Mapping human brain monoamine oxidase A and B with 11C-labeled suicide inactivators and PET. Science 1987, 235, 481–485. [PubMed: 3099392]
79. Bernard S; Fuseau C; Schmid L; Milcent R; Crouzel C Synthesis and in vivo studies of a specific monoamine oxidase B inhibitor: 5-[4-(benzyloxy)phenyl]-3-(2-cyanoethyl)-1,3,4-oxadiazol-[11C]-2(3H)-one. Eur. J. Nucl. Med 1996, 23, 150–156. [PubMed: 8925849]
80. Rusjan PM; Wilson AA; Miler L; Fan I; Mizrahi R; Houle S; Vasdev N; Meyer JH Kinetic modeling of the monoamine oxidase B radioligand [11C]SL25.1188 in human brain with high-resolution positron emission tomography. J. Cereb. Blood Flow Metab 2014, 34, 883–889. [PubMed: 24517979]
81. Villemagne VL; Harada R; Dore V; Furumoto S; Mulligan RS; Kudo Y; Burnham SC; Krishnadas N; Huang K; Yanai K; Rowe CC; Okamura N Evaluation of the novel 18F-labeled PET tracer SMBT-1 for imaging astrogliosis in healthy elderly controls and A+/T+/(N+) Alzheimer's disease patients. Alzheimer's & Dementia 2020, 16, e039858.
82. Tsai HC; Han MH Sphingosine-1-phosphate (S1P) and S1P signaling pathway: Therapeutic targets in autoimmunity and inflammation. Drugs 2016, 76, 1067–1079. [PubMed: 27318702]
83. Jin H; Yang H; Liu H; Zhang Y; Zhang X; Rosenberg AJ; Liu Y; Lapi SE; Tu Z A promising carbon-11-labeled sphingosine-1-phosphate receptor 1-specific PET tracer for imaging vascular injury. J. Nucl. Cardiol 2017, 24, 558–570. [PubMed: 26843200]

84. Luo Z; Han J; Liu H; Rosenberg AJ; Chen DL; Gropler RJ; Perlmutter JS; Tu Z Syntheses and in vitro biological evaluation of S1PR1 ligands and PET studies of four F-18 labeled radiotracers in the brain of nonhuman primates. Org Biomol Chem 2018, 16, 9171–9184. [PubMed: 30462126]

85. Tewari M; Seth P Emerging role of P2X7 receptors in CNS health and disease. Ageing Res. Rev 2015, 24, 328–342. [PubMed: 26478005]

86. Van Weehaeghe D; Koole M; Schmidt ME; Deman S; Jacobs AH; Souche E; Serdons K; Sunaert S; Bormans G; Vandenberghe W; Van Laere K [11C]JNJ54173717, a novel P2X7 receptor radioligand as marker for neuroinflammation: human biodistribution, dosimetry, brain kinetic modelling and quantification of brain P2X7 receptors in patients with Parkinson's disease and healthy volunteers. Eur. J. Nucl. Med. Mol. Imaging 2019, 46, 2051–2064. [PubMed: 31243495]

87. Koole M; Schmidt ME; Hijzen A; Ravenstijn P; Vandermeulen C; Van Weehaeghe D; Serdons K; Celen S; Bormans G; Ceusters M; Zhang W; Van Nueten L; Kolb H; de Hoon J; Van Laere K 18F-JNJ-64413739, a novel PET ligand for the P2X7 ion channel: radiation dosimetry, kinetic modeling, test-retest variability, and occupancy of the P2X7 antagonist JNJ-54175446. J. Nucl. Med 2019, 60, 683–690. [PubMed: 30262518]

88. Territo PR; Meyer JA; Peters JS; Riley AA; McCarthy BP; Gao M; Wang M; Green MA; Zheng QH; Hutchins GD Characterization of 11C-GSK1482160 for targeting the P2X7 receptor as a biomarker for neuroinflammation. J. Nucl. Med 2017, 58, 458–465. [PubMed: 27765863]

89. Hagens MHJ; Golla SSV; Janssen B; Vugts DJ; Beaino W; Windhorst AD; O'Brien-Brown J; Kassiou M; Schuit RC; Schwarte LA; de Vries HE; Killestein J; Barkhof F; van Berckel BNM; Lammertsma AA The P2X(7) receptor tracer [11C]SMW139 as an in vivo marker of neuroinflammation in multiple sclerosis: a first-in man study. Eur. J. Nucl. Med. Mol. Imaging 2020, 47, 379–389. [PubMed: 31705174]

90. Mildner A; Huang H; Radke J; Stenzel W; Priller J P2Y(12) receptor is expressed on human microglia under physiological conditions throughout development and is sensitive to neuroinflammatory diseases. Glia 2017, 65, 375–387. [PubMed: 27862351]

91. Janssen B; Vugts DJ; Molenaar GTT; Funke U; Kruijer PS; Dollé F; Bormans G; Lammertsma AA; Windhorst AD 18th European Symposium on Radiopharmacy and Radiopharmaceuticals: Synthesis of the first carbon-11 labelled P2Y12 receptor antagonist for imaging the anti-inflammatory phenotype of activated microglia. EJNMMI Radiopharm. Chem 2016, 1, 10.

92. De I; Steffen MD; Clark PA; Patros CJ; Sokn E; Bishop SM; Litscher S; Maklakova VI; Kuo JS; Rodriguez FJ; Collier LS CSF1 overexpression promotes high-grade glioma formation without impacting the polarization status of glioma-associated microglia and macrophages. Cancer Res. 2016, 76, 2552–2560. [PubMed: 27013192]

93. Tanzey SS; Shao X; Stauff J; Arteaga J; Sherman P; Scott PJH; Mossine AV Synthesis and initial in vivo evaluation of [11C]AZ683—A novel PET radiotracer for colony stimulating factor 1 receptor (CSF1R). Pharmaceuticals 2018, 11, 136.

94. Horti AG; Naik R; Foss CA; Minn I; Misheneva V; Du Y; Wang Y; Mathews WB; Wu Y; Hall A; LaCourse C; Ahn H-H; Nam H; Lesniak WG; Valentine H; Pletnikova O; Troncoso JC; Smith MD; Calabresi PA; Savonenko AV; Dannals RF; Pletnikov MV; Pomper MG PET imaging of microglia by targeting macrophage colony-stimulating factor 1 receptor (CSF1R). Proc. Natl. Acad. Sci 2019, 116, 1686–1691. [PubMed: 30635412]

95. Chuah YK; Basir R; Talib H; Tie TH; Nordin N Receptor for advanced glycation end products and its involvement in inflammatory diseases. Int. J. Inflam 2013, 2013, 403460. [PubMed: 24102034]

96. Cary BP; Brooks AF; Fawaz MV; Drake LR; Desmond TJ; Sherman P; Quesada CA; Scott PJH Synthesis and evaluation of [18F]RAGER: A first generation small-molecule PET radioligand targeting the receptor for advanced glycation endproducts. ACS Chem. Neurosci 2016, 7, 391–398. [PubMed: 26771209]

97. Drake LR; Brooks AF; Stauff J; Sherman PS; Arteaga J; Koeppe RA; Reed A; Montavon TJ; Skaddan MB; Scott PJH Strategies for PET imaging of the receptor for advanced glycation endproducts (RAGE). J. Pharm. Anal 2020, 10, 452–465. [PubMed: 33133729]

98. Tondo G; Perani D; Comi C TAM receptor pathways at the crossroads of neuroinflammation and neurodegeneration. Dis. Markers 2019, 2019, 2387614. [PubMed: 31636733]

99. Horti A; Dannals R; Pomper M [18F]JHU16907 for PET Imaging of MER tyrosine kinase (MERTK). J. Nucl. Med 2017, 58 (Suppl. 1), 209.

100. Kodani SD; Morisseau C Role of epoxy-fatty acids and epoxide hydrolases in the pathology of neuro-inflammation. Biochimie 2019, 159, 59–65. [PubMed: 30716359]

101. Coughlin JM; Slania S; Du Y; Shinehouse LK; Brosnan MK; Azad BB; Holt DP; Fan H; Lesniak WG; Minn I; Rowe SP; Dannals RF; Horti AG; Pomper MG First-in-human neuroimaging of soluble epoxide hydrolase using [18F]FNDP PET. Eur. J. Nucl. Med. Mol. Imaging 2021, 48, 3122–3128. [PubMed: 33585963]

102. Pearse DD; Hughes ZA PDE4B as a microglia target to reduce neuroinflammation. Glia 2016, 64, 1698–1709. [PubMed: 27038323]

103. Zhang L; Chen L; Beck EM; Chappie TA; Coelho RV; Doran SD; Fan KH; Helal CJ; Humphrey JM; Hughes Z; Kuszpit K; Lachapelle EA; Lazzaro JT; Lee C; Mather RJ; Patel NC; Skaddan MB; Sciabola S; Verhoest PR; Young JM; Zasadny K; Villalobos A The discovery of a novel phosphodiesterase (PDE) 4B-preferring radioligand for positron emission tomography (PET) imaging. J. Med. Chem 2017, 60, 8538–8551. [PubMed: 28957634]

104. Xiang J; Wang X; Gao Y; Li T; Cao R; Yan T; Ma Y; Niu Y; Xue J; Wang B Phosphodiesterase 4D gene modifies the functional network of patients with mild cognitive impairment and Alzheimer's disease. Front. Genet 2020, 11, 890. [PubMed: 32849849]

105. Wakabayashi Y; Telu S; Dick RM; Fujita M; Ooms M; Morse CL; Liow J-S; Hong JS; Gladding RL; Manly LS; Zoghbi SS; Mo X; D'Amato EC; Sindac JA; Nugent RA; Marron BE; Gurney ME; Innis RB; Pike VW Discovery, radiolabeling, and evaluation of subtype-selective inhibitors for positron emission tomography imaging of brain phosphodiesterase-4D. ACS Chem. Neurosci 2020, 11, 1311–1323. [PubMed: 32212718]

106. Morales-Garcia JA; Alonso-Gil S; Santos Á; Perez-Castillo A Phosphodiesterase 7 regulation in cellular and rodent models of Parkinson's disease. Mol. Neurobiol. 2020, 57, 806–822. [PubMed: 31473904]

107. Obokata N; Seki C; Hirata T; Maeda J; Ishii H; Nagai Y; Matsumura T; Takakuwa M; Fukuda H; Minamimoto T; Kawamura K; Zhang M-R; Nakajima T; Saijo T; Higuchi M Synthesis and preclinical evaluation of [11C]MTP38 as a novel PET ligand for phosphodiesterase 7 in the brain. Eur. J. Nucl. Med. Mol. Imaging 2021, 48, 3101–3112. [PubMed: 33674894]

108. Dénes Á; Ferenczi S; Halász J; Környei Z; Kovács KJ Role of CX3CR1 (fractalkine receptor) in brain damage and inflammation induced by focal cerebral ischemia in mouse. J. Cereb. Blood Flow Metab 2008, 28, 1707–1721. [PubMed: 18575457]

109. Mease R; Yang X; Foss C; Pomper M Radiosynthesis and initial in vivo evaluation of 2-[18F]FBTTP, a radiotracer targeting CX3CR1. J. Nucl. Med 2015, 56, 356–356.

110. He Y; Hara H; Núñez G Mechanism and regulation of NLRP3 inflammasome activation. Trends Biochem. Sci 2016, 41, 1012–1021. [PubMed: 27669650]

111. Hill JR; Shao X; Massey NL; Stauff J; Sherman PS; Robertson AAB; Scott PJH Synthesis and evaluation of NLRP3-inhibitory sulfonylurea [11C]MCC950 in healthy animals. Bioorg. Med. Chem. Lett 2020, 30, 127186. [PubMed: 32312583]

112. Maiocchi SL; Ku J; Thai T; Chan E; Rees MD; Thomas SR Myeloperoxidase: A versatile mediator of endothelial dysfunction and therapeutic target during cardiovascular disease. Pharmacol. Ther 2021, 221, 107711. [PubMed: 33137376]

113. Jucaite A; Svenningsson P; Rinne JO; Cselényi Z; Varnäs K; Johnström P; Amini N; Kirjavainen A; Helin S; Minkwitz M; Kugler AR; Posener JA; Budd S; Halldin C; Varrone A; Farde L Effect of the myeloperoxidase inhibitor AZD3241 on microglia: a PET study in Parkinson's disease. Brain 2015, 138, 2687–2700. [PubMed: 26137956]

114. Wang C; Keliher E; Zeller MWG; Wojtkiewicz GR; Aguirre AD; Buckbinder L; Kim H-Y; Chen J; Maresca K; Ahmed MS; Motlagh NJ; Nahrendorf M; Chen JW An activatable PET imaging radioprobe is a dynamic reporter of myeloperoxidase activity in vivo. Proc. Natl. Acad. Sci 2019, 116, 11966–11971. [PubMed: 31123149]

115. Leroy K; Brion J-P Developmental expression and localization of glycogen synthase kinase-3β in rat brain. J. Chem. Neuroanat 1999, 16, 279–293. [PubMed: 10450875]

116. Bernard-Gauthier V; Mossine AV; Knight A; Patnaik D; Zhao W-N; Cheng C; Krishnan HS; Xuan LL; Chindavong PS; Reis SA; Chen JM; Shao X; Stauff J; Arteaga J; Sherman P; Salem N; Bonsall D; Amaral B; Varlow C; Wells L; Martarello L; Patel S; Liang SH; Kurumbail RG;

Haggarty SJ; Scott PJH; Vasdev N Structural basis for achieving GSK-3β inhibition with high potency, selectivity, and brain exposure for positron emission tomography imaging and drug discovery. J. Med. Chem 2019, 62, 9600–9617. [PubMed: 31535859]

117. Aïd S; Bosetti F Targeting cyclooxygenases-1 and −2 in neuroinflammation: Therapeutic implications. Biochimie 2011, 93, 46–51. [PubMed: 20868723]
118. Yang H; Chen C Cyclooxygenase-2 in synaptic signaling. Curr. Pharm. Des 2008, 14, 1443–1451. [PubMed: 18537667]
119. Phillis JW; Horrocks LA; Farooqui AA Cyclooxygenases, lipoxygenases, and epoxygenases in CNS: Their role and involvement in neurological disorders. Brain Res.Rev 2006, 52, 201–243. [PubMed: 16647138]
120. Matousek SB; Hein AM; Shaftel SS; Olschowka JA; Kyrkanides S; O'Banion MK Cyclooxygenase-1 mediates prostaglandin E2 elevation and contextual memory impairment in a model of sustained hippocampal interleukin-1β expression. J. Neurochem 2010, 114, 247–258. [PubMed: 20412387]
121. Choi S-H; Bosetti F Cyclooxygenase-1 null mice show reduced neuroinflammation in response to beta-amyloid. Aging 2009, 1, 234–244. [PubMed: 20157512]
122. Choi S-H; Aid S; Caracciolo L; Sakura Minami S; Niikura T; Matsuoka Y; Turner RS; Mattson MP; Bosetti F Cyclooxygenase-1 inhibition reduces amyloid pathology and improves memory deficits in a mouse model of Alzheimer's disease. J. Neurochem 2013, 124, 59–68. [PubMed: 23083210]
123. Kikuchi T; Okada M; Nengaki N; Furutsuka K; Wakizaka H; Okamura T; Zhang M-R; Kato K Efficient synthesis and chiral separation of 11C-labeled ibuprofen assisted by DMSO for imaging of in vivo behavior of the individual isomers by positron emission tomography. Bioorg. Med. Chem 2011, 19, 3265–3273. [PubMed: 21515058]
124. Warner TD; Giuliano F; Vojnovic I; Bukasa A; Mitchell JA; Vane JR Nonsteroid drug selectivities for cyclo-oxygenase-1 rather than cyclo-oxygenase-2 are associated with human gastrointestinal toxicity: A full in vitro analysis. Proc. Natl. Acad. Sci 1999, 96, 7563–7568. [PubMed: 10377455]
125. Ohnishi A; Senda M; Yamane T; Sasaki M; Mikami T; Nishio T; Ikari Y; Nishida H; Shukuri M; Takashima T; Mawatari A; Doi H; Watanabe Y; Onoe H Human whole-body biodistribution and dosimetry of a new PET tracer, [11C]ketoprofen methyl ester, for imagings of neuroinflammation. Nucl. Med. Biol 2014, 41, 594–599. [PubMed: 24853403]
126. Singh P; Shrestha S; Cortes-Salva MY; Jenko KJ; Zoghbi SS; Morse CL; Innis RB; Pike VW 3-Substituted 1,5-diaryl-1H-1,2,4-triazoles as prospective PET radioligands for imaging brain COX-1 in monkey. Part 1: synthesis and pharmacology. ACS Chem. Neurosci 2018, 9, 2610–2619. [PubMed: 29678105]
127. Shrestha S; Singh P; Eldridge M; Cortes M; Gladding R; Morse C; Zoghbi S; Fujita M; Liow J-S; Pike V A novel PET radioligand, [11C]PS13, successfully images COX-1, a potential biomarker for neuroinflammation. J. Nucl. Med 2016, 57 (Suppl 2), 115–115. [PubMed: 26514178]
128. Kim M-J; Lee J-H; Juarez Anaya F; Hong J; Miller W; Telu S; Singh P; Cortes MY; Henry K; Tye GL; Frankland MP; Montero Santamaria JA; Liow J-S; Zoghbi SS; Fujita M; Pike VW; Innis RB First-in-human evaluation of [11C]PS13, a novel PET radioligand, to quantify cyclooxygenase-1 in the brain. Eur. J. Nucl. Med. Mol. Imaging 2020, 47, 3143–3151. [PubMed: 32399622]
129. Minghetti L Role of COX-2 in inflammatory and degenerative brain diseases. In Inflammation in the pathogenesis of chronic diseases: The COX-2 controversy, Harris RE; Bittman R; Dasgupta D; Engelhardt H; Flohe L; Herrmann H; Holzenburg A; Nasheuer HP; Rottem S; Wyss M; Zwickl P, Eds. Springer Netherlands: Dordrecht, 2007; pp 127–141.
130. Aid S; Langenbach R; Bosetti F Neuroinflammatory response to lipopolysaccharide is exacerbated in mice genetically deficient in cyclooxygenase-2. J. Neuroinflammation 2008, 5, 17. [PubMed: 18489773]
131. de Vries EFJ; van Waarde A; Buursma AR; Vaalburg W Synthesis and in vivo evaluation of 18F-desbromo-DuP-697 as a PET tracer for cyclooxygenase-2 expression. J. Nucl. Med 2003, 44, 1700–1706. [PubMed: 14530489]

132. Prabhakaran J; Majo VJ; Simpson NR; Van Heertum RL; Mann JJ; Kumar JSD Synthesis of [11C]celecoxib: a potential PET probe for imaging COX-2 expression. J. Labelled Comp. Radiopharm 2005, 48, 887–895.

133. Ji B; Kumata K; Onoe H; Kaneko H; Zhang M-R; Seki C; Ono M; Shukuri M; Tokunaga M; Minamihisamatsu T; Suhara T; Higuchi M Assessment of radioligands for PET imaging of cyclooxygenase-2 in an ischemic neuronal injury model. Brain Res. 2013, 1533, 152–162. [PubMed: 23973859]

134. Kumar JSD; Bai B; Zanderigo F; DeLorenzo C; Prabhakaran J; Parsey RV; Mann JJ In vivo brain imaging, biodistribution, and radiation dosimetry estimation of [11C]Celecoxib, a COX-2 PET ligand, in nonhuman primates. Molecules 2018, 23, 1929.

135. Prabhakaran J; Underwood MD; Parsey RV; Arango V; Majo VJ; Simpson NR; Van Heertum R; Mann JJ; Kumar JSD Synthesis and in vivo evaluation of [18F]-4-[5-(4-methylphenyl)-3-(trifluoromethyl)-1H-pyrazol-1-yl]benzenesulfonamide as a PET imaging probe for COX-2 expression. Bioorg. Med. Chem 2007, 15, 1802–1807. [PubMed: 17166726]

136. Fujisaki Y; Kawamura K; Wang W-F; Ishiwata K; Yamamoto F; Kuwano T; Ono M; Maeda M Radiosynthesis andin vivo evaluation of 11C-Iabeled 1,5-diarylpyrazole derivatives for mapping cyclooxygenases. Ann. Nucl. Med 2005, 19, 617. [PubMed: 16363629]

137. Kaur J; Tietz O; Bhardwaj A; Marshall A; Way J; Wuest M; Wuest F Design, synthesis, and evaluation of an 18F-labeled radiotracer based on Celecoxib–NBD for positron emission tomography (PET) imaging of cyclooxygenase-2 (COX-2). ChemMedChem 2015, 10, 1635–1640. [PubMed: 26287271]

138. Lebedev A; Jiao J; Lee J; Yang F; Allison N; Herschman H; Sadeghi S Radiochemistry on electrodes: Synthesis of an 18F-labelled and in vivo stable COX-2 inhibitor. PLOS One 2017, 12, e0176606. [PubMed: 28464017]

139. De Vries EFJ; Doorduin J; Dierckx RA; van Waarde A Evaluation of [11C]rofecoxib as PET tracer for cyclooxygenase 2 overexpression in rat models of inflammation. Nucl. Med. Biol 2008, 35, 35–42. [PubMed: 18158941]

140. Comley RA; Passchier J; Willemsen A; Wall A; Bergstrom M; Langstrom B; Pruim J; Wishart M; Rabiner E; Gunn RN; Antoni G; de Vries E; Matthews J Uptake and regional distribution of [11C]rofecoxib in human brain. NeuroImage 2010, 52, S135–S136.

141. Tanaka M; Fujisaki Y; Kawamura K; Ishiwata K; Qinggeletu Yamamoto, F.; Mukai T; Maeda M Radiosynthesis and evaluation of 11C-labeled diaryl-substituted imidazole and indole derivatives for mapping cyclooxygenase-2. Biol. Pharm. Bull 2006, 29, 2087–2094. [PubMed: 17015956]

142. Wuest F; Kniess T; Bergmann R; Pietzsch J Synthesis and evaluation in vitro and in vivo of a 11C-labeled cyclooxygenase-2 (COX-2) inhibitor. Bioorg. Med. Chem 2008, 16, 7662–7670. [PubMed: 18650097]

143. Elie J; Vercouillie J; Arlicot N; Lemaire L; Bidault R; Bodard S; Hosselet C; Deloye J-B; Chalon S; Emond P; Guilloteau D; Buron F; Routier S Design of selective COX-2 inhibitors in the (aza)indazole series. Chemistry, in vitro studies, radiochemistry and evaluations in rats of a [18F] PET tracer. J. Enzyme Inhib. Med. Chem 2019, 34, 1–7.

144. Toyokuni T; Dileep Kumar JS; Walsh JC; Shapiro A; Talley JJ; Phelps ME; Herschman HR; Barrio JR; Satyamurthy N Synthesis of 4-(5-[18F]fluoromethyl-3-phenylisoxazol-4-yl)benzenesulfonamide, a new [18F]fluorinated analogue of valdecoxib, as a potential radiotracer for imaging cyclooxygenase-2 with positron emission tomography. Bioorg. Med. Chem. Lett 2005, 15, 4699–4702. [PubMed: 16153836]

145. Kumar JSD; Zanderigo F; Prabhakaran J; Rubin-Falcone H; Parsey RV; Mann JJ In vivo evaluation of [11C]TMI, a COX-2 selective PET tracer, in baboons. Bioorg. Med. Chem. Lett 2018, 28, 3592–3595. [PubMed: 30396759]

146. Prabhakaran J; Underwood M; Zanderigo F; Simpson NR; Cooper AR; Matthew J; Rubin-Falcone H; Parsey RV; Mann JJ; Dileep Kumar JS Radiosynthesis and in vivo evaluation of [11C]MOV as a PET imaging agent for COX-2. Bioorg. Med. Chem. Lett 2018, 28, 2432–2435. [PubMed: 29929881]

147. Tietz O; Wuest M; Marshall A; Glubrecht D; Hamann I; Wang M; Bergman C; Way JD; Wuest F PET imaging of cyclooxygenase-2 (COX-2) in a pre-clinical colorectal cancer model. EJNMMI Res. 2016, 6, 37. [PubMed: 27112768]

148. Cortes M; Singh P; Morse C; Shrestha S; Jenko K; Kowalski A; Zoghbi S; Fujita M; Innis R; Pike V Synthesis of PET radioligands as potential probes for imaging COX-2 in neuroinflammation. J. Nucl. Med 2015, 56 (suppl 3), 1092–1092.

149. Kim M-J; Shrestha S; Eldridge M; Cortes M; Singh P; Liow J-S; Gladding R; Zoghbi S; Fujita M; Pike V; Innis R Novel PET radioligands show that, in rhesus monkeys, COX-1 is constitutively expressed and COX-2 is induced by inflammation. J. Nucl. Med 2017, 58 (suppl 1), 203–203.

150. Cortes-Salva MY; Shrestha S; Singh P; Morse CL; Jenko KJ; Montero Santamaria JA; Zoghbi SS; Innis RB; Pike VW 2-(4-Methylsulfonylphenyl)pyrimidines as prospective radioligands for imaging cyclooxygenase-2 with PET—Synthesis, triage, and radiolabeling. Molecules 2018, 23, 2850.

151. Gallagher E; Shrestha S; Eldridge M; Cortes M; Yu Z-X; Lehmann M; Kim M-J; Singh P; Fredericks M; Tye G; Saunders R; Gladding R; Liow J-S; Fujita M; Zoghbi S; Pike V; Innis R T80. Novel PET Radioligands Show That COX-2, but not COX-1, is Induced by Neuroinflammation in Rhesus Macaque. Biol. Psychiatry 2018, 83 (suppl 9), S160.

152. Kim M-J; Shrestha SS; Cortes M; Singh P; Morse C; Liow J-S; Gladding RL; Brouwer C; Henry K; Gallagher E; Tye GL; Zoghbi SS; Fujita M; Pike VW; Innis RB Evaluation of two potent and selective PET radioligands to image COX-1 and COX-2 in rhesus monkeys. J. Nucl. Med 2018, 59, 1907–1912. [PubMed: 29959215]

153. Valko M; Leibfritz D; Moncol J; Cronin MTD; Mazur M; Telser J Free radicals and antioxidants in normal physiological functions and human disease. Int. J. Biochem. Cell Biol 2007, 39, 44–84. [PubMed: 16978905]

154. Hsieh H-L; Yang C-M Role of redox signaling in neuroinflammation and neurodegenerative diseases. Biomed Res. Int 2013, 2013, 484613. [PubMed: 24455696]

155. Kuka S; Tatarkova Z; Racay P; Lehotsky J; Dobrota D; Kaplan P Effect of aging on formation of reactive oxygen species by mitochondria of rat heart. Gen. Physiol. Biophys. 2013, 32, 415–420. [PubMed: 23817642]

156. Shi Q; Gibson GE Oxidative stress and transcriptional regulation in Alzheimer disease. Alzheimer Dis. Assoc. Disord 2007, 21, 276–291. [PubMed: 18090434]

157. Jenner P; Olanow CW The pathogenesis of cell death in Parkinson's disease. Neurology 2006, 66, S24–S36. [PubMed: 16717250]

158. Carroll VN; Truillet C; Shen B; Flavell RR; Shao X; Evans MJ; VanBrocklin HF; Scott PJH; Chin FT; Wilson DM [11C]Ascorbic and [11C]dehydroascorbic acid, an endogenous redox pair for sensing reactive oxygen species using positron emission tomography. Chem. Commun 2016, 52, 4888–4890.

159. Chu W; Chepetan A; Zhou D; Shoghi KI; Xu J; Dugan LL; Gropler RJ; Mintun MA; Mach RH Development of a PET radiotracer for non-invasive imaging of the reactive oxygen species, superoxide, in vivo. Org. Biomol. Chem 2014, 12, 4421–4431. [PubMed: 24847866]

160. Cabral G; Marciano-Cabral F Cannabinoid receptors in microglia of the central nervous system: immune functional relevance. J. Leukoc. Biol 2005, 78, 1192–1197. [PubMed: 16204639]

161. Navarro G; Morales P; Rodriguez-Cueto C; Fernandez-Ruiz J; Jagerovic N; Franco R Targeting Cannabinoid CB2 Receptors in the Central Nervous System. Medicinal Chemistry Approaches with Focus on Neurodegenerative Disorders. Front Neurosci 2016, 10, 406. [PubMed: 27679556]

162. Di Marzo V New approaches and challenges to targeting the endocannabinoid system. Nat. Rev. Drug Discov 2018, 17, 623–639. [PubMed: 30116049]

163. López A; Aparicio N; Pazos MR; Grande MT; Barreda-Manso MA; Benito-Cuesta I; Vázquez C; Amores M; Ruiz-Pérez G; García-García E; Beatka M; Tolón RM; Dittel BN; Hillard CJ; Romero J Cannabinoid CB2 receptors in the mouse brain: relevance for Alzheimer's disease. J. Neuroinflammation 2018, 15, 158. [PubMed: 29793509]

164. Chen WW; Zhang X; Huang WJ Role of neuroinflammation in neurodegenerative diseases (Review). Mol. Med. Rep 2016, 13, 3391–3396. [PubMed: 26935478]

165. Turcotte C; Blanchet MR; Laviolette M; Flamand N The CB2 receptor and its role as a regulator of inflammation. Cell. Mol. Life Sci 2016, 73, 4449–4470. [PubMed: 27402121]

166. Acikalin MY; Gorgolewski KJ; Poldrack RA A coordinate-based meta-analysis of overlaps in regional specialization and functional connectivity across subjective value and default mode networks. Front. Neurosci 2017, 11, 1. [PubMed: 28154520]

167. Nevalainen T Recent development of CB2 selective and peripheral CB1/CB2 cannabinoid receptor ligands. Curr. Med. Chem 2014, 21, 187–203. [PubMed: 24164198]

168. Xing C; Zhuang Y; Xu TH; Feng Z; Zhou XE; Chen M; Wang L; Meng X; Xue Y; Wang J; Liu H; McGuire TF; Zhao G; Melcher K; Zhang C; Xu HE; Xie XQ Cryo-EM structure of the human cannabinoid receptor CB2-Gi signaling complex. Cell 2020, 180, 645–654.e13. [PubMed: 32004460]

169. Moldovan RP; Teodoro R; Gao Y; Deuther-Conrad W; Kranz M; Wang Y; Kuwabara H; Nakano M; Valentine H; Fischer S; Pomper MG; Wong DF; Dannals RF; Brust P; Horti AG Development of a high-affinity PET radioligand for imaging cannabinoid subtype 2 receptor. J. Med. Chem 2016, 59, 7840–7855. [PubMed: 27500461]

170. Savonenko AV; Melnikova T; Wang Y; Ravert H; Gao Y; Koppel J; Lee D; Pletnikova O; Cho E; Sayyida N; Hiatt A; Troncoso J; Davies P; Dannals RF; Pomper MG; Horti AG Cannabinoid CB2 receptors in a mouse model of Aβ amyloidosis: Immunohistochemical analysis and suitability as a PET biomarker of neuroinflammation. PLoS One 2015, 10, e0129618. [PubMed: 26086915]

171. Pottier G; Gomez-Vallejo V; Padro D; Boisgard R; Dolle F; Llop J; Winkeler A; Martin A PET imaging of cannabinoid type 2 receptors with [11C]A-836339 did not evidence changes following neuroinflammation in rats. J. Cereb. Blood Flow Metab 2017, 37, 1163–1178. [PubMed: 28079433]

172. Ahmad R; Koole M; Evens N; Serdons K; Verbruggen A; Bormans G; Van Laere K Whole-body biodistribution and radiation dosimetry of the cannabinoid type 2 receptor ligand [11C]-NE40 in healthy subjects. Mol. Imaging Biol 2013, 15, 384–90. [PubMed: 23508466]

173. Raitio KH; Savinainen JR; Vepsäläinen J; Laitinen JT; Poso A; Järvinen T; Nevalainen T Synthesis and SAR studies of 2-oxoquinoline derivatives as CB2 receptor inverse agonists. J. Med. Chem 2006, 49, 2022–2027. [PubMed: 16539390]

174. Evens N; Muccioli GG; Houbrechts N; Lambert DM; Verbruggen AM; Van Laere K; Bormans GM Synthesis and biological evaluation of carbon-11- and fluorine-18-labeled 2-oxoquinoline derivatives for type 2 cannabinoid receptor positron emission tomography imaging. Nucl. Med. Biol 2009, 36, 455–465. [PubMed: 19423014]

175. Ahmad R; Postnov A; Bormans G; Versijpt J; Vandenbulcke M; Van Laere K Decreased in vivo availability of the cannabinoid type 2 receptor in Alzheimer's disease. Eur. J. Nucl. Med. Mol. Imaging 2016, 43, 2219–2227. [PubMed: 27488857]

176. Slavik R; Herde AM; Bieri D; Weber M; Schibli R; Kramer SD; Ametamey SM; Mu L Synthesis, radiolabeling and evaluation of novel 4-oxo-quinoline derivatives as PET tracers for imaging cannabinoid type 2 receptor. Eur. J. Med. Chem 2015, 92, 554–564. [PubMed: 25599952]

177. Mu L; Bieri D; Slavik R; Drandarov K; Muller A; Cermak S; Weber M; Schibli R; Kramer SD; Ametamey SM Radiolabeling and in vitro /in vivo evaluation of N-(1-adamantyl)-8-methoxy-4-oxo-1-phenyl-1,4-dihydroquinoline-3-carboxamide as a PET probe for imaging cannabinoid type 2 receptor. J. Neurochem 2013, 126, 616–624. [PubMed: 23795580]

178. Meletta R; Slavik R; Mu L; Rancic Z; Borel N; Schibli R; Ametamey SM; Kramer SD; Muller Herde A Cannabinoid receptor type 2 (CB2) as one of the candidate genes in human carotid plaque imaging: Evaluation of the novel radiotracer [11C]RS-016 targeting CB2 in atherosclerosis. Nucl. Med. Biol 2017, 47, 31–43. [PubMed: 28104528]

179. Slavik R; Muller Herde A; Haider A; Kramer SD; Weber M; Schibli R; Ametamey SM; Mu L Discovery of a fluorinated 4-oxo-quinoline derivative as a potential positron emission tomography radiotracer for imaging cannabinoid receptor type 2. J. Neurochem 2016, 138, 874–886. [PubMed: 27385045]

180. Haider A; Spinelli F; Herde AM; Mu B; Keller C; Margelisch M; Weber M; Schibli R; Mu L; Ametamey SM Evaluation of 4-oxo-quinoline-based CB2 PET radioligands in R6/2 chorea huntington mouse model and human ALS spinal cord tissue. Eur. J. Med. Chem 2018, 145, 746–759. [PubMed: 29353725]

181. Ahamed M; van Veghel D; Ullmer C; Van Laere K; Verbruggen A; Bormans GM Synthesis, biodistribution and in vitro evaluation of brain permeable high affinity type 2 cannabinoid receptor agonists [11C]MA2 and [18F]MA3. Front. Neurosci 2016, 10, 431. [PubMed: 27713686]

182. Attili B; Celen S; Ahamed M; Koole M; Haute CVD; Vanduffel W; Bormans G Preclinical evaluation of [18F]MA3: a CB2 receptor agonist radiotracer for PET. Br. J. Pharmacol 2019, 176, 1481–1491. [PubMed: 30588600]

183. Hortala L; Arnaud J; Roux P; Oustric D; Boulu L; Oury-Donat F; Avenet P; Rooney T; Alagille D; Barret O; Tamagnan G; Barth F Synthesis and preliminary evaluation of a new fluorine-18 labelled triazine derivative for PET imaging of cannabinoid CB2 receptor. Bioorg. Med. Chem. Lett 2014, 24, 283–287. [PubMed: 24291040]

184. Yrjola S; Sarparanta M; Airaksinen AJ; Hytti M; Kauppinen A; Pasonen-Seppanen S; Adinolfi B; Nieri P; Manera C; Keinanen O; Poso A; Nevalainen TJ; Parkkari T Synthesis, in vitro and in vivo evaluation of 1,3,5-triazines as cannabinoid CB2 receptor agonists. Eur. J. Pharm. Sci 2015, 67, 85–96. [PubMed: 25447744]

185. Slavik R; Grether U; Muller Herde A; Gobbi L; Fingerle J; Ullmer C; Kramer SD; Schibli R; Mu L; Ametamey SM Discovery of a high affinity and selective pyridine analog as a potential positron emission tomography imaging agent for cannabinoid type 2 receptor. J. Med. Chem 2015, 58, 4266–4277. [PubMed: 25950914]

186. Xaio H; Banks WA; Niehoff ML; Morley JE Effect of LPS on the permeability of the blood-brain barrier to insulin. Brain Res. 2001, 896, 36–42. [PubMed: 11277970]

187. Haider A; Kretz J; Gobbi L; Ahmed H; Atz K; Bürkler M; Bartelmus C; Fingerle J; Guba W; Ullmer C; Honer M; Knuesel I; Weber M; Brink A; Herde AM; Keller C; Schibli R; Mu L; Grether U; Ametamey SM Structure–activity relationship studies of pyridine-based ligands and identification of a fluorinated derivative for positron emission tomography imaging of cannabinoid type 2 receptors. J. Med. Chem 2019, 62, 11165–11181. [PubMed: 31751140]

188. Shih JC; Wu JB; Chen K Transcriptional regulation and multiple functions of MAO genes. J. Neural. Transm 2011, 118, 979–986. [PubMed: 21359973]

189. Wang CC; Borchert A; Ugun-Klusek A; Tang LY; Lui WT; Chu CY; Billett E; Kuhn H; Ufer C Monoamine oxidase a expression is vital for embryonic brain development by modulating developmental apoptosis. J. Biol. Chem 2011, 286, 28322–28330. [PubMed: 21697081]

190. Tong J; Meyer JH; Furukawa Y; Boileau I; Chang L-J; Wilson AA; Houle S Distribution of monoamine oxidase proteins in human vrain: Implications for brain imaging studies. J. Cereb. Blood Flow Metab 2013, 33, 863–871. [PubMed: 23403377]

191. Sánchez-Rodríguez R; Munari F; Angioni R; Venegas F; Agnellini A; Castro-Gil MP; Castegna A; Luisetto R; Viola A; Canton M Targeting monoamine oxidase to dampen NLRP3 inflammasome activation in inflammation. Cell. Mol. Immunol 2020.

192. Liu Y; Feng S; Subedi K; Wang H Attenuation of ischemic ctroke-caused brain injury by a monoamine oxidase inhibitor involves improved proteostasis and reduced neuroinflammation. Mol. Neurobiol 2020, 57, 937–948. [PubMed: 31620993]

193. Cusin C; Serretti A; Lattuada E; Lilli R; Lorenzi C; Smeraldi E Association study of MAO-A, COMT, 5-HT2A, DRD2, and DRD4 polymorphisms with illness time course in mood disorders. Am. J. Med. Genet 2002, 114, 380–390. [PubMed: 11992560]

194. Serretti A; Cristina S; Lilli R; Cusin C; Lattuada E; Lorenzi C; Corradi B; Grieco G; Costa A; Santorelli F; Barale F; Nappi G; Smeraldi E Family-based association study of 5-HTTLPR, TPH, MAO-A, and DRD4 polymorphisms in mood disorders. Am. J. Med. Genet 2002, 114, 361–369. [PubMed: 11992558]

195. Serretti A; Lorenzi C; Lilli R; Mandelli L; Pirovano A; Smeraldi E Pharmacogenetics of lithium prophylaxis in mood disorders: Analysis of COMT, MAO-A, and Gβ3 variants. Am. J. Med. Genet. 2002, 114, 370–379. [PubMed: 11992559]

196. Serretti A; Mandelli L; Lorenzi C; Landoni S; Calati R; Insacco C; Cloninger CR Temperament and character in mood disorders: Influence of DRD4, SERTPR, TPH and MAO-A polymorphisms. Neuropsychobiology 2006, 53, 9–16. [PubMed: 16319504]

197. Bortolato M; Chen K; Shih JC Monoamine oxidase inactivation: From pathophysiology to therapeutics. Adv. Drug Deliv. Rev 2008, 60, 1527–1533. [PubMed: 18652859]

198. Shoulson I DATATOP: a decade of neuroprotective inquiry. Parkinson study group. Deprenyl and tocopherol antioxidative therapy of parkinsonism. Ann Neurol. 1998, 44, S160–166. [PubMed: 9749589]

199. Checkoway H; Franklin GM; Costa-Mallen P; Smith-Weller T; Dilley J; Swanson PD; Costa LG A genetic polymorphism of MAO-B modifies the association of cigarette smoking and Parkinson's disease. Neurology 1998, 50, 1458–1461. [PubMed: 9596006]

200. Foley P; Gerlach M; Youdim MBH; Riederer P MAO-B inhibitors: multiple roles in the therapy of neurodegenerative disorders? Parkinsonism Relat. Disord 2000, 6, 25–47. [PubMed: 18591148]

201. Mandel S; Grünblatt E; Riederer P; Gerlach M; Levites Y; Youdim MBH Neuroprotective strategies in Parkinson's disease : an update on progress. CNS drugs 2003, 17, 729–762. [PubMed: 12873156]

202. Lecht S; Haroutiunian S; Hoffman A; Lazarovici P Rasagiline - a novel MAO B inhibitor in Parkinson's disease therapy. Ther. Clin. Risk Manag 2007, 3, 467–474. [PubMed: 18488080]

203. Mallajosyula JK; Kaur D; Chinta SJ; Rajagopalan S; Rane A; Nicholls DG; Di Monte DA; Macarthur H; Andersen JK MAO-B elevation in mouse brain astrocytes results in Parkinson's pathology. PLoS One 2008, 3, e1616. [PubMed: 18286173]

204. Gökhan-Kelekçi N; Yabanoğlu S; Küpeli E; Salgın U; Özgen Ö; Uçar G; Yeşilada E; Kendi E; Yeşilada A; Bilgin AA A new therapeutic approach in Alzheimer disease: Some novel pyrazole derivatives as dual MAO-B inhibitors and antiinflammatory analgesics. Bioorg. Med. Chem 2007, 15, 5775–5786. [PubMed: 17611112]

205. Huang L; Lu C; Sun Y; Mao F; Luo Z; Su T; Jiang H; Shan W; Li X Multitarget-directed benzylideneindanone derivatives: Anti-β-amyloid (Aβ) aggregation, antioxidant, metal chelation, and monoamine oxidase B (MAO-B) inhibition properties against Alzheimer's disease. J. Med. Chem 2012, 55, 8483–8492. [PubMed: 22978824]

206. Tong J; Rathitharan G; Meyer JH; Furukawa Y; Ang L-C; Boileau I; Guttman M; Hornykiewicz O; Kish SJ Brain monoamine oxidase B and A in human parkinsonian dopamine deficiency disorders. Brain 2017, 140, 2460–2474. [PubMed: 29050386]

207. Fowler CJ; Mantle TJ; Tipton KF The nature of the inhibition of rat liver monoamine oxidase types A and B by the acetylenic inhibitors clorgyline, L-deprenyl and pargyline. Biochem. Pharmacol 1982, 31, 3555–3561. [PubMed: 6817759]

208. MacGregor RR; Halldin C; Fowler JS; Wolf AP; Arnett CD; Langström B; Alexoff D Selective, irreversible in vivo binding of [11C]clorgyline and [11C]-L-deprenyl in mice: Potential for measurement of functional monoamine oxidase activity in brain using positron emission tomography. Biochem. Pharmacol 1985, 34, 3207–3210. [PubMed: 3929788]

209. Gulyás B; Pavlova E; Kása P; Gulya K; Bakota L; Várszegi S; Keller É; Horváth MC; Nag S; Hermecz I; Magyar K; Halldin C Activated MAO-B in the brain of Alzheimer patients, demonstrated by [11C]-L-deprenyl using whole hemisphere autoradiography. Neurochem. Int 2011, 58, 60–68. [PubMed: 21075154]

210. Nag S; Varrone A; TÓth M; Thiele A; Kettschau G; Heinrich T; Lehmann L; Halldin C In vivo evaluation in cynomolgus monkey brain and metabolism of [18F]fluorodeprenyl: A new MAO-B pet radioligand. Synapse 2012, 66, 323–330. [PubMed: 22124971]

211. Macgregor RR; Fowler JS; Wolf AP; Halldin C; Langström B Synthesis of suicide inhibitors of monoamine oxidase: Carbon-11 labeled clorgyline, L-deprenyl and D-deprenyl. J. Labelled Comp. Radiopharm 1988, 25, 1–9.

212. Nag S; Fazio P; Lehmann L; Kettschau G; Heinrich T; Thiele A; Svedberg M; Amini N; Leesch S; Catafau AM; Hannestad J; Varrone A; Halldin C In vivo and in vitro characterization of a novel MAO-B inhibitor radioligand, 18F-labeled deuterated fluorodeprenyl. J. Nucl. Med 2016, 57, 315–320. [PubMed: 26585057]

213. Hirvonen J; Kailajärvi M; Haltia T; Koskimies S; Någren K; Virsu P; Oikonen V; Sipilä H; Ruokoniemi P; Virtanen K; Scheinin M; Rinne JO Assessment of MAO-B occupancy in the brain

with PET and [11C]-L-deprenyl-D2: A dose-finding study with a novel MAO-B inhibitor, EVT 301. Clin. Pharmacol. Ther 2009, 85, 506–512. [PubMed: 19129751]

214. Fowler JS; Volkow ND; Wang GJ; Pappas N; Logan J; Macgregor R; Alexoff D; Wolf AP; Warner D; Cilento R; Zezulkova I Neuropharmacological actions of cigarette smoke. J. Addict. Dis 1998, 17, 23–34. [PubMed: 9549600]
215. Fowler JS; Wang GJ; Volkow ND; Franceschi D; Logan J; Pappas N; Shea C; MacGregor RR; Garza V Smoking a single cigarette does not produce a measurable reduction in brain MAO B in non-smokers. Nicotine Tob. Res 1999, 1, 325–329. [PubMed: 11072429]
216. Kumlien E; Bergström M; Lilja A; Andersson J; Szekeres V; Westerberg C-E; Westerberg G; Antoni G; Långström B Positron emission tomography with [11C]deuterium-deprenyl in temporal lobe epilepsy. Epilepsia 1995, 36, 712–721. [PubMed: 7555990]
217. Bergström M; Kumlien E; Lilja A; Tyrefors N; Westerberg G; Långström B Temporal lobe epilepsy visualized with PET with 11C-L-deuterium-deprenyl – analysis of kinetic data. Acta Neurol. Scand 1998, 98, 224–231. [PubMed: 9808270]
218. Kumlien E; Nilsson A; Hagberg G; Långström B; Bergström M PET with 11C-deuterium-deprenyl and 18F-FDG in focal epilepsy. Acta Neurol. Scand 2001, 103, 360–366. [PubMed: 11421848]
219. Carter SF; Schöll M; Almkvist O; Wall A; Engler H; Långström B; Nordberg A Evidence for astrocytosis in prodromal Alzheimer disease provided by 11C-deuterium-L-deprenyl: A multitracer PET paradigm combining 11C-pittsburgh compound B and 18F-FDG. J. Nucl. Med 2012, 53, 37–46. [PubMed: 22213821]
220. Choo ILH; Carter SF; Schöll ML; Nordberg A Astrocytosis measured by 11C-deprenyl PET correlates with decrease in gray matter density in the parahippocampus of prodromal Alzheimer's patients. Eur. J. Nucl. Med. Mol. Imaging 2014, 41, 2120–2126. [PubMed: 25077930]
221. Nag S; Lehmann L; Kettschau G; Heinrich T; Thiele A; Varrone A; Gulyas B; Halldin C Synthesis and evaluation of [18F]fluororasagiline, a novel positron emission tomography (PET) radioligand for monoamine oxidase B (MAO-B). Bioorg. Med. Chem 2012, 20, 3065–3071. [PubMed: 22436387]
222. Nag S; Lehmann L; Kettschau G; Toth M; Heinrich T; Thiele A; Varrone A; Halldin C Development of a novel fluorine-18 labeled deuterated fluororasagiline ([18F]fluororasagiline-D2) radioligand for PET studies of monoamino oxidase B (MAO-B). Bioorg. Med. Chem 2013, 21, 6634–6641. [PubMed: 24012376]
223. Shiue C-Y; Shiue GG; Rysavy JA; Pleus RC; Huang H; Bai L-Q; Cornish KG; Sunderland JJ; Frick MP Fluorine-18 and carbon-11 labeled amphetamine analogs—Synthesis, distribution, binding characteristics in mice and rats and a PET study in monkey. Nucl. Med. Biol 1993, 20, 973–981. [PubMed: 8298577]
224. Beer HF; Frey LD; Häberli M; Schubiger PA [123I/18F] N-(2-aminoethyl)-5-halogeno-2-pyridinecarbox-amides, site specific tracers for MAO-B mapping with SPET and PET. Nucl. Med. Biol 1995, 22, 999–1004. [PubMed: 8998478]
225. Bläuenstein P; Rémy N; Buck A; Ametamey S; Häberli M; Schubiger PA In vivo properties of N-(2-aminoethyl)-5-halogeno-2-pyridinecarboxamide 18F- and 123I-labelled reversible inhibitors of monoamine oxidase B. Nucl. Med. Biol 1998, 25, 47–52. [PubMed: 9466361]
226. Yoshimoto M; Hirata M; Kagawa S; Magata Y; Ohmomo Y; Temma T Synthesis and characterization of novel radiofluorinated probes for positron emission tomography imaging of monoamine oxidase B. J. Labelled Comp. Radiopharm 2019, 62, 580–587. [PubMed: 31215665]
227. Vasdev N; Sadovski O; Garcia A; Dollé F; Meyer JH; Houle S; Wilson AA Radiosynthesis of [11C]SL25.1188 via [11C]CO2 fixation for imaging monoamine oxidase B. J. Labelled Comp. Radiopharm 2011, 54, 678–680.
228. Saba W; Valette H; Peyronneau M-A; Bramoullé Y; Coulon C; Curet O; George P; Dollé F; Bottlaender M [11C]SL25.1188, a new reversible radioligand to study the monoamine oxidase type B with PET: Preclinical characterisation in nonhuman primate. Synapse 2010, 64, 61–69. [PubMed: 19728365]
229. Hicks JW; Sadovski O; Parkes J; Houle S; Hay BA; Carter RL; Wilson AA; Vasdev N Radiosynthesis and ex vivo evaluation of [18F]-(S)-3-(6-(3-fluoropropoxy)benzo[d]isoxazol-3-

yl)-5-(methoxymethyl)oxazolidin-2-one for imaging MAO-B with PET. Bioorg. Med. Chem. Lett 2015, 25, 288–291. [PubMed: 25488845]

230. Harada R; Hayakawa Y; Ezura M; Lerdsirisuk P; Du Y; Ishikawa Y; Iwata R; Shidahara M; Ishiki A; Kikuchi A; Arai H; Kudo Y; Yanai K; Furumoto S; Okamura N 18F-SMBT-1: A selective and reversible positron-emission tomography tracer for monoamine oxidase-B imaging. J. Nucl. Med 2021, 62, 253–258. [PubMed: 32646880]
231. Harada R; Okamura N; Furumoto S; Furukawa K; Ishiki A; Tomita N; Tago T; Hiraoka K; Watanuki S; Shidahara M; Miyake M; Ishikawa Y; Matsuda R; Inami A; Yoshikawa T; Funaki Y; Iwata R; Tashiro M; Yanai K; Arai H; Kudo Y 18F-THK5351: A novel PET radiotracer for imaging neurofibrillary pathology in Alzheimer disease. J. Nucl. Med 2016, 57, 208–214. [PubMed: 26541774]
232. Moerlein SM; Stöcklin G; Pawlik G; Wienhard K; Heiss W-D Regional cerebral pharmacokinetics of the dopaminergic neurotoxin 1-methyl-4-phenyl-1,2,3,6-tetrahydropyridine as examined by positron emission tomography in a baboon is altered by tranylcypromine. Neurosci. Lett 1986, 66, 205–209. [PubMed: 3487753]
233. Shinotoh H; Inoue O; Suzuki K; Yamasaki T; Iyo M; Hashimoto K; Tominaga T; Itoh T; Tateno Y; Ikehira H Kinetics of [11C]N,N-dimethylphenylethylamine in mice and humans: Potential for measurement of brain MAO-B activity. J. Nucl. Med 1987, 28, 1006–1011. [PubMed: 3495646]
234. Brooks AF; Shao X; Quesada CA; Sherman P; Scott PJH; Kilbourn MR In vivo metabolic trapping radiotracers for imaging monoamine oxidase-A and -B enzymatic activity. ACS Chem. Neurosci 2015, 6, 1965–1971. [PubMed: 26393369]
235. O'Sullivan C; Dev KK The structure and function of the S1P1 receptor. Trends Pharmacol. Sci 2013, 34, 401–412. [PubMed: 23763867]
236. Proia RL; Hla T Emerging biology of sphingosine-1-phosphate: its role in pathogenesis and therapy. J. Clin. Invest 2015, 125, 1379–1387. [PubMed: 25831442]
237. Kono M; Proia RL Imaging S1P1 activation in vivo. Exp. Cell Res 2015, 333, 178–182. [PubMed: 25498971]
238. Blaho VA; Hla T An update on the biology of sphingosine 1-phosphate receptors. J. Lipid Res 2014, 55, 1596–1608. [PubMed: 24459205]
239. Farooqui AA; Ong WY; Farooqui T Lipid mediators in the nucleus: Their potential contribution to Alzheimer's disease. Biochim. Biophys. Acta 2010, 1801, 906–916. [PubMed: 20170745]
240. Rutherford C; Childs S; Ohotski J; McGlynn L; Riddick M; MacFarlane S; Tasker D; Pyne S; Pyne NJ; Edwards J; Palmer TM Regulation of cell survival by sphingosine-1-phosphate receptor S1P1 via reciprocal ERK-dependent suppression of Bim and PI-3-kinase/protein kinase C-mediated upregulation of Mcl-1. Cell Death Dis. 2013, 4, e927. [PubMed: 24263101]
241. Lee MJ; Van Brocklyn JR; Thangada S; Liu CH; Hand AR; Menzeleev R; Spiegel S; Hla T Sphingosine-1-phosphate as a ligand for the G protein-coupled receptor EDG-1. Science 1998, 279, 1552–1555. [PubMed: 9488656]
242. Maceyka M; Spiegel S Sphingolipid metabolites in inflammatory disease. Nature 2014, 510, 58–67. [PubMed: 24899305]
243. Garris CS; Wu L; Acharya S; Arac A; Blaho VA; Huang Y; Moon BS; Axtell RC; Ho PP; Steinberg GK; Lewis DB; Sobel RA; Han DK; Steinman L; Snyder MP; Hla T; Han MH Defective sphingosine 1-phosphate receptor 1 (S1P1) phosphorylation exacerbates TH17-mediated autoimmune neuroinflammation. Nat. Immunol 2013, 14, 1166–1172. [PubMed: 24076635]
244. Ceccom J; Loukh N; Lauwers-Cances V; Touriol C; Nicaise Y; Gentil C; Uro-Coste E; Pitson S; Maurage CA; Duyckaerts C; Cuvillier O; Delisle MB Reduced sphingosine kinase-1 and enhanced sphingosine 1-phosphate lyase expression demonstrate deregulated sphingosine 1-phosphate signaling in Alzheimer's disease. Acta Neuropathol. Commun 2014, 2, 12. [PubMed: 24468113]
245. Badawy SMM; Okada T; Kajimoto T; Hirase M; Matovelo SA; Nakamura S; Yoshida D; Ijuin T; Nakamura SI Extracellular α-synuclein drives sphingosine 1-phosphate receptor subtype 1 out of lipid rafts, leading to impaired inhibitory G-protein signaling. J. Biol. Chem 2018, 293, 8208–8216. [PubMed: 29632069]

246. Czubowicz K; Jęśko H; Wencel P; Lukiw WJ; Strosznajder RP The role of ceramide and sphingosine-1-phosphate in Alzheimer's disease and other neurodegenerative disorders. Mol. Neurobiol 2019, 56, 5436–5455. [PubMed: 30612333]

247. Choi JW; Gardell SE; Herr DR; Rivera R; Lee C-W; Noguchi K; Teo ST; Yung YC; Lu M; Kennedy G; Chun J FTY720 (fingolimod) efficacy in an animal model of multiple sclerosis requires astrocyte sphingosine 1-phosphate receptor 1 (S1P1) modulation. Proc. Natl. Acad. Sci 2011, 108, 751–756. [PubMed: 21177428]

248. Chiba K; Adachi K Sphingosine 1-phosphate receptor 1 as a useful target for treatment of multiple sclerosis. Pharmaceuticals 2012, 5, 514–528. [PubMed: 24281561]

249. Tsai H-C; Nguyen K; Hashemi E; Engleman E; Hla T; Han MH Myeloid sphingosine-1-phosphate receptor 1 is important for CNS autoimmunity and neuroinflammation. J. Autoimmun 2019, 105, 102290. [PubMed: 31202617]

250. Tintore M; Vidal-Jordana A; Sastre-Garriga J Treatment of multiple sclerosis - success from bench to bedside. Nat. Rev. Neurol 2019, 15, 53–58. [PubMed: 30315270]

251. La Mantia L; Tramacere I; Firwana B; Pacchetti I; Palumbo R; Filippini G Fingolimod for relapsing-remitting multiple sclerosis. Cochrane Database Syst. Rev 2016, 4, CD009371. [PubMed: 27091121]

252. Van Doorn R; Van Horssen J; Verzijl D; Witte M; Ronken E; Van Het Hof B; Lakeman K; Dijkstra CD; Van Der Valk P; Reijerkerk A; Alewijnse AE; Peters SL; De Vries HE Sphingosine 1-phosphate receptor 1 and 3 are upregulated in multiple sclerosis lesions. Glia 2010, 58, 1465–1476. [PubMed: 20648639]

253. Brinkmann V; Billich A; Baumruker T; Heining P; Schmouder R; Francis G; Aradhye S; Burtin P Fingolimod (FTY720): discovery and development of an oral drug to treat multiple sclerosis. Nat. Rev. Drug Discov 2010, 9, 883–897. [PubMed: 21031003]

254. Cohen JA; Barkhof F; Comi G; Hartung HP; Khatri BO; Montalban X; Pelletier J; Capra R; Gallo P; Izquierdo G; Tiel-Wilck K; de Vera A; Jin J; Stites T; Wu S; Aradhye S; Kappos L; Group, T. S. Oral fingolimod or intramuscular interferon for relapsing multiple sclerosis. N. Engl. J. Med 2010, 362, 402–415. [PubMed: 20089954]

255. Briard E; Orain D; Beerli C; Billich A; Streiff M; Bigaud M; Auberson YP BZM055, an iodinated radiotracer candidate for PET and SPECT imaging of myelin and FTY720 brain distribution. ChemMedChem 2011, 6, 667–677. [PubMed: 21280229]

256. Shaikh RS; Schilson SS; Wagner S; Hermann S; Keul P; Levkau B; Schafers M; Haufe G Synthesis and evaluation of fluorinated fingolimod (FTY720) analogues for sphingosine-1-phosphate receptor molecular imaging by positron emission tomography. J. Med. Chem 2015, 58, 3471–3484. [PubMed: 25826109]

257. Prasad VP; Wagner S; Keul P; Hermann S; Levkau B; Schafers M; Haufe G Synthesis of fluorinated analogues of sphingosine-1-phosphate antagonists as potential radiotracers for molecular imaging using positron emission tomography. Bioorg. Med. Chem 2014, 22, 5168–5181. [PubMed: 25216968]

258. Luo Z; Gu J; Dennett RC; Gaehle GG; Perlmutter JS; Chen DL; Benzinger TLS; Tu Z Automated production of a sphingosine-1 phosphate receptor 1 (S1P1) PET radiopharmaceutical [11C]CS1P1 for human use. Appl. Radiat. Isot 2019, 152, 30–36. [PubMed: 31280104]

259. Rosenberg AJ; Liu H; Jin H; Yue X; Riley S; Brown SJ; Tu Z Design, Synthesis, and In Vitro and In Vivo Evaluation of an (18)F-Labeled Sphingosine 1-Phosphate Receptor 1 (S1P1) PET Tracer. J Med Chem 2016, 59, 6201–6220. [PubMed: 27280499]

260. Luo Z; Rosenberg AJ; Liu H; Han J; Tu Z Syntheses and in vitro evaluation of new S1PR1 compounds and initial evaluation of a lead F-18 radiotracer in rodents. Eur. J. Med. Chem 2018, 150, 796–808. [PubMed: 29604582]

261. Benzinger TLS Investigation of inflammation using [C-11]-CS1P1 (CS1P1). https://clinicaltrials.gov/ct2/show/NCT04517552?term=S1P&cntry=US&draw=2&rank=5 (2020).

262. Rust R; Grönnert L; Gantner C; Enzler A; Mulders G; Weber RZ; Siewert A; Limasale YDP; Meinhardt A; Maurer MA; Sartori AM; Hofer AS; Werner C; Schwab ME Nogo-A targeted therapy promotes vascular repair and functional recovery following stroke. Proc. Natl. Acad. Sci 2019, 116, 14270–14279. [PubMed: 31235580]

263. Cruz-Orengo L; Daniels BP; Dorsey D; Basak SA; Grajales-Reyes JG; McCandless EE; Piccio L; Schmidt RE; Cross AH; Crosby SD; Klein RS Enhanced sphingosine-1-phosphate receptor 2 expression underlies female CNS autoimmunity susceptibility. J. Clin. Invest 2014, 124, 2571–2584. [PubMed: 24812668]

264. Li C; Chi XX; Xie W; Strong JA; Zhang JM; Nicol GD Sphingosine 1-phosphate receptor 2 antagonist JTE-013 increases the excitability of sensory neurons independently of the receptor. J. Neurophysiol 2012, 108, 1473–1483. [PubMed: 22673325]

265. Yue X; Jin H; Liu H; Rosenberg AJ; Klein RS; Tu Z A potent and selective C-11 labeled PET tracer for imaging sphingosine-1-phosphate receptor 2 in the CNS demonstrates sexually dimorphic expression. Org. Biomol. Chem 2015, 13, 7928–7939. [PubMed: 26108234]

266. Luo Z; Liang Q; Liu H; Sumit J; Jiang H; Klein RS; Tu Z Synthesis and characterization of [125I]TZ6544, a promising radioligand for investigating sphingosine-1-phosphate receptor 2. Nucl. Med. Biol 2020, 88-89, 52–61. [PubMed: 32791475]

267. Cekic C; Linden J Purinergic regulation of the immune system. Nat. Rev. Immunol 2016, 16, 177–192. [PubMed: 26922909]

268. Burnstock G Purinergic signalling and disorders of the central nervous system. Nat. Rev. Drug Discov 2008, 7, 575–590. [PubMed: 18591979]

269. Tozaki-Saitoh H; Tsuda M; Inoue K Role of purinergic receptors in CNS function and neuroprotection. Adv. Pharmacol 2011, 61, 495–528. [PubMed: 21586368]

270. Burnstock G An introduction to the roles of purinergic signalling in neurodegeneration, neuroprotection and neuroregeneration. Neuropharmacology 2016, 104, 4–17. [PubMed: 26056033]

271. Beamer E; Gölöncsér F; Horváth G; Bekő K; Otrokocsi L; Koványi B; Sperlágh B Purinergic mechanisms in neuroinflammation: An update from molecules to behavior. Neuropharmacology 2016, 104, 94–104. [PubMed: 26384652]

272. Zarrinmayeh H; Territo PR Purinergic receptors of the central nervous system: Biology, PET ligands, and their applications. Mol. Imaging 2020, 19, 1536012120927609. [PubMed: 32539522]

273. Narayanaswami V; Dahl K; Bernard-Gauthier V; Josephson L; Cumming P; Vasdev N Emerging PET Radiotracers and Targets for Imaging of Neuroinflammation in Neurodegenerative Diseases: Outlook Beyond TSPO. Mol Imaging 2018, 17, 1536012118792317. [PubMed: 30203712]

274. Khakh BS; North RA Neuromodulation by extracellular ATP and P2X receptors in the CNS. Neuron 2012, 76, 51–69. [PubMed: 23040806]

275. Imura Y; Morizawa Y; Komatsu R; Shibata K; Shinozaki Y; Kasai H; Moriishi K; Moriyama Y; Koizumi S Microglia release ATP by exocytosis. Glia 2013, 61, 1320–1330. [PubMed: 23832620]

276. Sperlágh B; Heinrich A; Csölle C P2 receptor-mediated modulation of neurotransmitter release-an update. Purinergic signal. 2007, 3, 269–284. [PubMed: 18404441]

277. Karasawa A; Kawate T Structural basis for subtype-specific inhibition of the P2X7 receptor. eLife 2016, 5, e22153. [PubMed: 27935479]

278. Jain P; Chaney AM; Carlson ML; Jackson IM; Rao A; James ML Neuroinflammation PET imaging: Current opinion and future directions. J. Nucl. Med 2020, 61, 1107–1112. [PubMed: 32620705]

279. Monif M; Burnstock G; Williams DA Microglia: proliferation and activation driven by the P2X7 receptor. Int. J. Biochem. Cell Biol 2010, 42, 1753–1756. [PubMed: 20599520]

280. Takenouchi T; Sekiyama K; Sekigawa A; Fujita M; Waragai M; Sugama S; Iwamaru Y; Kitani H; Hashimoto M P2X7 receptor signaling pathway as a therapeutic target for neurodegenerative diseases. Arch. Immunol. Ther. Exp. (Warsz) 2010, 58, 91–96. [PubMed: 20143170]

281. Ory D; Celen S; Gijsbers R; Van Den Haute C; Postnov A; Koole M; Vandeputte C; Andrés JI; Alcazar J; De Angelis M; Langlois X; Bhattacharya A; Schmidt M; Letavic MA; Vanduffel W; Van Laere K; Verbruggen A; Debyser Z; Bormans G Preclinical evaluation of a P2X7 receptor-selective radiotracer: PET studies in a rat model with local overexpression of the human P2X7 receptor and in nonhuman primates. J. Nucl. Med 2016, 57, 1436–1441. [PubMed: 27199364]

282. Kolb HC; Barret O; Bhattacharya A; Chen G; Constantinescu C; Huang C; Letavic M; Tamagnan G; Xia CA; Zhang W; Szardenings AK Preclinical evaluation and nonhuman primate receptor occupancy study of 18F-JNJ-64413739, a PET radioligand for P2X7 receptors. J. Nucl. Med 2019, 60, 1154–1159. [PubMed: 30733317]

283. Berdyyeva T; Xia C; Taylor N; He Y; Chen G; Huang C; Zhang W; Kolb H; Letavic M; Bhattacharya A; Szardenings AK PET imaging of the P2X7 ion channel with a novel tracer [18F]JNJ-64413739 in a rat model of neuroinflammation. Mol. Imaging Biol 2019, 21, 871–878. [PubMed: 30632003]

284. Janssen B; Vugts DJ; Funke U; Spaans A; Schuit RC; Kooijman E; Rongen M; Perk LR; Lammertsma AA; Windhorst AD Synthesis and initial preclinical evaluation of the P2X7 receptor antagonist [^{11}C]A-740003 as a novel tracer of neuroinflammation. J. Labelled Comp. Radiopharm 2014, 57, 509–516. [PubMed: 24995673]

285. Fantoni ER; Dal Ben D; Falzoni S; Di Virgilio F; Lovestone S; Gee A Design, synthesis and evaluation in an LPS rodent model of neuroinflammation of a novel 18F-labelled PET tracer targeting P2X7. EJNMMI Res. 2017, 7, 31. [PubMed: 28374288]

286. Gao M; Wang M; Green MA; Hutchins GD; Zheng QH Synthesis of [11C]GSK1482160 as a new PET agent for targeting P2X(7) receptor. Bioorg. Med. Chem. Lett 2015, 25, 1965–70. [PubMed: 25819093]

287. Han J; Liu H; Liu C; Jin H; Perlmutter JS; Egan TM; Tu Z Pharmacologic characterizations of a P2X7 receptor-specific radioligand, [11C]GSK1482160 for neuroinflammatory response. Nucl. Med. Commun 2017, 38, 372–382. [PubMed: 28338530]

288. Gao M; Wang M; Glick-Wilson BE; Meyer JA; Peters JS; Territo PR; Green MA; Hutchins GD; Zarrinmayeh H; Zheng QH Synthesis and preliminary biological evaluation of a novel P2X7R radioligand [18F]IUR-1601. Bioorg. Med. Chem. Lett 2018, 28, 1603–1609. [PubMed: 29628324]

289. Wilkinson SM; Barron ML; O'Brien-Brown J; Janssen B; Stokes L; Werry EL; Chishty M; Skarratt KK; Ong JA; Hibbs DE; Vugts DJ; Fuller S; Windhorst AD; Kassiou M Pharmacological evaluation of novel bioisosteres of an adamantanyl benzamide P2X(7) receptor antagonist. ACS Chem. Neurosci 2017, 8, 2374–2380. [PubMed: 28841278]

290. Janssen B; Vugts DJ; Wilkinson SM; Ory D; Chalon S; Hoozemans JJM; Schuit RC; Beaino W; Kooijman EJM; van den Hoek J; Chishty M; Doméné A; Van der Perren A; Villa A; Maggi A; Molenaar GT; Funke U; Shevchenko RV; Baekelandt V; Bormans G; Lammertsma AA; Kassiou M; Windhorst AD Identification of the allosteric P2X(7) receptor antagonist [11C]SMW139 as a PET tracer of microglial activation. Sci. Rep 2018, 8, 6580. [PubMed: 29700413]

291. Walker DG; Tang TM; Mendsaikhan A; Tooyama I; Serrano GE; Sue LI; Beach TG; Lue LF Patterns of expression of purinergic receptor P2RY12, a putative marker for non-activated microglia, in aged and Alzheimer's disease brains. Int. J. Mol. Sci 2020, 21, 678.

292. Beaino W; Janssen B; Kooij G; van der Pol SMA; van Het Hof B; van Horssen J; Windhorst AD; de Vries HE Purinergic receptors P2Y12R and P2X7R: potential targets for PET imaging of microglia phenotypes in multiple sclerosis. J. Neuroinflammation 2017, 14, 259. [PubMed: 29273052]

293. Weisman GA; Woods LT; Erb L; Seye CI P2Y receptors in the mammalian nervous system: pharmacology, ligands and therapeutic potential. CNS Neurol. Disord. Drug Targets 2012, 11, 722–738. [PubMed: 22963441]

294. Dorsam RT; Kunapuli SP Central role of the P2Y12 receptor in platelet activation. J. Clin. Invest 2004, 113, 340–345. [PubMed: 14755328]

295. Amadio S; Parisi C; Montilli C; Carrubba AS; Apolloni S; Volonté C P2Y(12) receptor on the verge of a neuroinflammatory breakdown. Mediators Inflamm. 2014, 2014, 975849. [PubMed: 25180027]

296. Bach P; Boström J; Brickmann K; van Giezen JJJ; Groneberg RD; Harvey DM; O'Sullivan M; Zetterberg F Synthesis, structure–property relationships and pharmacokinetic evaluation of ethyl 6-aminonicotinate sulfonylureas as antagonists of the P2Y12 receptor. Eur.J. Med. Chem 2013, 65, 360–375. [PubMed: 23747805]

297. Villa A; Klein B; Janssen B; Pedragosa J; Pepe G; Zinnhardt B; Vugts DJ; Gelosa P; Sironi L; Beaino W; Damont A; Dollé F; Jego B; Winkeler A; Ory D; Solin O; Vercouillie J; Funke

U; Laner-Plamberger S; Blomster LV; Christophersen P; Vegeto E; Aigner L; Jacobs A; Planas AM; Maggi A; Windhorst AD Identification of new molecular targets for PET imaging of the microglial anti-inflammatory activation state. Theranostics 2018, 8, 5400–5418. [PubMed: 30555554]

298. Mitrasinovic OM; Grattan A; Robinson CC; Lapustea NB; Poon C; Ryan H; Phong C; Murphy GM Microglia overexpressing the macrophage colony-stimulating factor receptor are neuroprotective in a microglial-hippocampal organotypic coculture system. J. Neurosci 2005, 25, 4442–4451. [PubMed: 15858070]
299. Pyonteck SM; Akkari L; Schuhmacher AJ; Bowman RL; Sevenich L; Quail DF; Olson OC; Quick ML; Huse JT; Teijeiro V; Setty M; Leslie CS; Oei Y; Pedraza A; Zhang J; Brennan CW; Sutton JC; Holland EC; Daniel D; Joyce JA CSF-1R inhibition alters macrophage polarization and blocks glioma progression. Nat. Med 2013, 19, 1264–1272. [PubMed: 24056773]
300. Olmos-Alonso A; Schetters STT; Sri S; Askew K; Mancuso R; Vargas-Caballero M; Holscher C; Perry VH; Gomez-Nicola D Pharmacological targeting of CSF1R inhibits microglial proliferation and prevents the progression of Alzheimer's-like pathology. Brain 2016, 139, 891–907. [PubMed: 26747862]
301. Sassi C; Nalls MA; Ridge PG; Gibbs JR; Lupton MK; Troakes C; Lunnon K; Al-Sarraj S; Brown KS; Medway C; Lord J; Turton J; Bras J; Passmore P; Craig D; Johnston J; McGuinness B; Todd S; Heun R; Kölsch H; Kehoe PG; Vardy ERLC; Hooper NM; Mann DM; Pickering-Brown S; Brown K; Lowe J; Morgan K; Smith AD; Wilcock G; Warden D; Holmes C; Blumenau S; Thielke M; Josties C; Freyer D; Dietrich A; Hammer M; Baier M; Dirnagl U; Powell JF; Kauwe JS; Cruchaga C; Goate AM; Singleton AB; Guerreiro R; Hodges A; Hardy J Mendelian adult-onset leukodystrophy genes in Alzheimer's disease: critical influence of CSF1R and NOTCH3. Neurobiol. Aging 2018, 66, 179.e17–179.e29.
302. Spangenberg E; Severson PL; Hohsfield LA; Crapser J; Zhang J; Burton EA; Zhang Y; Spevak W; Lin J; Phan NY; Habets G; Rymar A; Tsang G; Walters J; Nespi M; Singh P; Broome S; Ibrahim P; Zhang C; Bollag G; West BL; Green KN Sustained microglial depletion with CSF1R inhibitor impairs parenchymal plaque development in an Alzheimer's disease model. Nat. Commun 2019, 10, 3758. [PubMed: 31434879]
303. Hagan N; Kane JL; Grover D; Woodworth L; Madore C; Saleh J; Sancho J; Liu J; Li Y; Proto J; Zelic M; Mahan A; Kothe M; Scholte AA; Fitzgerald M; Gisevius B; Haghikia A; Butovsky O; Ofengeim D CSF1R signaling is a regulator of pathogenesis in progressive MS. Cell Death Dis. 2020, 11, 904. [PubMed: 33097690]
304. Hu X; Li S; Doycheva DM; Huang L; Lenahan C; Liu R; Huang J; Xie S; Tang J; Zuo G; Zhang JH Rh-CSF1 attenuates neuroinflammation via the CSF1R/PLCG2/PKCε pathway in a rat model of neonatal HIE. J. Neuroinflammation 2020, 17, 182. [PubMed: 32522286]
305. Akiyama H; Nishimura T; Kondo H; Ikeda K; Hayashi Y; McGeer PL Expression of the receptor for macrophage colony stimulating factor by brain microglia and its upregulation in brains of patients with Alzheimer's disease and amyotrophic lateral sclerosis. Brain Res. 1994, 639, 171–174. [PubMed: 7514086]
306. Walker DG; Tang TM; Lue L-F Studies on colony stimulating factor receptor-1 and ligands colony stimulating factor-1 and interleukin-34 in Alzheimer's disease brains and human microglia. Front. Aging Neurosci 2017, 9, 244. [PubMed: 28848420]
307. Bernard-Gauthier V; Schirrmacher R 5-(4-((4-[18F]fluorobenzyl)oxy)-3-methoxybenzyl)pyrimidine-2,4-diamine: A selective dual inhibitor for potential PET imaging of Trk/CSF-1R. Bioorg. Med. Chem. Lett 2014, 24, 4784–4790. [PubMed: 25257201]
308. Conway JG; McDonald B; Parham J; Keith B; Rusnak DW; Shaw E; Jansen M; Lin P; Payne A; Crosby RM; Johnson JH; Frick L; Lin M-HJ; Depee S; Tadepalli S; Votta B; James I; Fuller K; Chambers TJ; Kull FC; Chamberlain SD; Hutchins JT Inhibition of colony-stimulating-factor-1 signaling in vivo with the orally bioavailable cFMS kinase inhibitor GW2580. Proc. Natl. Acad. Sci 2005, 102, 16078–16083. [PubMed: 16249345]
309. Zhou X; Ji B; Seki C; Nagai Y; Minamimoto T; Fujinaga M; Zhang M-R; Saito T; Saido TC; Suhara T; Kimura Y; Higuchi M PET imaging of colony-stimulating factor 1 receptor: A head-to-head comparison of a novel radioligand, 11C-GW2580, and 11C-CPPC, in mouse

models of acute and chronic neuroinflammation and a rhesus monkey. J. Cereb. Blood Flow Metab 2021, 41, 2410–2422. [PubMed: 33757319]

310. Knight AC; Varlow C; Zi T; Liang SH; Josephson L; Schmidt K; Patel S; Vasdev N In vitro evaluation of [3H]CPPC as a tool radioligand for CSF-1R. ACS Chem. Neurosci 2021, 12, 998–1006. [PubMed: 33667059]
311. Lue L-F; Walker DG; Jacobson S; Sabbagh M Receptor for advanced glycation end products: its role in Alzheimer's disease and other neurological diseases. Future Neurol. 2009, 4, 167–177. [PubMed: 19885375]
312. Kong Y; Hua F; Guan Y; Zhao B RAGE-specific probe 18F-FPS-ZM1 may be a promising biomarker for early detection of Diabetes with Alzheimer's disease. J. Nucl. Med 2016, 57 (Suppl 2), 1049.
313. Drake L; Brooks A; Scott P Imaging the receptor for advanced glycation endproducts with [18F]RAGER. J. Nucl. Med 2017, 58 (suppl 1), 551.
314. Savickas V; Bongarzone S; Luzi F; Singh N; Gee TD Development and evaluation of a novel positron emission tomography radiotracer for imaging the receptor for advanced glycation endproducts in Alzheimer's disease. Alzheimer's Dementia 2017, 13 (Suppl), P1536–P1537.
315. Luzi F; Savickas V; Taddei C; Hader S; Singh N; Gee AD; Bongarzone S Radiolabeling of [11C]FPS-ZM1, a receptor for advanced glycation end products-targeting positron emission tomography radiotracer, using a [11C]CO2-to-[11C]CO chemical conversion. Future Med. Chem 2020, 12, 511–521. [PubMed: 32100545]
316. Pierce AM; Keating AK TAM receptor tyrosine kinases: Expression, disease and oncogenesis in the central nervous system. Brain Res. 2014, 1542, 206–220. [PubMed: 24184575]
317. Ma GZM; Stankovich J; The A; New Zealand Multiple Sclerosis Genetics, C.; Kilpatrick TJ; Binder MD; Field J Polymorphisms in the receptor tyrosine kinase MERTK gene are associated with multiple sclerosis susceptibility. PLOS One 2011, 6, e16964. [PubMed: 21347448]
318. Weinger JG; Omari KM; Marsden K; Raine CS; Shafit-Zagardo B Up-regulation of soluble Axl and Mer receptor tyrosine kinases negatively correlates with Gas6 in established multiple sclerosis lesions. Am. J. Pathol 2009, 175, 283–293. [PubMed: 19541935]
319. Horti AG; Wang Y; Minn I; Lan X; Wang J; Koehler RC; Alkayed NJ; Dannals RF; Pomper MG 18F-FNDP for PET Imaging of Soluble Epoxide Hydrolase. J. Nucl. Med 2016, 57, 1817–1822. [PubMed: 27417650]
320. Du Y; Minn I; Foss C; Lesniak WG; Hu F; Dannals RF; Pomper MG; Horti AG PET imaging of soluble epoxide hydrolase in non-human primate brain with [18F]FNDP. EJNMMI Res. 2020, 10, 67. [PubMed: 32572592]
321. Thomae D; Servaes S; Vazquez N; wyffels L; Dedeurwaerdere S; Van der Veken P; Joossens J; Augustyns K; Stroobants S; Staelens S Synthesis and preclinical evaluation of an 18F labeled PDE7 inhibitor for PET neuroimaging. Nucl. Med. Biol 2015, 42, 975–981. [PubMed: 26330158]
322. Schröder S; Wenzel B; Deuther-Conrad W; Scheunemann M; Brust P Novel radioligands for cyclic nucleotide phosphodiesterase imaging with positron emission tomography: An update on developments since 2012. Molecules 2016, 21, 650.
323. Nakajima T; Hayashi N; Ishizawa K; Tsuzaki Y; Iwamura R; Tsuboike K Bicyclic nitrogenated heterocyclic compound. WO2018038265, 2018.
324. Kubota M; Seki C; Kimura Y; Takahata K; Shimada H; Takado Y; Matsuoka K; Tagai K; Sano Y; Yamamoto Y; Okada M; Kikuchi T; Ichise M; Kawamura K; Zhang M-R; Higuchi M A first-in-human study of 11C-MTP38, a novel PET ligand for phosphodiesterase 7. Eur. J. Nucl. Med. Mol. Imaging 2021, 48, 2846–2855. [PubMed: 33566152]
325. Auffray C; Fogg DK; Narni-Mancinelli E; Senechal B; Trouillet C; Saederup N; Leemput J; Bigot K; Campisi L; Abitbol M; Molina T; Charo I; Hume DA; Cumano A; Lauvau G; Geissmann F CX3CR1+ CD115+ CD135+ common macrophage/DC precursors and the role of CX3CR1 in their response to inflammation. J. Exp. Med 2009, 206, 595–606. [PubMed: 19273628]
326. Karlström S; Nordvall G; Sohn D; Hettman A; Turek D; Åhlin K; Kers A; Claesson M; Slivo C; Lo-Alfredsson Y; Petersson C; Bessidskaia G; Svensson PH; Rein T; Jerning E; Malmberg Å; Ahlgen C; Ray C; Vares L; Ivanov V; Johansson R Substituted 7-amino-5-thio-thiazolo[4,5-

d]pyrimidines as potent and selective antagonists of the fractalkine receptor (CX3CR1). J. Med. Chem 2013, 56, 3177–3190. [PubMed: 23516963]

327. Pissarek M Small-molecule ligands as challenge for positron emission tomography of peptide receptors in neurons and microglia of the brain. World J. Neurol 2019, 9, 294–327.
328. Luehmann HP; Detering L; Fors BP; Pressly ED; Woodard PK; Randolph GJ; Gropler RJ; Hawker CJ; Liu Y PET/CT imaging of chemokine receptors in inflammatory atherosclerosis using targeted nanoparticles. J. Nucl. Med 2016, 57, 1124–1129. [PubMed: 26795285]
329. Xu Y; Xu Y; Blevins H; Lan Y; Liu Y; Yuan G; Striar R; Zagaroli JS; Tocci DR; Langan AG; Zhang C; Zhang S; Wang C Discovery of carbon-11 labeled sulfonamide derivative: A PET tracer for imaging brain NLRP3 inflammasome. Bioorg. Med. Chem. Lett 2021, 34, 127777. [PubMed: 33418063]
330. Robertwoodgett J cDNA cloning and properties of glycogen synthase kinase-3. In Methods in Enzymology, Academic Press: 1991; Vol. 200, pp 564–577. [PubMed: 1659660]
331. Woodgett JR Molecular cloning and expression of glycogen synthase kinase-3/factor A. EMBO J. 1990, 9, 2431–2438. [PubMed: 2164470]
332. Patel P; Woodgett JR Chapter Eight - Glycogen synthase kinase 3: A kinase for all pathways? In Current Topics in Developmental Biology, Jenny A, Ed. Academic Press: 2017; Vol. 123, pp 277–302. [PubMed: 28236969]
333. Hooper C; Killick R; Lovestone S The GSK3 hypothesis of Alzheimer's disease. J. Neurochem. 2008, 104, 1433–1439. [PubMed: 18088381]
334. Bhat RV; Budd Haeberlein SL; Avila J Glycogen synthase kinase 3: a drug target for CNS therapies. J. Neurochem 2004, 89, 1313–1317. [PubMed: 15189333]
335. Lei P; Ayton S; Bush AI; Adlard PA GSK-3 in Neurodegenerative Diseases. Int. J. Alzheimers Dis 2011, 2011, 189246. [PubMed: 21629738]
336. Kaplanski J; Nassar A; Sharon-Granit Y; Jabareen A; Kobal SL; Azab AN Lithium attenuates lipopolysaccharide-induced hypothermia in rats. Eur. Rev. Med. Pharmacol. Sci 2014, 18, 1829–1837. [PubMed: 24992627]
337. Pei J-J; Tanaka T; Tung Y-C; Braak E; Iqbal K; Grundke-Iqbal I Distribution, levels, and activity of glycogen synthase kinase-3 in the Alzheimer disease brain. J. Neuropathol. Exp. Neurol 1997, 56, 70–78. [PubMed: 8990130]
338. Blalock EM; Geddes JW; Chen KC; Porter NM; Markesbery WR; Landfield PW Incipient Alzheimer's disease: Microarray correlation analyses reveal major transcriptional and tumor suppressor responses. Proc. Natl. Acad. Sci 2004, 101, 2173–2178. [PubMed: 14769913]
339. Leroy K; Yilmaz Z; Brion JP Increased level of active GSK-3β in Alzheimer's disease and accumulation in argyrophilic grains and in neurones at different stages of neurofibrillary degeneration. Neuropathol. Appl. Neurobiol 2007, 33, 43–55. [PubMed: 17239007]
340. Vasdev N; Garcia A; Stableford WT; Young AB; Meyer JH; Houle S; Wilson AA Synthesis and ex vivo evaluation of carbon-11 labelled N-(4-methoxybenzyl)-N′-(5-nitro-1,3-thiazol-2-yl)urea ([11C]AR-A014418): A radiolabelled glycogen synthase kinase-3β specific inhibitor for PET studies. Bioorg. Med. Chem. Lett 2005, 15, 5270–5273. [PubMed: 16202587]
341. Hicks JW; Wilson AA; Rubie EA; Woodgett JR; Houle S; Vasdev N Towards the preparation of radiolabeled 1-aryl-3-benzyl ureas: Radiosynthesis of [11C-carbonyl] AR-A014418 by [11C]CO2 fixation. Bioorg. Med. Chem. Lett 2012, 22, 2099–2101. [PubMed: 22321216]
342. Cole EL; Shao X; Sherman P; Quesada C; Fawaz MV; Desmond TJ; Scott PJH Synthesis and evaluation of [11C]PyrATP-1, a novel radiotracer for PET imaging of glycogen synthase kinase-3β (GSK-3β). Nucl. Med. Biol 2014, 41, 507–512. [PubMed: 24768148]
343. Kumata K; Yui J; Xie L; Zhang Y; Nengaki N; Fujinaga M; Yamasaki T; Shimoda Y; Zhang M-R Radiosynthesis and preliminary PET evaluation of glycogen synthase kinase 3β (GSK-3β) inhibitors containing [11C]methylsulfanyl, [11C]methylsulfinyl or [11C]methylsulfonyl groups. Bioorg. Med. Chem. Lett 2015, 25, 3230–3233. [PubMed: 26067173]
344. Li L; Shao X; Cole EL; Ohnmacht SA; Ferrari V; Hong YT; Williamson DJ; Fryer TD; Quesada CA; Sherman P; Riss PJ; Scott PJH; Aigbirhio FI Synthesis and initial in vivo studies with [11C]SB-216763: The first radiolabeled brain penetrative inhibitor of GSK-3. ACS Med. Chem. Lett 2015, 6, 548–552. [PubMed: 26005531]

345. Hu K; Patnaik D; Collier TL; Lee KN; Gao H; Swoyer MR; Rotstein BH; Krishnan HS; Liang SH; Wang J; Yan Z; Hooker JM; Vasdev N; Haggarty SJ; Ngai M-Y Development of [18F]maleimide-based glycogen synthase kinase-3β ligands for positron emission tomography imaging. ACS Med. Chem. Lett 2017, 8, 287–292. [PubMed: 28337318]

346. Liang SH; Chen JM; Normandin MD; Chang JS; Chang GC; Taylor CK; Trapa P; Plummer MS; Para KS; Conn EL; Lopresti-Morrow L; Lanyon LF; Cook JM; Richter KEG; Nolan CE; Schachter JB; Janat F; Che Y; Shanmugasundaram V; Lefker BA; Enerson BE; Livni E; Wang L; Guehl NJ; Patnaik D; Wagner FF; Perlis R; Holson EB; Haggarty SJ; El Fakhri G; Kurumbail RG; Vasdev N Discovery of a highly selective glycogen synthase kinase-3 inhibitor (PF-04802367) that modulates tau phosphorylation in the brain: Translation for PET neuroimaging. Angew. Chem. Int. Ed 2016, 55, 9601–9605.

347. Rojas A; Ganesh T; Lelutiu N; Gueorguieva P; Dingledine R Inhibition of the prostaglandin EP2 receptor is neuroprotective and accelerates functional recovery in a rat model of organophosphorus induced status epilepticus. Neuropharmacology 2015, 93, 15–27. [PubMed: 25656476]

348. Yang Y; Kim SC; Yu T; Yi Y-S; Rhee MH; Sung G-H; Yoo BC; Cho JY Functional roles of p38 mitogen-activated protein kinase in macrophage-mediated inflammatory responses. Mediators Inflamm. 2014, 2014, 352371. [PubMed: 24771982]

349. Olmos G; Lladó J Tumor necrosis factor alpha: A link between neuroinflammation and excitotoxicity. Mediators Inflamm. 2014, 2014, 861231. [PubMed: 24966471]

350. Zhang X; Li M; Yin N; Zhang J The expression regulation and biological function of autotaxin. Cells 2021, 10, 939. [PubMed: 33921676]

351. Chen Z; Mori W; Zhang X; Yamasaki T; Dunn PJ; Zhang G; Fu H; Shao T; Zhang Y; Hatori A; Ma L; Fujinaga M; Xie L; Deng X; Li H; Yu Q; Rong J; Josephson L; Ma J-A; Shao Y; Tomita S; Zhang M-R; Liang SH Synthesis, pharmacology and preclinical evaluation of 11C-labeled 1,3-dihydro-2H-benzo[d]imidazole-2-ones for imaging γ8-dependent transmembrane AMPA receptor regulatory protein. Eur. J. Med. Chem 2018, 157, 898–908. [PubMed: 30145376]

352. Chen J; Gan J; Sun J; Chen Z; Fu H; Rong J; Deng X; Shang J; Gong J; Shao T; Collier L; Wang L; Xu H; Liang SH Radiosynthesis and preliminary evaluation of 11C-labeled 4-cyclopropyl-7-(3-methoxyphenoxy)-3,4-dihydro-2H-benzo[e] [1,2,4] thiadiazine 1,1-dioxide for PET imaging AMPA receptors. Tetrahedron Lett. 2020, 61, 151635. [PubMed: 32153306]

353. Zhang X; Zhang Y; Chen Z; Shao T; Van R; Kumata K; Deng X; Fu H; Yamasaki T; Rong J; Hu K; Hatori A; Xie L; Yu Q; Ye W; Xu H; Sheffler DJ; Cosford NDP; Shao Y; Tang P; Wang L; Zhang M-R; Liang SH Synthesis and preliminary studies of 11C-labeled tetrahydro-1,7-naphthyridine-2-carboxamides for PET imaging of metabotropic glutamate receptor 2. Theranostics 2020, 10, 11178–11196. [PubMed: 33042277]

354. Sun J.-y.; Kumata K; Chen Z; Zhang Y.-d.; Chen J.-h.; Hatori A; Fu H.-l.; Rong J; Deng X.-y.; Yamasaki T; Xie L; Hu K; Fujinaga M; Yu Q.-z.; Shao T; Collier TL; Josephson L; Shao Y.-h.; Du Y.-f.; Wang L; Xu H; Zhang M.-r.; Liang SH Synthesis and preliminary evaluation of novel 11C-labeled GluN2B-selective NMDA receptor negative allosteric modulators. Acta Pharmacologica Sinica 2021, 42, 491–498. [PubMed: 32661351]

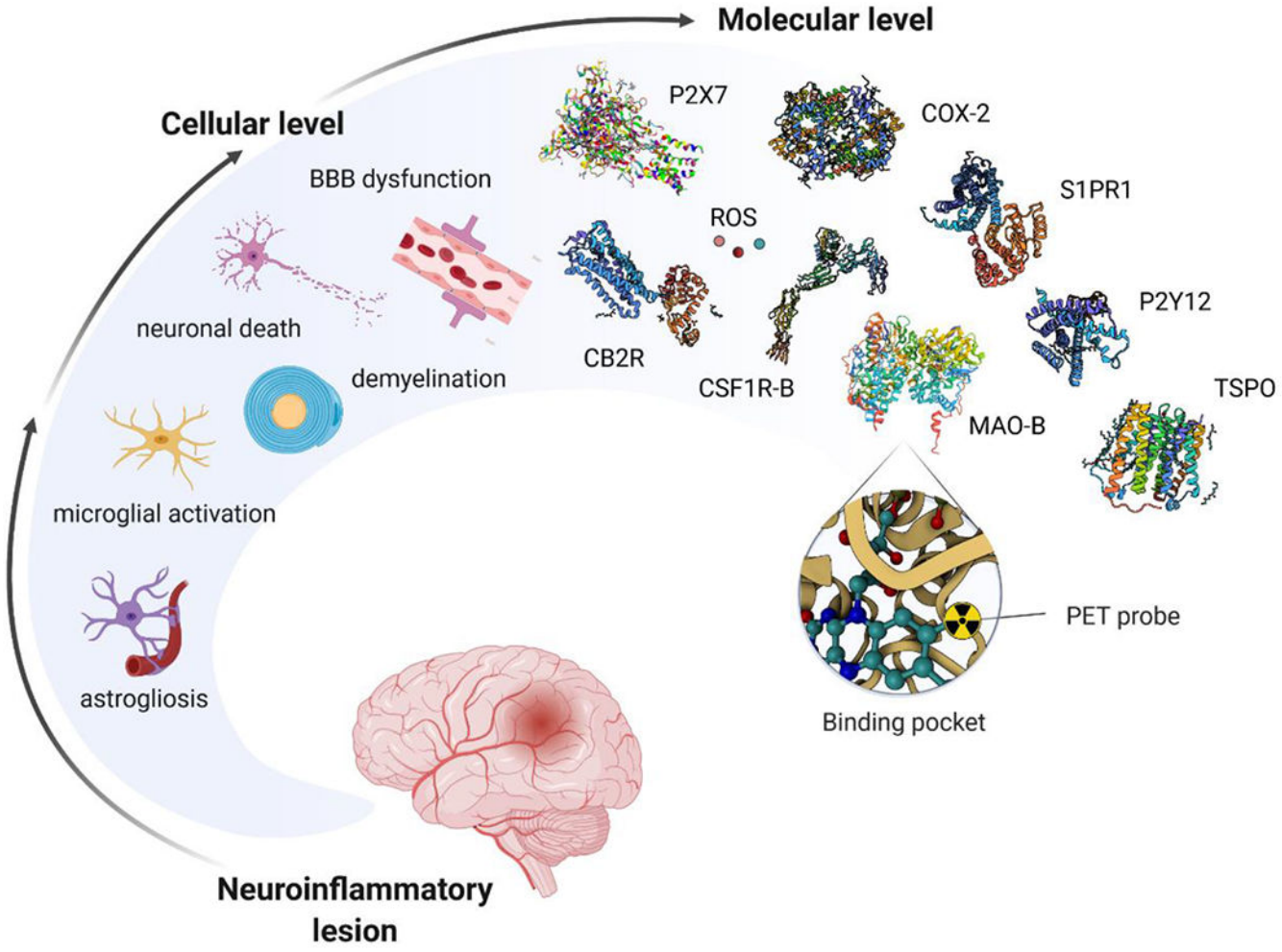

Figure 1.
Cellular and molecular hallmarks of neuroinflammation.

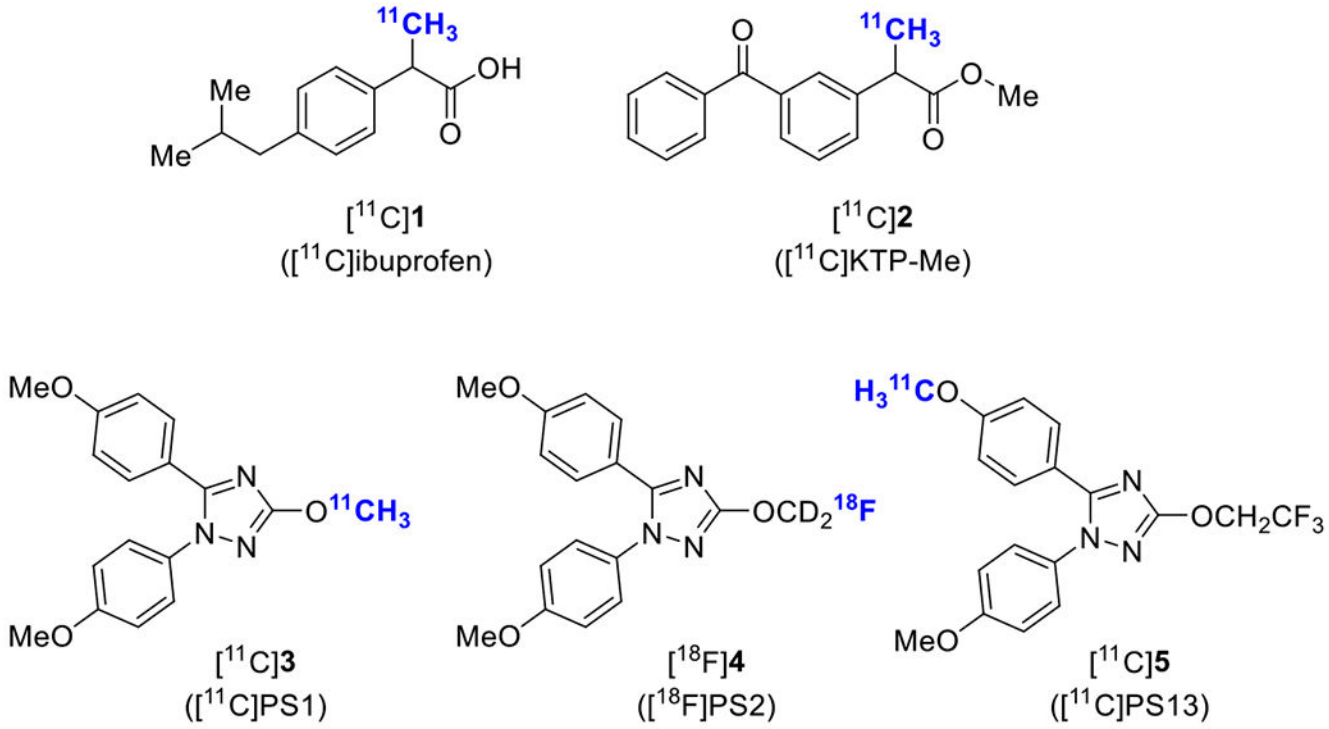

Figure 2.
Representative PET probes for COX-1.

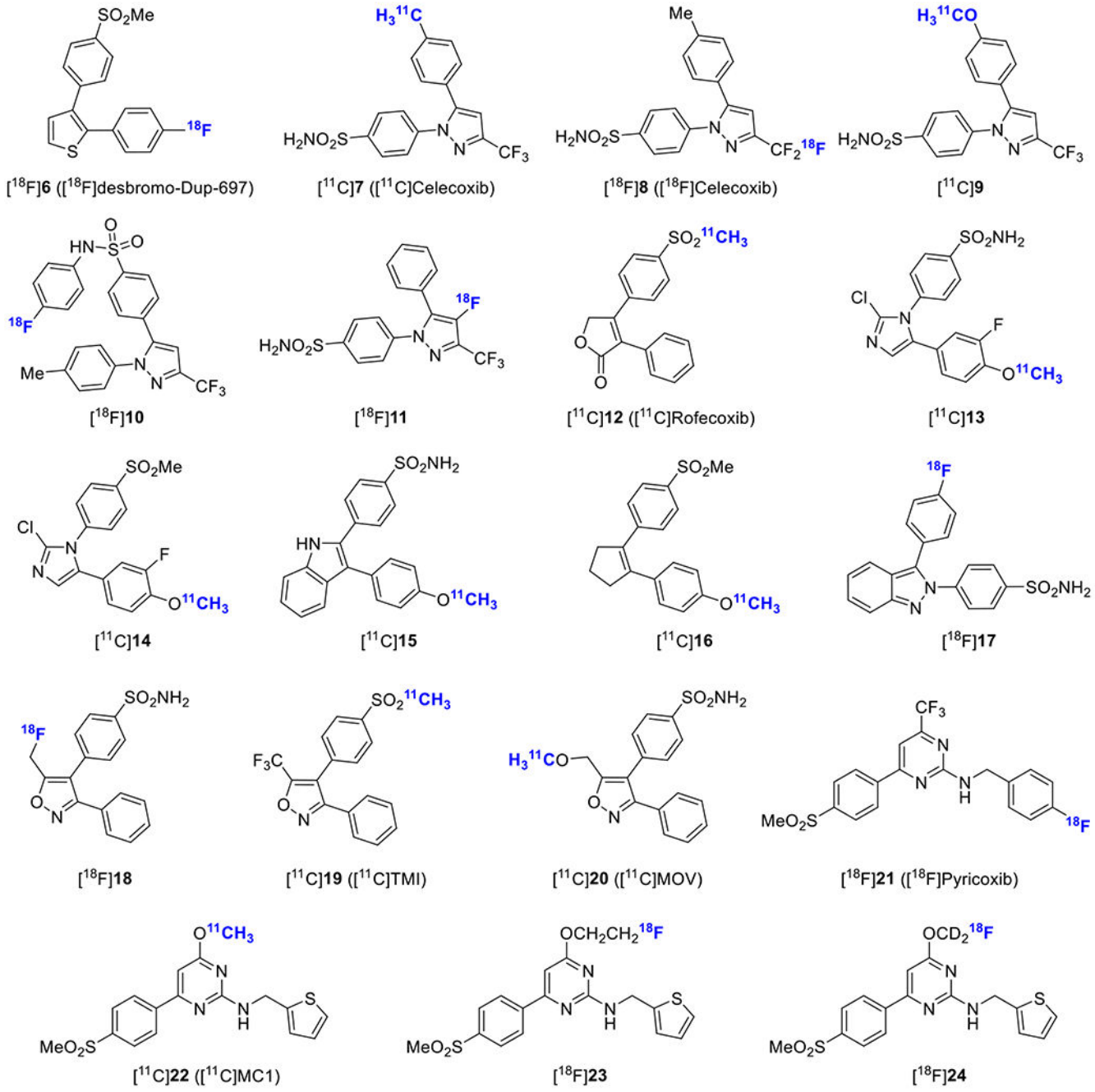

Figure 3.
Representative PET probes for COX-2.

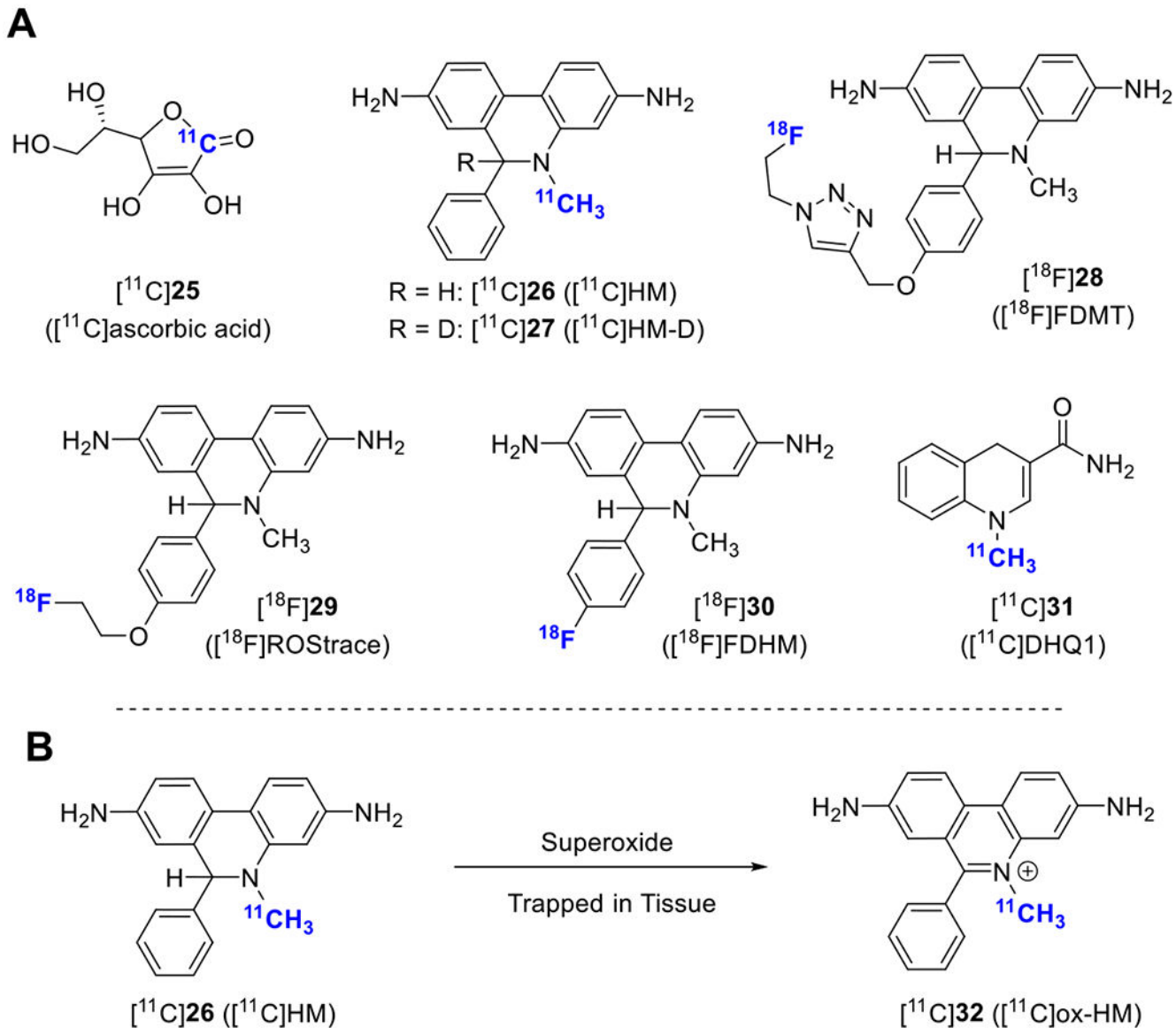

Figure 4.

A) Representative PET probes for ROS and **B)** mode of action of [11C]**26**.

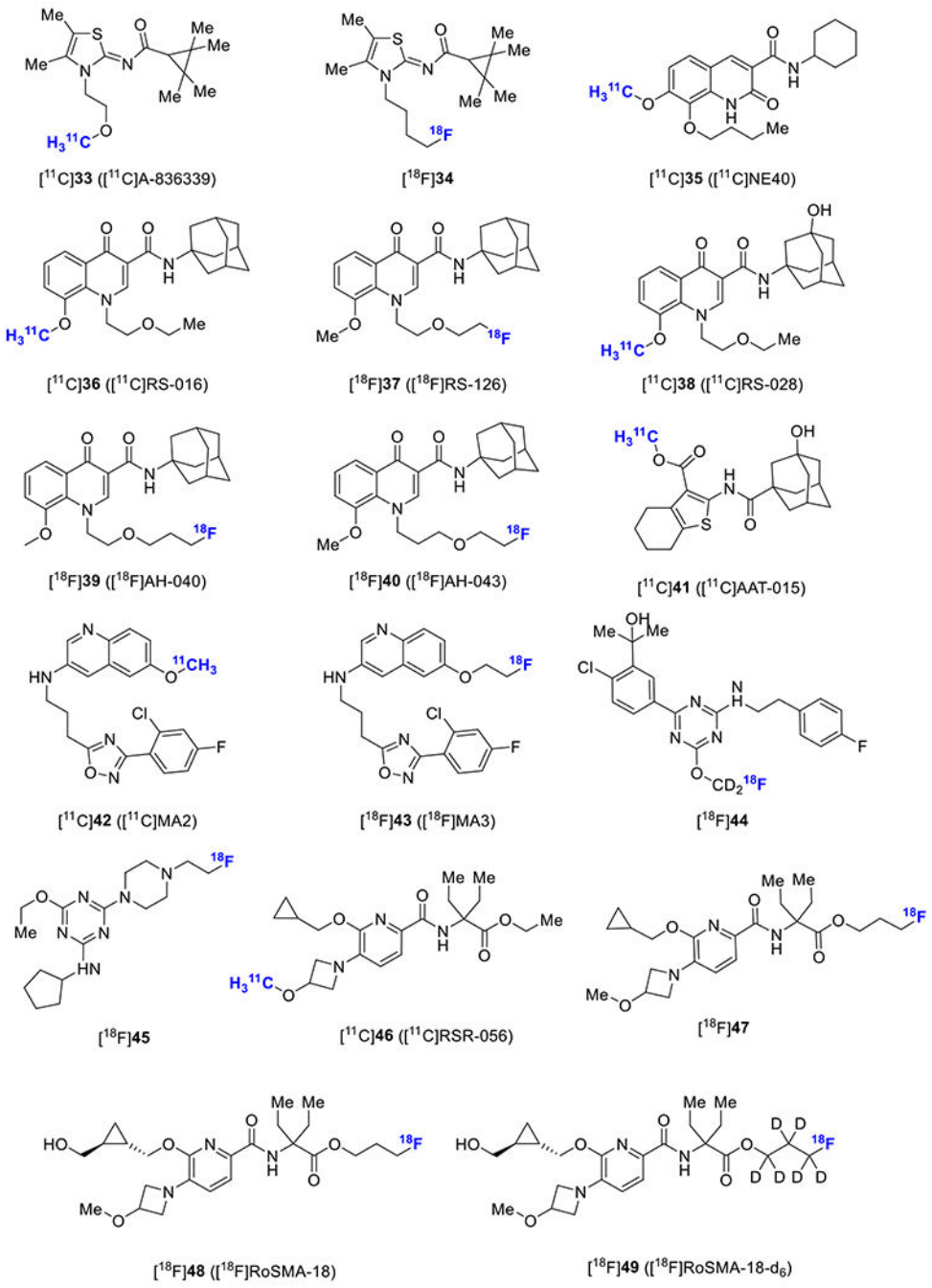

Figure 5.
Representative PET probes for CB2R.

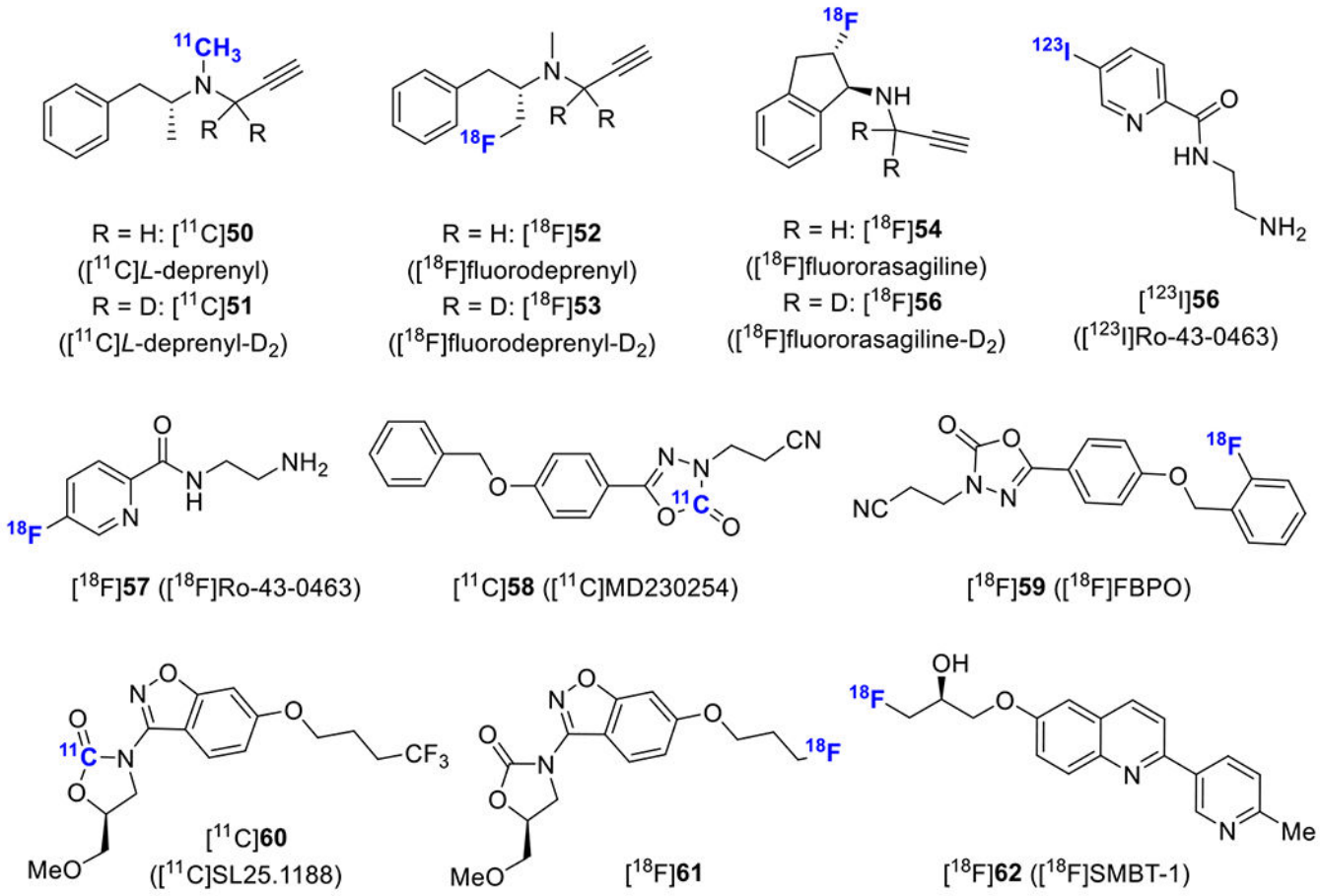

Figure 6.
Chemical structures of MAO-B selective PET probes.

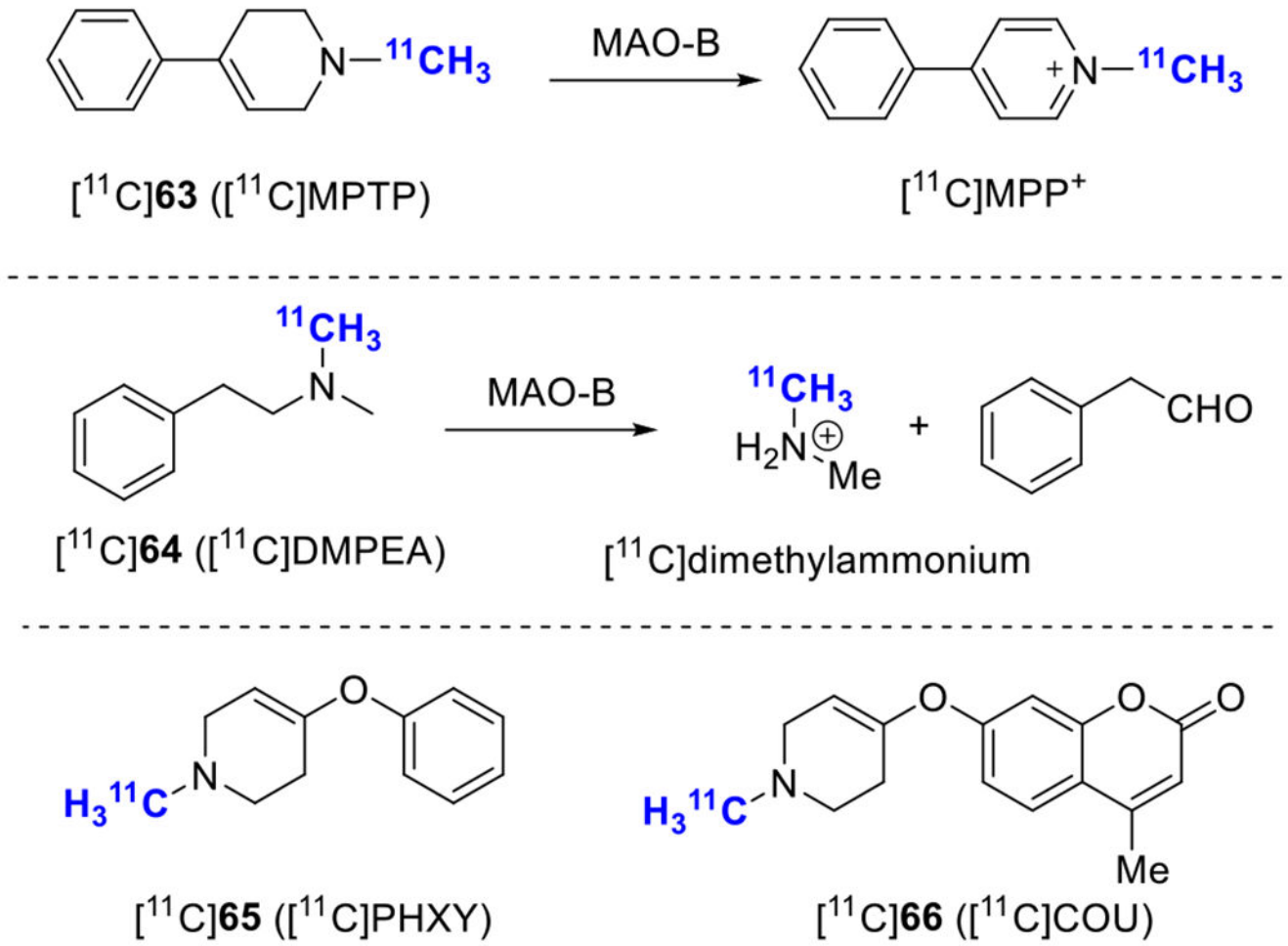

Figure 7.
Chemical structures of metabolic trapping agents for MAO.

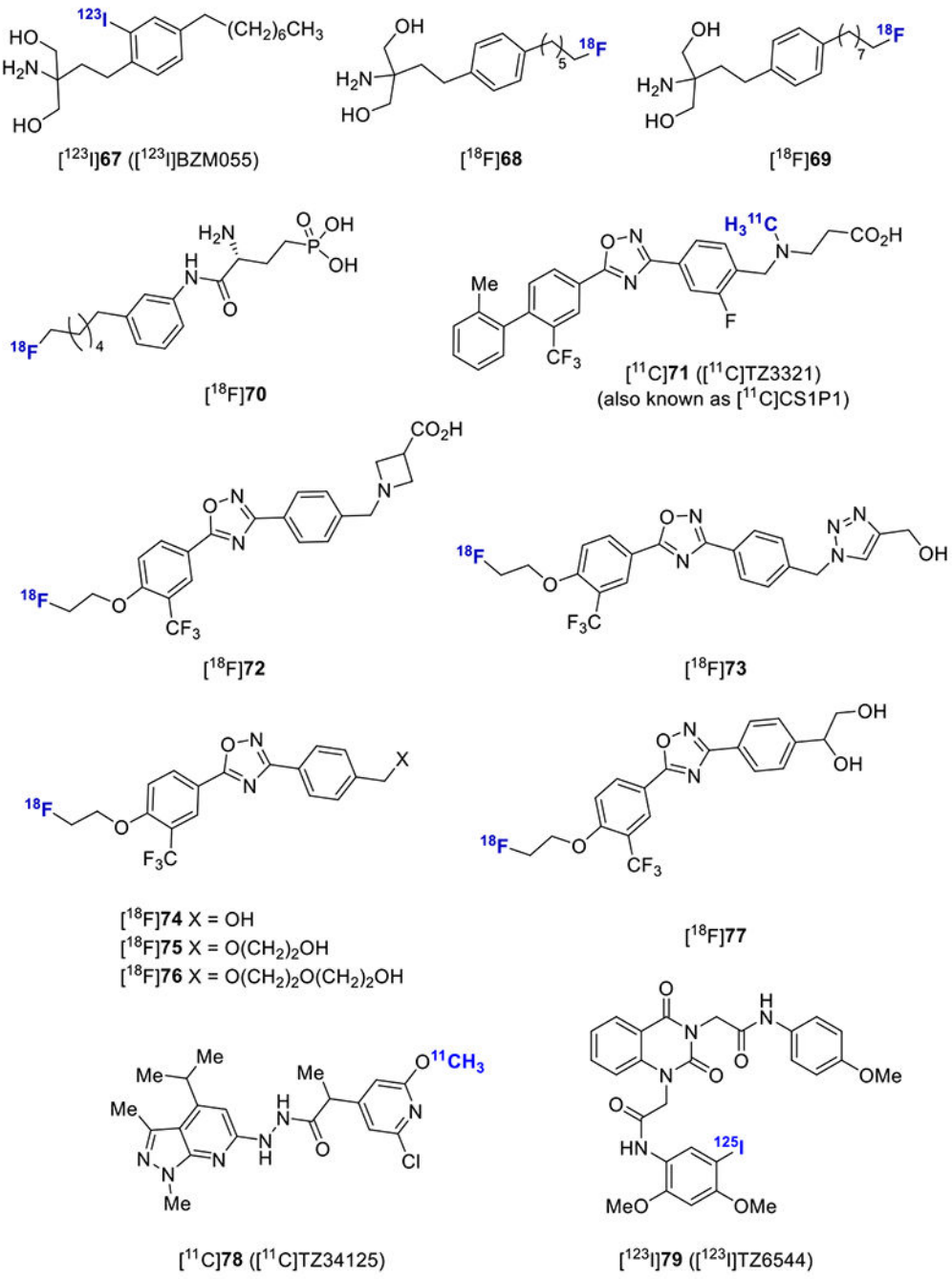

Figure 8.
Representative imaging probes for S1PR1 (**67-78**) and S1PR2 (**78** and **79**).

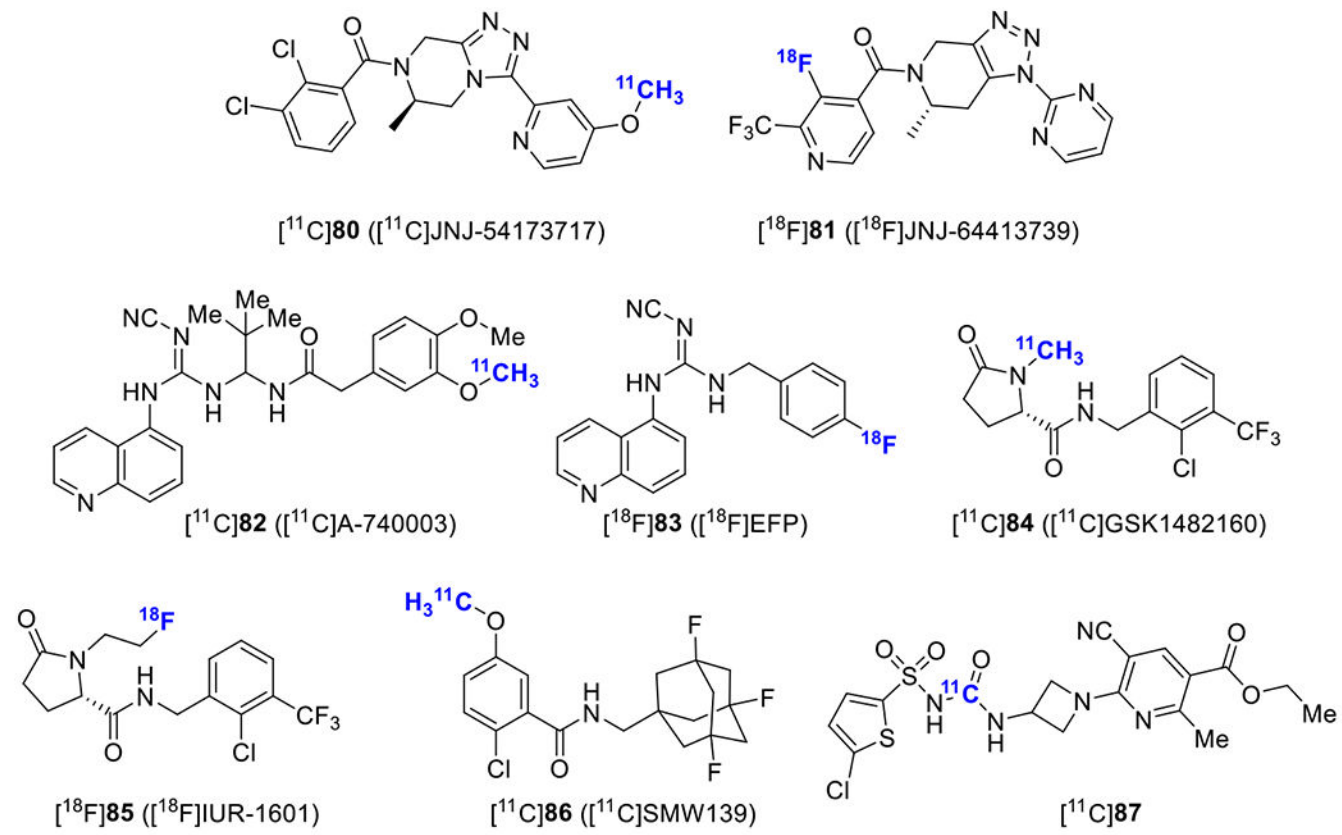

Figure 9.

Representative PET probes for purinergic receptors (compounds **80-86** for P2X7R, compound **87** for P2Y12R).

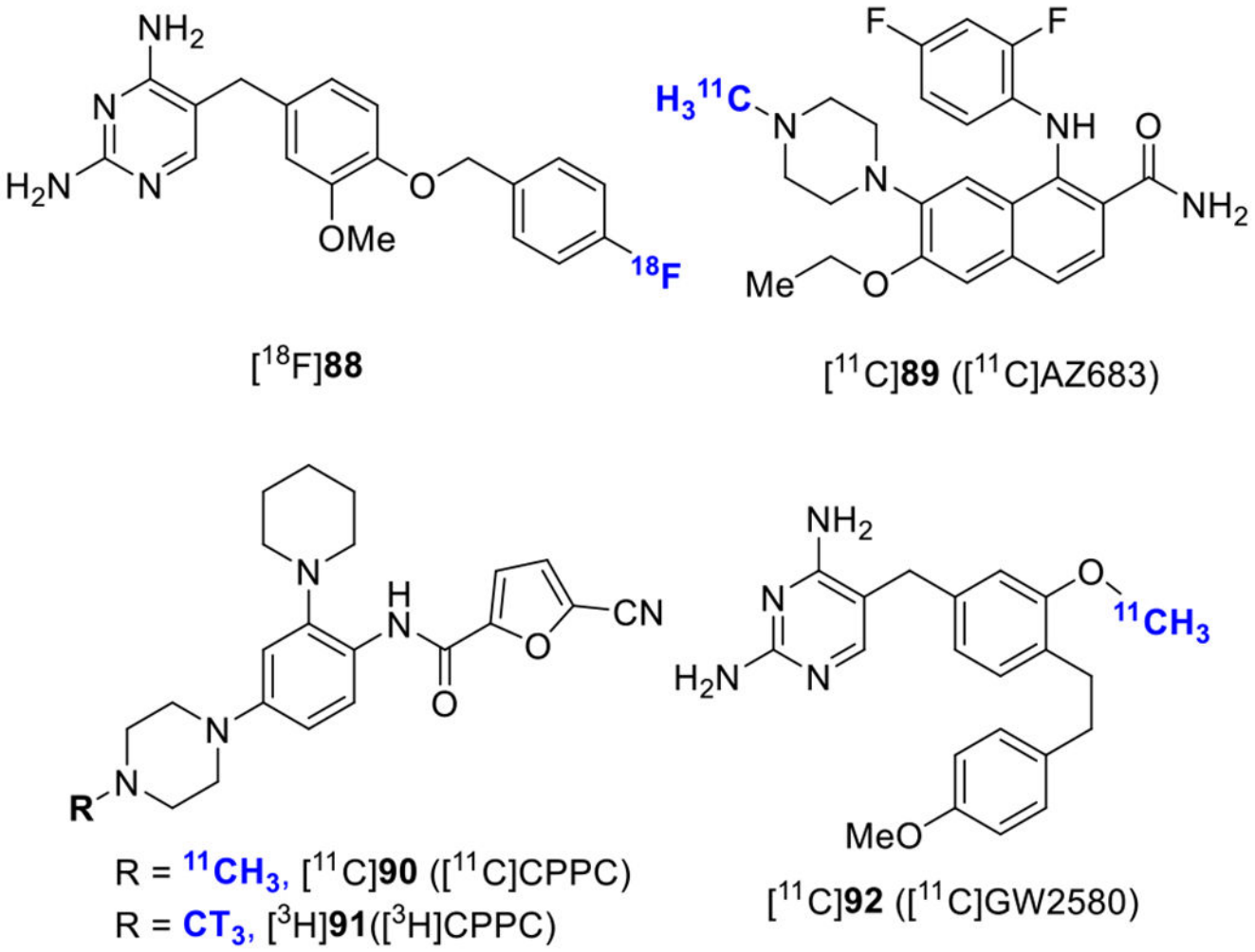

Figure 10.
Representative PET probes for CSF1R.

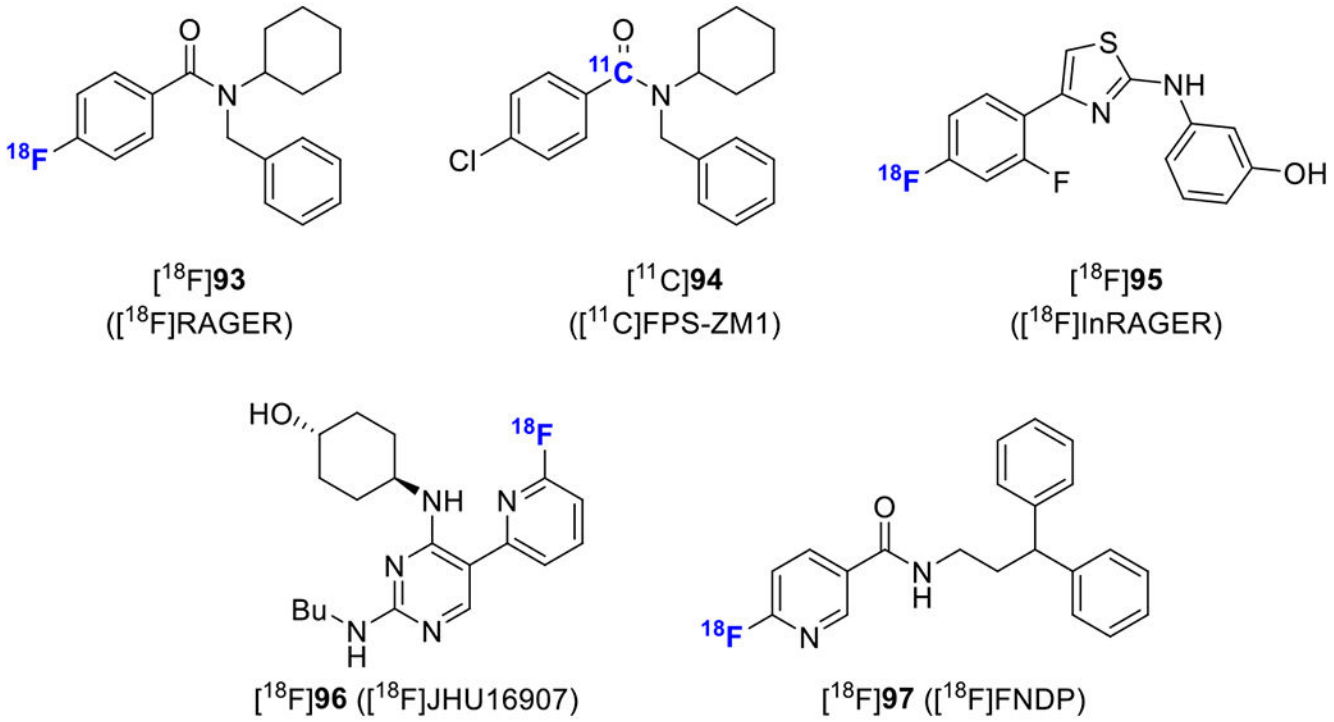

Figure 11.

Representative PET probes for RAGE (compounds **93**-**95**), MERTK (compound **96**) and sEH (compound **97**).

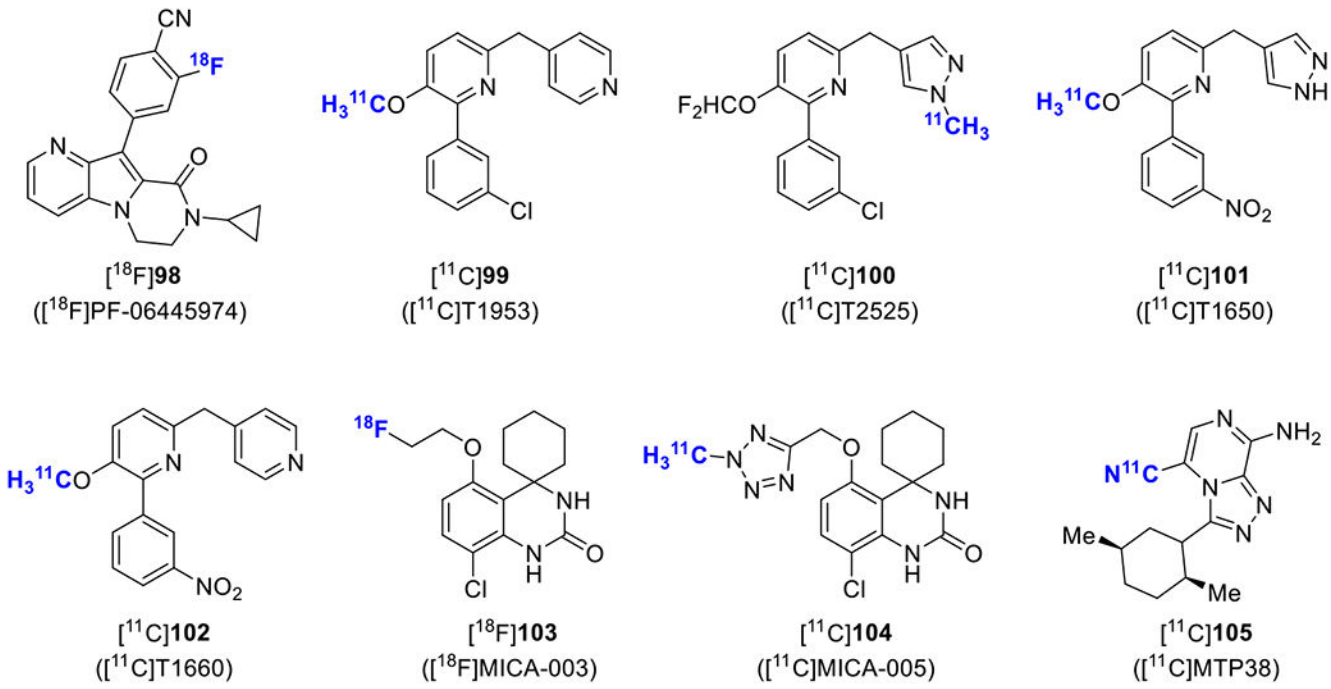

Figure 12.
Representative PET probes for PDE4B (**98**), PDE4D (**99-102**), and PDE7 (**103-105**)

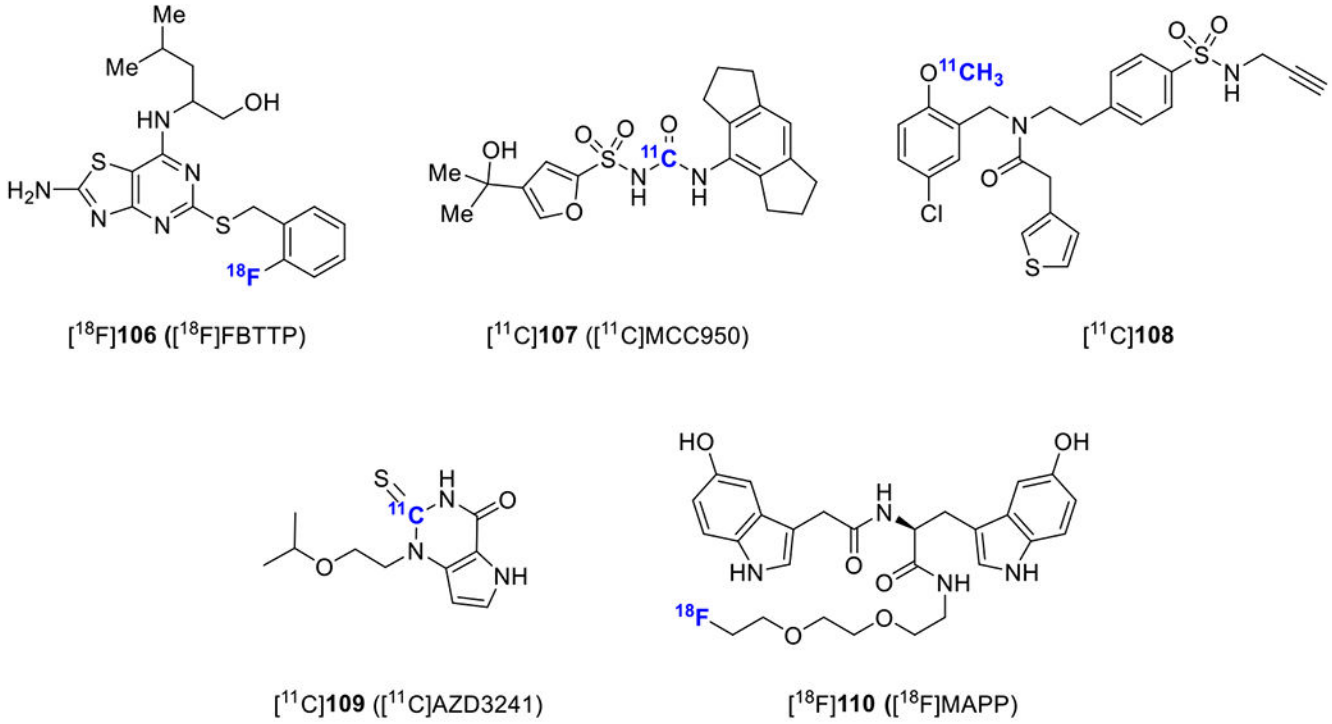

Figure 13.

Representative imaging probes for CX3CR1 (compound **106**), NLRP3 (compound **107** & **108**) and MPO (compound **109** & **110**)

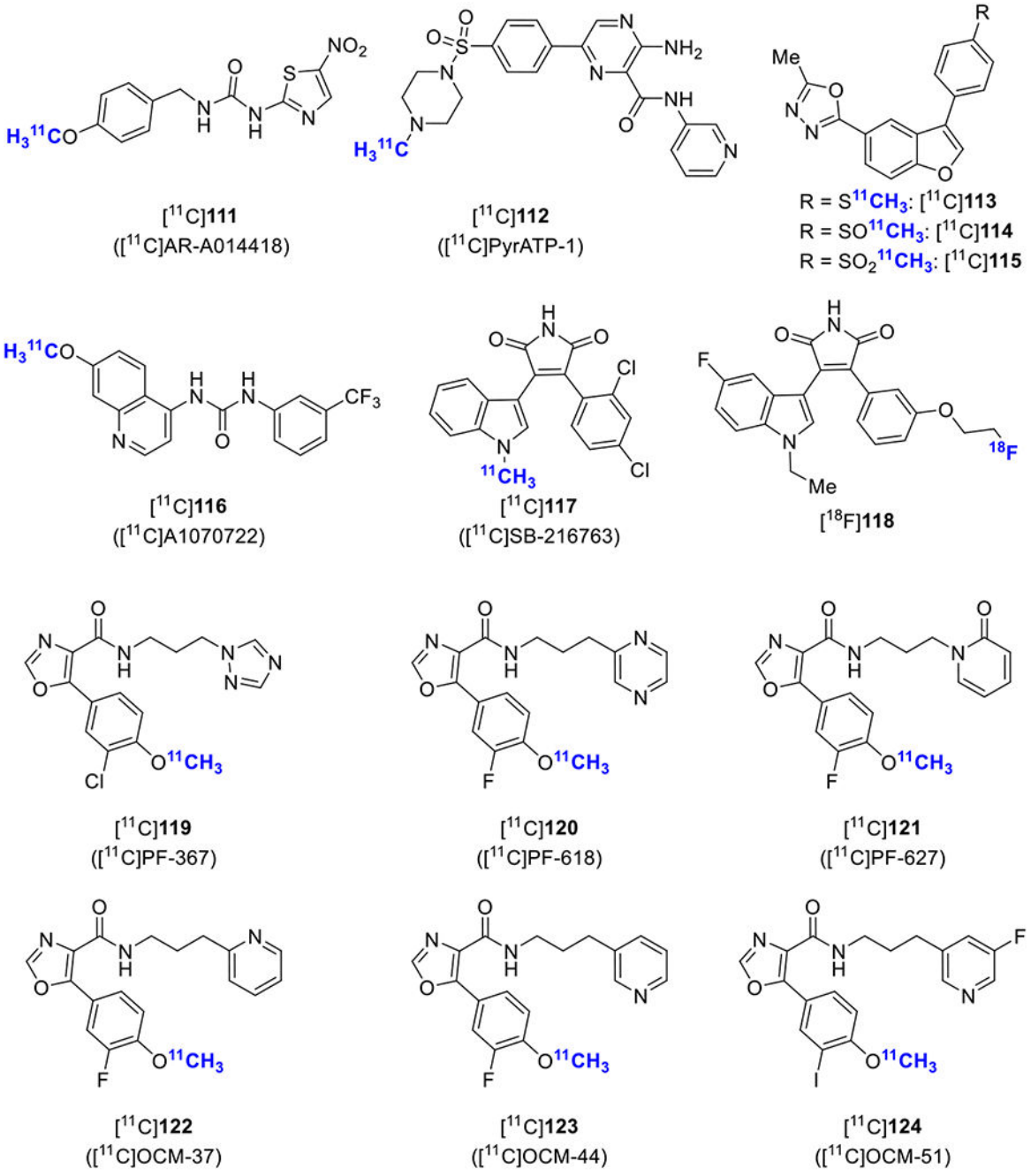

Figure 14.
Representative PET probes for GSK-3.

Table 1.

PET imaging of neuroinflammation: Potential targets and respective probes beyond TSPO imaging.[a–c]

Target	Cell expression	Expression in neuroinflammation	Representative PET probes[a]	Binding affinity	Stage of research	comments or current status[b]
COX-1[63]	Microglia	Upregulated	[^{11}C]KTP-Me[64]	IC_{50} = 47 nM	humans	Rapid metabolic rate
			[^{11}C]PS13[65]	IC_{50} = 1 nM	humans	CE
COX-2[66]	Microglia	Upregulated	[^{11}C]MC1[67]	IC_{50} = 1 nM	humans	CE
ROS[68]	Microglia	Upregulated	[^{11}C]HM-D[69] [^{18}F]ROStrace[70] [^{18}F]FDHM[71] [^{11}C]DHQ1[72]	--[c]	rodents	CE
CB2R[73]	Microglia Astrocyte	Upregulated	[^{11}C]A-836339[74]	K_i = 0.7 nM	rodents	CE
			[^{11}C]NE40[75]	K_i = 9.6 nM	humans	No correlation between tracer uptake and amyloid load
			^{18}F]RoSMA-18-d_6[76]	K_i = 0.7 nM	rodents	CE
MAO-B[77]	Astrocyte>>Microglia	Upregulated	[^{11}C]*L*-deprenyl-D_2[78]	K_i = 0.97 μM	humans	Irreversible binding
			[^{11}C]MD230254[79]	IC_{50} = 4 nM	NHPs	CE, reversible binding
			[^{11}C]SL25.1188[80]	K_i = 2.9 nM	humans	CE, reversible binding
			[^{18}F]SMBT-1[81]	K_d = 3.7 nM	humans	CE, reversible binding
S1PR1[82]	Microglia >> Astrocyte	Upregulated	[^{11}C]TZ3321[83]	IC_{50} = 2.13 nM	humans	CE
			[^{18}F]**74**[84]	IC_{50} = 6.7 nM	NHPs	CE
P2X7R[85]	Microglia >> Astrocyte	Upregulated	[^{11}C]JNJ-54173717[86]	IC_{50} = 4.2 nM	humans	CE
			[^{18}F]JNJ-64413739[87]	IC_{50} = 1 nM	humans	CE
			[^{11}C]GSK1482160[88]	IC_{50} = 3 nM	NHPs	CE
			[^{11}C]SMW139[89]	IC_{50} = 24.5 nM	humans	CE
P2Y12R[90]	Microglia (M2)	Downregulated	[^{11}C]**87**[91]	IC_{50} = 6 nM	rodents	Limited brain uptake
CSF1R[92]	Microglia	Upregulated	[^{11}C]AZ683[93]	IC_{50} = 6 nM	NHPs	CE
			[^{11}C]CPPC[94]	IC_{50} = 0.8 nM	NHPs	Low specific binding
RAGE[95]	Microglia	flRAGE: upregulated sRAGE: downregulated	[^{18}F]RAGER[96]	K_d = 15 nM	NHPs	CE
			[^{18}F]InRAGER[97]	K_d = 1 nM	rodents	Lack of efficient radiolabeling method
MERTK[98]	Microglia Astrocyte	Upregulated	[^{18}F]JHU16907[99]	IC_{50} = 2.5 nM	rodents	CE

Target	Cell expression	Expression in neuroinflammation	Representative PET probes[a]	Binding affinity	Stage of research	comments or current status[b]
sEH[100]	Astrocyte	Upregulated	[^{18}F]FNDP[101]	IC_{50} = 8.7 nM	humans	CE
PDE4B[102]	Microglia	Upregulated	[^{18}F]PF-06445974[103]	IC_{50} < 1 nM	NHPs	CE
PDE4D[104]	Microglia	Upregulated	[^{11}C]T1650[105]	IC_{50} = 3.9 nM	humans	Problematic brain penetrant radiometabolites
PDE7[106]	Microglia	Upregulated	[^{11}C]MTP38[107]	IC_{50} < 10 nM	humans	CE
CX3CR1[108]	Microglia	Upregulated	[^{18}F]FBTTP[109]	K_i = 23 nM	rodents	CE
NLRP3[110]	Microglia	Upregulated	[^{11}C]MCC950[111]	IC_{50} = 8 nM	NHPs	Limited brain uptake
MPO[112]	Microglia	Upregulated	[^{11}C]AZD3241[113]	IC_{50} = 1.2 μM	NHPs	Irreversible binding
			[^{18}F]MAPP[114]	--	rodents	CE
GSK-3[115]	Microglia Astrocyte	Upregulated	[^{11}C]PF-618[116]	IC_{50} = 2.5 nM	NHPs	CE
			[^{11}C]OCM-37[116]	IC_{50} = 1.5 nM	NHPs	CE
			[^{11}C]OCM-44[116]	IC_{50} = 2 nM	NHPs	CE

Notes:

a. This is a representative but not exhaustive list.

b. "CE" is indicated as Continued Efforts (CE) on the evaluation (advantages or shortcomings) of referred radioligands; it is premature to conclude that whether they are successful before completing in-depth study.

c. --, not applicable